

# Ginzburg-Landau Theory for Bosonic Gases in Optical Lattices



im Fachbereich Physik der  
Freien Universität Berlin  
eingereichte Dissertation

von

Francisco Ednilson Alves dos Santos

October 2011

Die in vorliegender Dissertation dargestellte Arbeit wurde in der Zeit zwischen April 2007 und August 2011 im Fachbereich Physik an der Freien Universität Berlin unter Betreuung von Priv.- Doz. Dr. Axel Pelster durchgeführt.

Erstgutachter: Priv.-Doz. Dr. Axel Pelster

Zweitgutachter: Prof. Dr. Jürgen Bosse

Disputationsdatum: 07.11.2011

# Abstract

In this thesis the quantum phase transition of spinless bosons in optical lattices is described within a Ginzburg-Landau theory. To this end the underlying effective action is derived from the microscopic Bose-Hubbard Hamiltonian by developing diagrammatic techniques for a resummed hopping expansion. Thus, this Ginzburg-Landau theory inaugurates a new approach for determining the properties of bosonic atoms in lattice systems. Already in second hopping order it exhibits a relative error of less than 3 % for the boundary between the superfluid and the Mott insulator phase of a three-dimensional cubic optical lattice when compared with the most recent results of Quantum Monte Carlo simulations. In addition, the Ginzburg-Landau theory also allows to calculate near-equilibrium as well as non-equilibrium quantities. Thus, this thesis shows that, although comparable with numerical methods in terms of accuracy, the analytical Ginzburg-Landau theory presented here offers a much better qualitative understanding of the respective system properties.

The thesis starts in Chapter 1 with a brief introduction of the experimental achievements and the theoretical description of Bose-Einstein condensation in general and lattice physics in particular. Afterwards, Chapter 2 discusses in more detail the theory of laser-generated optical lattices. Second-order phase transitions are then covered in Chapter 3 with special emphasis on the physics of the quantum phase transition between a Mott insulator and a superfluid.

The Ginzburg-Landau theory itself is developed systematically in Chapter 4. It contains the diagrammatic techniques, which are used to calculate the effective action of the lattice system in a power series of the hopping parameter. To this end symmetry-breaking currents are coupled to the bosonic operators and, by applying a Legendre transformation to the free energy, the resulting effective action is obtained. This procedure leads to an effective resummation of the free energy which makes it possible to analytically describe the properties of the different phases of the lattice system.

Various applications of the Ginzburg-Landau theory are presented in Chapters 5 and 6. In Chapter 5, the effective action is used to calculate various static and dynamical properties of cubic bosonic lattices at both zero and finite temperature. It shows an impressive accordance with the numerically calculated quantum phase diagrams for two and three dimensions already at second hopping order. In addition, the equivalence between condensate and superfluid density is demonstrated at first hopping order. Furthermore, the spectra of the various collective excitations appearing in both the Mott insulator and the superfluid phase are analyzed in detail. In Chapter 6, the Ginzburg-Landau theory is then adapted to deal with the collapse and revival dynamics of matter waves in an optical lattice loaded with  $^{87}\text{Rb}$  atoms according to the experiment performed in Ref. [1]. Our method is used to reproduce at least qualitatively the observed damped oscillations of the coherence.



# Kurzzusammenfassung

In der vorliegenden Arbeit wird der Quantenphasenübergang spinloser Bosonen in optischen Gittern im Rahmen einer Ginzburg-Landau-Theorie beschrieben. Hierzu wird die zugrunde liegende effektive Wirkung ausgehend vom mikroskopischen Bose-Hubbard-Hamiltonian abgeleitet, indem eine diagrammatische Technik zur Resummation einer Tunnel-Entwicklung ausgearbeitet wird. Die so erhaltene Ginzburg-Landau-Theorie eröffnet einen neuen Zugang, um die Eigenschaften bosonischer Atome in einem Gittersystem zu bestimmen. Schon in zweiter Hopping-Ordnung ergibt sich ein Fehler von nur 3 % für die Grenze zwischen der superfluiden und der Mott-Isolator-Phase eines dreidimensionalen kubischen optischen Gitters im Vergleich zu neuesten Quanten Monte-Carlo-Simulationen. Außerdem erlaubt die Ginzburg-Landau-Theorie, physikalische Größen nahe des Gleichgewichtes und im Nichtgleichgewicht zu berechnen. Die Arbeit zeigt daher, dass die hier vorgestellte analytische Ginzburg-Landau-Theorie ein viel besseres qualitatives Verständnis der jeweiligen Systemeigenschaften ermöglicht, auch wenn die Genauigkeit der Ergebnisse mit denen durch numerische Methoden erzielten Ergebnisse vergleichbar ist.

Die Arbeit beginnt in Kapitel 1 mit einer kurzen Einführung in die experimentelle Errungenschaften und die theoretische Beschreibung der Bose-Einstein-Kondensation im allgemeinen und der Gitterphysik im besonderen. Anschließend diskutiert Kapitel 2 detaillierter die Theorie der durch Laser erzeugten optischen Gitter. Phasenübergänge zweiter Ordnung werden dann im Kapitel 3 behandelt, wobei besonders die Physik des Quantenphasenübergangs vom Mott-Isolator zum Superfluid betont wird.

Die eigentliche Ginzburg-Landau-Theorie wird systematisch in Kapitel 4 entwickelt. Sie beinhaltet die diagrammatischen Techniken, die zur Berechnung der effektiven Wirkung eines Gittersystems als Potenzreihe des Tunnelparameters verwendet werden. Hierzu werden Symmetrie brechende Ströme an die bosonischen Operatoren gekoppelt und die effektive Wirkung folgt durch eine Legendre-Transformation der freien Energie. Dieses Verfahren führt zu einer effektiven Resummation der freien Energie, die eine analytische Beschreibung der Eigenschaften in den verschiedenen Phasen des Gittersystems ermöglicht.

Verschiedene Anwendungen der Ginzburg-Landau-Theorie werden in den Kapiteln 5 und 6 vorgestellt. In Kapitel 5 wird die effektive Wirkung verwendet, um die verschiedenen statischen und dynamischen Eigenschaften von kubischen bosonischen Gittern sowohl bei verschwindender als auch bei endlicher Temperatur zu berechnen. Es zeigt sich, dass die Quantenphasendiagramme für zwei und drei Dimensionen schon in zweiter Tunnelordnung beeindruckend mit numerisch erzielten Ergebnissen übereinstimmen. Ferner wird gezeigt, dass Kondensatdichte und superfluide Dichte in erster Tunnelordnung äquivalent sind. Außerdem werden die Spektren der verschiedenen kollektiven Anregungen genauer analysiert, die sowohl in der Mott-Isolator als auch in der superfluiden Phase auftreten. In Kapitel 6 wird die Ginzburg-Landau-Theorie angewandt, um die Kollaps-und-Wiederkehr-Dynamik von Ma-

teriewellen in einem mit  $^{87}\text{Rb}$  Atome beladenen optischen Gitter zu behandeln, die im Experiment der Ref. [1] beobachtet wurde. Unsere Methode ist in der Lage, die beobachteten gedämpften Oszillationen der Kohärenz zumindest qualitativ zu reproduzieren.

Wir halten zusammenfassend fest, dass unsere Ginzburg-Landau-Theorie für Bosonen in optischen Gittern verschiedene Überprüfungen beim Vergleich mit numerischen Simulationen und experimentellen Resultaten erfolgreich bestanden hat. Daher erwarten wir, dass sie zur Planung und Analyse künftiger Gitterexperimente nützlich sein wird.

# Contents

<b>1. Introduction</b>	<b>9</b>
1.1. Bose-Einstein Condensation . . . . .	9
1.2. Bosons in optical lattices . . . . .	10
1.3. Overview . . . . .	14
<b>2. Optical Lattice Potentials</b>	<b>17</b>
2.1. Laser forces . . . . .	17
2.2. Band structure . . . . .	20
2.3. Bose-Hubbard Hamiltonian . . . . .	23
2.3.1. Hamiltonian Parameters . . . . .	25
2.3.2. Corrections due to Laser Inhomogeneity . . . . .	28
<b>3. Quantum Phase Transitions</b>	<b>33</b>
3.1. Second-Order Quantum Phase Transitions . . . . .	33
3.2. Quantum Phase Transitions in Bosonic Lattices . . . . .	35
3.3. Mean-Field Theory . . . . .	40
<b>4. Bosonic Lattices at Finite Temperature</b>	<b>47</b>
4.1. Perturbation Theory . . . . .	49
4.2. Lattice Diagrammatics . . . . .	50
4.3. Diagrammatic Representation . . . . .	51
4.4. Effective Action and 1-Particle Irreducible Diagrams . . . . .	53
4.5. Matsubara Representation . . . . .	55
4.6. Zeroth-Hopping Order Effective Action . . . . .	57
4.7. First-hopping order effective action . . . . .	63
4.8. Second-hopping order effective action . . . . .	64
<b>5. Homogeneous Lattices</b>	<b>69</b>
5.1. Quasi-Momentum Representation . . . . .	69
5.2. Static Properties . . . . .	71
5.2.1. First Hopping Order . . . . .	71
5.2.2. Second Hopping Order . . . . .	73
5.3. Dynamical Properties . . . . .	76
5.3.1. Superfluid Density . . . . .	76
5.3.2. Excitation Spectra . . . . .	78

5.3.3. Critical Exponents . . . . .	89
<b>6. Collapse and Revival of Matter Waves</b>	<b>95</b>
6.1. Equations of motion for $J = 0$ . . . . .	95
6.2. Exact solution for $J = 0$ . . . . .	96
6.3. Initial conditions . . . . .	97
6.4. Momentum distributions . . . . .	97
6.5. Comparison with Experiments . . . . .	100
<b>7. Summary and Conclusion</b>	<b>103</b>
<b>A. Appendix 1</b>	<b>109</b>
<b>B. Appendix 2</b>	<b>113</b>
<b>Bibliography</b>	<b>115</b>



# 1. Introduction

## 1.1. Bose-Einstein Condensation

By applying the new quantum statistics developed by Satyendra N. Bose [2], Albert Einstein predicted the possibility of a new state of matter emerging in extremely cold bosonic gases: the Bose-Einstein Condensate (BEC) [3,4]. According to his theory, when a non-interacting bosonic gas is cooled until it reaches a certain critical temperature, a phase transition occurs. Below such temperature, the number of particles occupying the ground state of the system becomes macroscopic. Following these ideas, in 1938 [5], F. London was the first to suggest the formation of a BEC as the explanation for superfluidity in  $^4\text{He}$ . Although Einstein's theory concerns only with ideal Bose gases, the prediction of London was later experimentally confirmed by using neutron scattering techniques [6].

Despite all the theoretical predictions, it took more 70 years before the extremely low temperatures necessary for the realization of the first BEC became available. It was only in the early 1980s that laser cooling techniques turned temperatures of the order of micro-Kelvin accessible to experiments. For this achievement, Chu, Cohen-Tannoudji, and Phillips received the physics Nobel prize in 1997.

The basic idea of laser cooling is to use the Doppler effect due to the thermal motion of the atoms in such a way that they absorb more photons when moving towards the light source than in other directions. This effect is obtained by tuning the laser to a frequency a little smaller than an electronic transition of the atom. This way, when an atom moves in the direction of the laser source, its transition frequency matches the laser frequency due to the Doppler effect. By using two laser beams pointing in opposite directions, the atom will absorb more photons whenever it moves towards a light source, thus reducing its momentum. Later, when the excited atom spontaneously emits the absorbed photon, it will receive the photon momentum in an arbitrary direction. The net effect of such a cycle of an absorption and an emission process is an overall decrease in the speed of atom and, therefore, the cooling of the gas.

Alkali atoms are particularly accessible to laser-based methods due to their peculiar electronic structure and because their transitions are reachable by available lasers. Such methods provided the basis for the next step in achieving even lower temperatures by using a procedure called *evaporative cooling* [7]. This technique consists in successively lowering the trapping potential so that the most energetic atoms fly from the sample leaving behind a cooler gas. This finally made possible the temperatures of only a few nano-Kelvin which are necessary to produce a BEC.

Finally in 1995, the first BECs were experimentally produced using rubidium atoms by Wiemann and Cornell [8], and using sodium atoms by Ketterle [9]. In these experiments the ultracold gas is released from its magnetic trap so that the atomic cloud can freely expand for a few milliseconds before a picture of the expanded cloud is taken by shining resonant laser light on it and capturing its shadow using a CCD-camera. As the density distribution of the expanded cloud reproduces almost exactly the

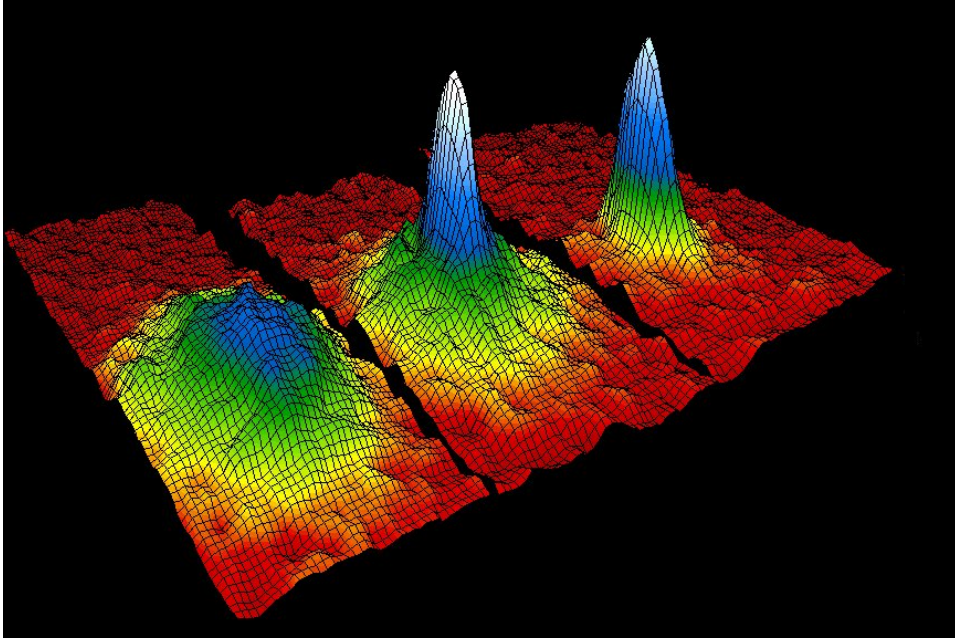


Figure 1.1.: Observed ultracold rubidium gas at 400, 200, 50 nano-Kelvin from right to left [8]. High momentum peaks at 200 and 50 nano-Kelvin indicates the presence of a BEC while at 50 Kelvin the system is still too hot to condensate.

momentum distribution before the expansion, the observed spike in the captured image corresponds to a macroscopic population of atoms in low-momentum states, i.e., of a BEC inside the magnetic trap (see Fig. 1.1).

The creation of these first condensates was soon followed by intense theoretical and experimental activities. Unlike superfluid  $^4\text{He}$ , which exhibits strong inter-particle interactions, the weak interactions between alkali atoms allows a theoretical picture where all atoms belong to a BEC and are described by a single macroscopic wave function which is a solution of the so called Gross-Pitaevskii equation (GPE) [10,11]. A more precise theory, which takes into account quantum and thermal fluctuations, was already developed by Bogouliubov [12]. In this theory, these fluctuations are responsible for the depletion of particles from the condensate. As typically the depletion in alkali BECs are only a few percent, GPE together with the Bogouliubov theory turns out to be capable of covering nearly all experimental measurements of BECs.

## 1.2. Bosons in optical lattices

Cubic optical lattices are produced by using electromagnetic standing waves generated by pairs of laser beams orthogonally aligned to each other, with their crossing point positioned at the center of a BEC. This way each atom feels an oscillating electric field which induces an electric dipole in the atom. Due to the ac Stark effect, the combination of the oscillatory electric field and the induced dipole causes a shift in the electronic energy levels according to  $\Delta\epsilon = -\frac{1}{2}\alpha(\omega)\langle E^2(t)\rangle$ , where  $\alpha(\omega)$  is the dynamical polarizability,  $\omega$  is the laser frequency, and  $\langle\cdot\rangle$  stands for the average over a time much larger than the period of the light wave. When the laser frequency is slightly smaller than a given atomic resonance

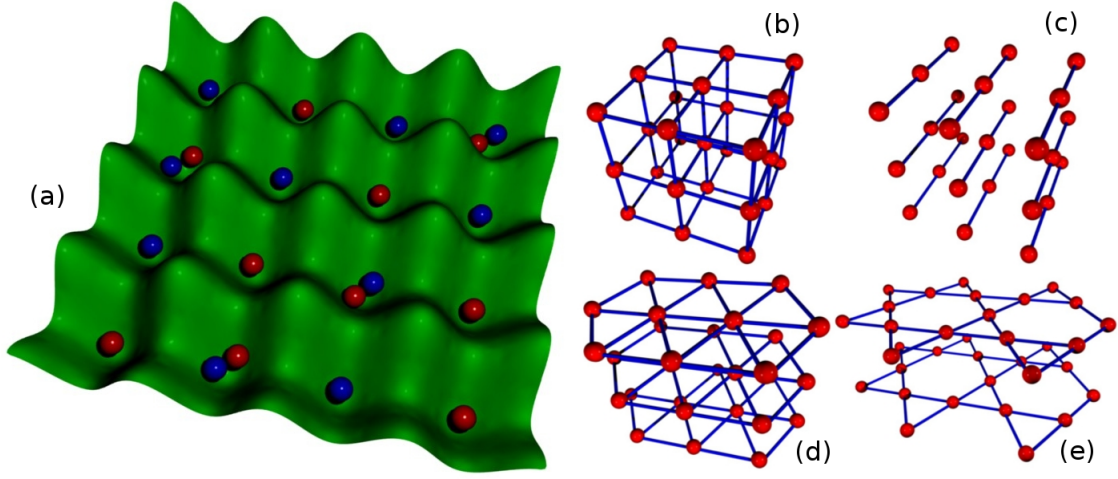


Figure 1.2.: Schematic drawing of optical lattices. (a) Trapping of atoms due to the periodic potential generated by orthogonal standing waves. (b) Three-dimensional lattice [20]. (c) Grid of one-dimensional lattices generated when the potential barriers are much weaker along the lattices than in its orthogonal directions [13]. (d) Array of two-dimensional triangular lattices generated by a strong periodic potential perpendicular to the lattice and three pairs of laser beams propagating in the lattice plane [21]. (e) Array of two-dimensional Kagomé lattices generated by a strong periodic potential perpendicular to the lattice and four pairs of laser beams propagating in the lattice plane [22].

frequency (*red detuned*),  $\alpha(\omega)$  will be positive and, therefore, the potential maxima occur at the points where  $\langle E^2(t) \rangle = 0$  while the potential minima occur at the maxima of  $\langle E^2(t) \rangle$ . The opposite scenario happens when the laser frequency is larger than a given atomic resonance frequency (*blue detuned*), i.e.,  $\alpha(\omega)$  is negative and the lattice potential is in phase with  $\langle E^2(t) \rangle$ . By using different frequencies for each pair of laser beams, it is possible to create optical lattices in one [13–16], two [17–19], or three dimensions [20,19]. In addition, by changing the angle between the laser, it is also possible to build different lattice topologies such as triangular [21] or Kagomé [22] as depicted in Fig. 1.2.

According to Bloch’s theorem, the periodic potential of the lattice modifies the energy spectrum of the atoms so that it exhibits a band structure, i.e., energy gaps appear between the energy bands which are limited within the first Brillouin zone. This periodicity makes it possible to study models originally developed in condensed matter physics with many advantages over the solid-state systems. Besides being practically perfect, optical lattices allow the creation of a vast number of potentials with almost complete control over its respective parameters. Actually the potential can even be made time dependent [1] or be completely switched off during the experiment to study time-of-flight experiments.

The role of the band structure in optical lattices was observed even before the creation of BEC [23,24] where gases with temperatures of the order of micro-Kelvin subjected to strong external forces induced non-adiabatic transition between Bloch bands. This phenomenon, known as Landau-Zener tunneling, leads to a splitting of the wavefunctions of the atoms each time a band gap is crossed. The inclusion of BEC in optical lattices offered even more possibilities for studying these effects. A striking demonstration of the Landau-Zener tunneling involving a BEC in optical lattices was made by Anderson and Kasevich [25], where the authors used the gravitational force of the earth on a vertically oriented lattice in order drive the condensate through the lattice. In Fig. 1.3 we see the successive

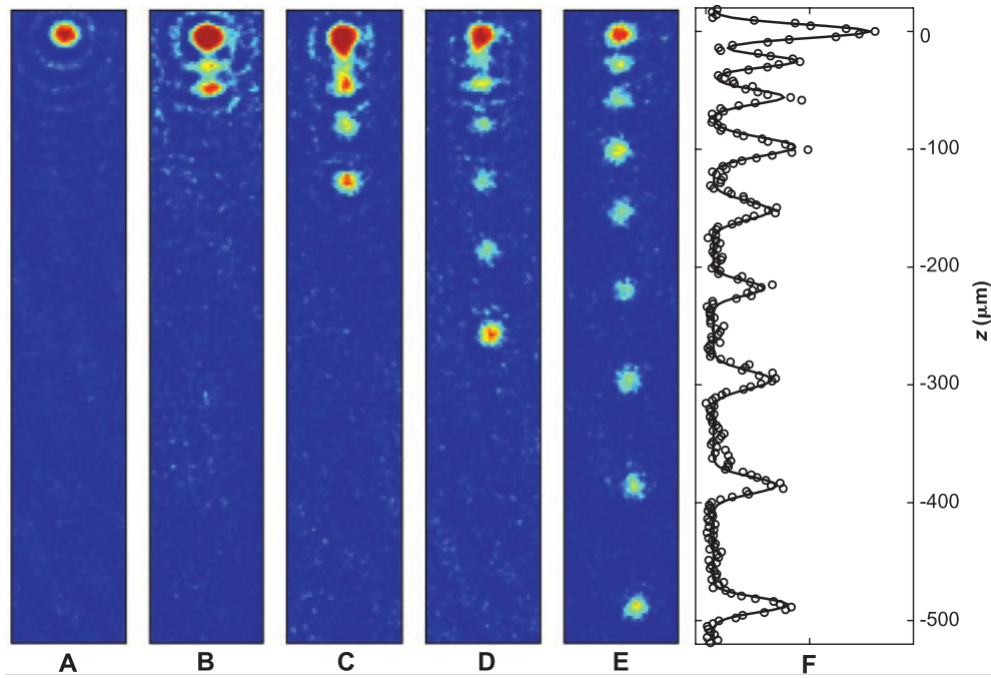


Figure 1.3.: Absorption image of a BEC falling through an optical lattice at different times. (a) 0 ms, (b) 3 ms, (c) 5 ms, (d) 7 ms, and (e) 10 ms. (f) Integrated absorption profile for (e). Figure from Ref. [25].

splinting of the macroscopic matter wave as it crosses the Brillouin zone edges.

BECs in optical lattices exhibit a much richer physics than that of cold atoms in magneto-optical traps. This is due to the fact that gases with temperatures of the order of micro-Kelvin have typically densities around  $10^{10} \text{ cm}^{-3}$ , whereas BECs have temperatures on the order of nano-Kelvin and densities around  $10^{14}$  or even higher [26]. The incredible low temperature of BECs assures that when the optical lattice is adiabatically switched on, the system will remain very close to its ground state. In addition, the high densities of BECs can lead to lattice filling factors higher than unity, in contrast to cold atoms which have filling factors around  $10^{-3}$ . This increases dramatically the relevance of inter-atomic interactions in BECs while they are practically negligible in just cold atoms.

When a BEC is loaded in a shallow lattice the system is in the weakly interacting regime and most of the atoms remain condensed. However, by increasing the lattice potential, the system becomes strongly interacting. This increase of the lattice potential leads to larger separations of the Bloch bands in such a way that interband band transitions are highly suppressed. In this case, it is a good approximation to assume that all atoms are confined in the lowest Bloch band so that, in this regime, the system can be very well described by the so called Bose-Hubbard Hamiltonian. Optical lattices were first proposed as a nearly perfect realization of the Bose-Hubbard Hamiltonian by Jaksch *et al.* [27].

Perhaps the most impressive demonstration of the role of interparticle interactions in the strongly correlated regime is the superfluid-Mott insulator transition which was predicted with the help of the Bose-Hubbard Hamiltonian by Fisher *et al.* [28] and experimentally realized by Greiner *et al.* [29]. From the Bose-Hubbard Hamiltonian follows that bosonic gases in optical lattices can exist in two

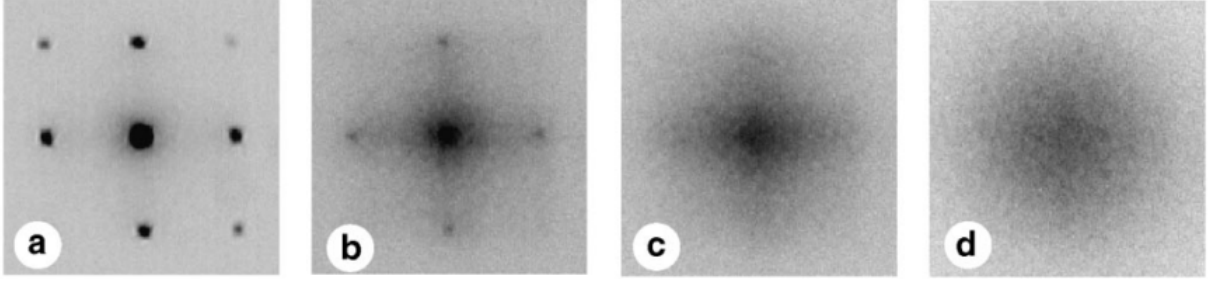


Figure 1.4.: Figure from Ref. [31] of absorption pictures of ultracold gases released from an optical lattice for various lattice depths: (a)  $8E_R$ , (b)  $14E_R$ , (c)  $18E_R$ , and (d)  $30E_R$ .  $E_R$  is the recoil energy defined in Chapter 2. The figures from left to right indicates the transition from a superfluid phase to a Mott phase which are characterized by the clear interference peaks in (a) and the broad pattern in (d), respectively.

different phases which can be chosen by tuning the depth of the potential wells generated by the optical waves. This model is characterized by two energies: the tunneling energy, which determines the probability of an atom to tunnel from a lattice site to one of its neighboring sites, and the on-site interaction energy which is the interaction energy between two atoms located in the same lattice site. When the on-site interaction is small compared to the hopping amplitude, the ground state is superfluid (SF), as the bosons are delocalized and the phase is coherent over the entire lattice. In the opposite limit, where the on-site interaction dominates the hopping energy, the ground state is a Mott insulator (MI) which is characterized by an integer number of bosons trapped in each potential minimum. These different phases are observable, for instance, in time-of-flight absorption pictures which are taken after switching off the lattice potential. While the superfluid phase yields to distinct Bragg-like interference peaks, the Mott phase is characterized by a broad diffusive interference pattern [30,31], as we can see in Fig. 1.4.

In addition to the SF-MI transition, the loss of coherence in bosonic lattices, as the system approaches the strongly correlated regime, can be demonstrated in other experiments. For instance, Bloch *et al.* [1] observed the interesting behavior of the macroscopic matter wave as the parameters of the system are rapidly switched from the SF to the MI regime. In particular, the authors observed the collapse and revival of the condensate after a sudden change of the potential depth from a small to a large value. Besides the main frequency dependency of the collapse and revival process, the authors observed a damping in the matter wave and suggested that it was caused by coherency loss due to the harmonic trapping potential.

There are several numerical and analytical methods available in order to describe in- and out-of-equilibrium bosons in optical lattices. Among the numerical methods we have density-matrix renormalization group (DMRG) [32], applied to one-dimensional systems, and quantum Monte Carlo methods (QMC) [33–35] which were applied in one, two, and three spatial dimensions. Former analytical methods are in general based on mean field theories [28,36], renormalization group analysis [28,37,36] or on a strong coupling expansion [37,32,38]. However, if we compare the results for the SF-MI phase boundary obtained by mean-field theory and strong-coupling expansion with the numerical results from high-precision Monte-Carlo simulations, as shown in Fig. 1.5 for the three-dimensional case, we observe that the mean-field theory underestimates the critical hopping parameter which characterizes

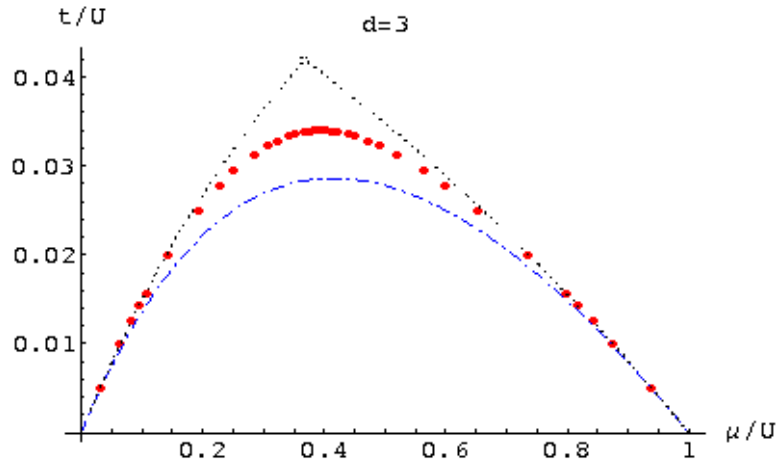


Figure 1.5.: Quantum phase diagram of the first MI-SF lobe at  $T = 0$  for three-dimensional cubic optical lattice. Dot-dashed blue line is the mean field result [28], dotted black line is from the third-order strong expansion [37], red dots are high-precision Monte-Carlo data [34]. The mean-field theory gives a relative error of 16% at the tip of the lobe while the third-order strong-coupling expansion not only gives a relative error of 24% but also predicts an unphysical cusp at the tip of the lobe.

the quantum phase transition, while the strong-coupling approach overestimates it. Thus, in view of a more quantitative comparison with the experimental results, it was indispensable to further develop analytical approximation methods [39,40]. In particular, to obtain accurate analytical results for the phase boundary at arbitrary dimensions as well as chemical potentials can yield new insights beyond the purely numerical data provided by Monte-Carlo simulations.

Motivated by the necessity of new precise analytical tools, this thesis was dedicated to the elaboration of such tools. The effort culminated with the development of an elegant and powerful strong-coupling effective potential method [39,40]. This method turned out to provide not only a better qualitative understanding of the lattice system, but also to improve the former analytical methods. Actually, a second-order hopping expansion already exhibits a relative error of less than 3% for the phase boundary in the three-dimensional case which can be taken as exact for most practical purposes. Higher-order calculations of the phase boundary were carried out in Refs. [41–44] and demonstrate an impressive convergence for the hopping expansion. As this method is based in the imaginary-time formalism, it had to be adapted to real time in order to make it able to deal with out-of-equilibrium problems at zero temperature. In Chapter 6, this real-time effective action formalism is used to describe not only the collapse and revival of matter waves observed in [1] but also the damping caused by the presence of the overall harmonic trap. A proposal for the generalization of this method for out-of-equilibrium system at finite temperature by combining it with the Keldish formalism is found in Refs. [45,46].

### 1.3. Overview

In the first three chapters of this thesis, including this introduction, I include an overview of some subjects necessary for a better the understanding of this thesis. The last three chapters contain the

original contributions of my PhD work.

In Chapter 2, the general theory of optical lattices is discussed. It is described how laser generated standing waves are used to produce periodic trapping potentials. These potentials are capable of reproducing many features of solid-state systems with the advantage of a defect-free lattice for which the tunnel coupling between different potential wells can be tuned by both the intensity and the frequency of the lasers. Due to the ac-Stark effect, the atoms are trapped in the maxima or minima of the laser field depending on whether the laser are red or blue detuned, respectively [20].

In Chapter 3, a general introduction to second-order phase transitions according to the modern classification of phase transitions is made. In particular, I address the symmetry breakdown mechanism which applies when the system passes from one more ordered to a less ordered phase of system. A discussion is also made about the role of the order parameter and concept of *universality* as well as its relation to the different critical exponents characterizing different systems. Special attention is given to quantum phase transitions which are transitions that can happen even in systems at zero temperature. Most of these discussions are made in the context of bosons in optical lattices so that the theory of second-order phase transitions is specifically applied to the Mott insulator-superfluid transition. Explicit calculation of the quantum phase diagram is performed by using mean-field theory and the properties of the two different phases are discussed.

In Chapter 4, a perturbation theory is developed by taking advantage of a diagrammatic notation specially developed to deal with bosons in optical lattices. The calculation of the effective action, which is defined through a Legendre transformation of the free energy, leads to an automatic resummation of the hopping expansion. This allows the description of the system properties in both the Mott insulator and superfluid phase. By using a set of diagrammatic rules, the effective action is calculated up to second hopping order.

In Chapter 5, the effective action is used to calculate various static and dynamical properties of cubic bosonic lattices at finite and zero temperature. By comparing the compressibility in the superfluid phase with the mean-field result, it is shown some advantages of the effective-action approach over the mean-field theory. The second-hopping order calculation of the quantum phase diagram exhibits an impressive accordance with the numerically calculated phase diagrams for two and three dimensions. This indicates that already at second-hopping order, our theory has enough precision for most practical applications. In addition, the equivalence between condensed density and superfluid density is demonstrated at first hopping order. The spectra of the various excitations appearing in the Mott phase and superfluid phase are calculated. In particular, the gaps and masses of the gapped modes are calculated as well as the sound velocity associated with the Goldstone mode.

In Chapter 6, is discussed the formation and dynamics of matter waves in a optical lattice loaded with  $^{87}\text{Rb}$  atoms which was experimentally observed by Greiner et. al [1]. I use the results from our effective action theory to reproduce the observed features in Ref. [1] and test our theory against the experimental results.

In order to facilitate the comprehension of calculations in Matsubara space, some extra computational details are included in the appendices A and B.





## 2. Optical Lattice Potentials

In this chapter the general theory of optical lattices is discussed. It is described how laser generated standing waves are used in order to produce periodic trapping potentials. These potential are capable of reproducing many features of solid-state systems with the advantages of a defect-free lattice whose tunnel coupling between different potential wells can be tuned by both the intensity and the frequency of the lasers. Due to the AC Stark effect, the atoms are trapped in maxima or minima of the laser field depending on whether the lasers are red or blue detuned, respectively [20].

### 2.1. Laser forces

First, consider the Hamiltonian of a freely moving atom

$$\hat{H}_{\text{Free}} = \frac{1}{2m} \hat{\mathbf{p}}^2 + \sum_n E_n |n\rangle \langle n|, \quad (2.1)$$

where  $m$  is the mass of the atom,  $\hat{\mathbf{p}}$  is the center-of-mass momentum operator, and  $|n\rangle$  are the internal electronic states with energy  $E_n$ .

Now, let us consider the laser-generated electric field

$$\mathcal{E}(t) = \mathcal{E}_0 \boldsymbol{\epsilon} \cos(\omega t), \quad (2.2)$$

where  $\boldsymbol{\epsilon}$  indicates the direction of polarization of the laser light.

In the dipole approximation [47,48], the effect of the oscillating electric field on the atom is taken into account by adding the interaction term

$$\hat{I}(t) = -\hat{\mathbf{d}} \cdot \mathcal{E}(t) \quad (2.3)$$

to the Hamiltonian  $\hat{H}_{\text{Free}}$ , with the dipole momentum operator defined as

$$\hat{\mathbf{d}} = -e \sum_i \hat{\mathbf{r}}_i, \quad (2.4)$$

where  $e$  is the electric charge of the electron and  $\hat{\mathbf{r}}_i$  is the position operator of the  $i$ -th atomic electron relative to the nucleus.

As we are interested in systems at very low temperatures, the atom is considered to be in its electronic ground state  $|0\rangle$ . In this case, the first non-vanishing contribution to the ground-state energy is of second order and is given by [11,47]

$$\Delta E = -\frac{1}{2} \alpha(\omega) \overline{|\mathcal{E}(t)|^2}, \quad (2.5)$$

## 2. Optical Lattice Potentials

where  $\overline{f(t)}$  stands for the time average of an arbitrary function  $f(t)$  over a period much larger than  $2\pi/\omega$  and the frequency-dependent polarizability  $\alpha(\omega)$  is given by

$$\begin{aligned}\alpha(\omega) &= \Re \left\{ i \lim_{\eta \rightarrow 0} \int_0^\infty dt e^{it(\omega+i\eta)} \langle 0 | \frac{1}{\hbar} [\boldsymbol{\epsilon} \cdot \hat{\mathbf{d}}(t), \boldsymbol{\epsilon} \cdot \hat{\mathbf{d}}] | 0 \rangle \right\} \\ &\approx \sum_{n \neq 0} \left| \langle n | \boldsymbol{\epsilon} \cdot \hat{\mathbf{d}} | 0 \rangle \right|^2 \left[ \frac{E_n - E_0 - \hbar\omega}{(E_n - E_m - \hbar\omega)^2 + (\hbar\Gamma_n/2)^2} + (\omega \rightarrow -\omega) \right],\end{aligned}\quad (2.6)$$

where in the last line, the finite lifetime of excited atomic states was approximately accounted for by writing  $\langle n | \boldsymbol{\epsilon} \cdot \hat{\mathbf{d}}(t) | 0 \rangle \approx \langle n | \boldsymbol{\epsilon} \cdot \hat{\mathbf{d}} | 0 \rangle e^{it(E_n - E_0)/\hbar - |t|\Gamma_n/2}$ . In practice, the long lifetime of electronic states implies  $\Gamma_n, \Gamma_m \ll |E_n - E_m|/\hbar$  for any two atomic states  $|n\rangle$  and  $|m\rangle$ . Therefore, the frequency-dependent polarizability in the vicinity of the  $n$ -th atomic excitation frequency, i.e, for frequencies  $\omega = (E_n - E_m)/\hbar + \delta_n$  with  $|\delta_n| = \mathcal{O}(\Gamma_n) \ll |E_n - E_m|/\hbar$ , will be dominated by only a single term in the above sum over excited states:

$$\alpha(\omega) \approx \left| \langle n | \boldsymbol{\epsilon} \cdot \hat{\mathbf{d}} | 0 \rangle \right|^2 \frac{1}{\hbar} \frac{(-\delta_n)}{\delta_n^2 + \Gamma_n^2/4}, \quad \delta_n = \omega - (E_n - E_0)/\hbar. \quad (2.7)$$

Inserting this into Eq. (2.5), one finds for the second-order shift of the atomic ground-state energy

$$\Delta E = \frac{\hbar\Omega_R^2}{2} \frac{\delta_n}{\delta_n^2 + \Gamma_n^2/4}, \quad (2.8)$$

with the Rabi frequency

$$\Omega_R = \frac{1}{\hbar} \sqrt{\left| \langle n | \hat{\mathbf{d}} \cdot \boldsymbol{\mathcal{E}}(t) | 0 \rangle \right|^2}. \quad (2.9)$$

Besides inducing an  $\mathbf{r}$ -dependent shift  $\Delta E$  to the atomic ground-state energy which resembles an external potential experienced by atoms, the laser light will also be absorbed and excite atoms which will make transitions  $|0\rangle \rightarrow |n\rangle$  at a rate  $w_{0 \rightarrow n} \propto (\Gamma_n/\delta_n)\Delta E$  which, in view of Eq. (2.8), will be maximal at resonance ( $\delta_n = 0$ ). In order to avoid strong absorption which would be associated with heating up the ultra-cold gas, the lasers must be detuned with  $\delta_n$  as large as possible.

Now we must take into account the fact that the laser generated standing wave possesses not only a time-dependent electric field but also has a space dependency. Therefore, instead of Eq. (2.2), we consider

$$\boldsymbol{\mathcal{E}}(\mathbf{r}, t) = \mathcal{E}_0(\mathbf{r}) \boldsymbol{\epsilon} \cos(\omega t) \quad (2.10)$$

As the spatial variation of the electric field  $\boldsymbol{\mathcal{E}}(\mathbf{r}, t)$  is negligible inside the atoms, we may assume that the laser-induced electric field produces an effective external potential  $V_{\text{full}}$  felt by each atom, this spatio-temporal dependent electric field produces the spatially dependent potential

$$V_{\text{full}}(\mathbf{r}) = -\frac{1}{2} \alpha(\omega) \overline{|\boldsymbol{\mathcal{E}}(\mathbf{r}, t)|^2}. \quad (2.11)$$

The intensity profile of a single Gaussian laser beams in cylindrical coordinates is given by [49]

$$I(\mathbf{r}) = |\overline{\mathcal{E}(\mathbf{0}, t)}|^2 \frac{w_0}{w(z)} e^{-\frac{2}{w(z)^2} r^2} \cos^2(k_L z), \quad (2.12)$$

where  $z$  is the direction of propagation of the laser beam,  $w(z) = w_0 \sqrt{1 + (z/z_R)^2}$  is the radius at which the intensity drops to  $1/e^2$  of its maximum,  $z_R = \pi w_0^2/\lambda$  is the Rayleigh length,  $\lambda$  is the wave length of the lattice, and  $w_0$  is the beam waist size. The laser beams must be aligned so that the location of their respective waists coincide. In this way, the approximation  $w(z) \approx w_0$  can be made leading to a potential of the form

$$V_{\text{full}}(\mathbf{r}) = -V_0 e^{-2\frac{x^2+y^2}{w_0^2}} \cos^2(k_L z) - V_0 e^{-2\frac{x^2+z^2}{w_0^2}} \cos^2(k_L y) - V_0 e^{-2\frac{y^2+z^2}{w_0^2}} \cos^2(k_L x). \quad (2.13)$$

This can be rearranged to the form

$$V_{\text{full}}(\mathbf{r}) = V_{\text{trap}}(\mathbf{r}) + V_{\text{OL}}(\mathbf{r}) \quad (2.14)$$

with trap and optical-lattice contributions

$$V_{\text{trap}}(\mathbf{r}) = -V_0 \left( e^{-2\frac{x^2+y^2}{w_0^2}} + e^{-2\frac{y^2+z^2}{w_0^2}} + e^{-2\frac{x^2+z^2}{w_0^2}} \right) \approx -3V_0 + \frac{4V_0}{w_0^2} |\mathbf{r}|^2, \quad (2.15)$$

$$V_{\text{OL}}(\mathbf{r}) = V_x(\mathbf{r}) \sin^2(k_L x) + V_y(\mathbf{r}) \sin^2(k_L y) + V_z(\mathbf{r}) \sin^2(k_L z), \quad (2.16)$$

and the abbreviations

$$V_x(\mathbf{r}) = V_0 e^{-2\frac{y^2+z^2}{w_0^2}} \approx V_0 - \frac{2V_0}{w_0^2} (y^2 + z^2), \quad (2.17)$$

$$V_y(\mathbf{r}) = V_0 e^{-2\frac{x^2+z^2}{w_0^2}} \approx V_0 - \frac{2V_0}{w_0^2} (x^2 + z^2), \quad (2.18)$$

$$V_z(\mathbf{r}) = V_0 e^{-2\frac{x^2+y^2}{w_0^2}} \approx V_0 - \frac{2V_0}{w_0^2} (x^2 + y^2). \quad (2.19)$$

Finally the full Hamiltonian which describes the motion of a single atom in a far detuned laser field can be written as

$$\hat{H}_{\text{full}} = \frac{1}{2m} \hat{\mathbf{p}}^2 + V_{\text{full}}(\hat{\mathbf{r}}). \quad (2.20)$$

In most applications, the atoms are concentrated in a region  $|\mathbf{r}| \ll w_0$  near the center of the trap. For this reason, deviations from periodicity in the full external potential  $V_{\text{full}}(\mathbf{r})$  may be ignored, i.e.,  $V_{\text{full}}(\mathbf{r}) \approx -3V_0 + V(\mathbf{r})$ . Therefore, the only part that will be considered in following is

$$V(\mathbf{r}) = V_0 [\sin^2(k_L x) + \sin^2(k_L y) + \sin^2(k_L z)], \quad (2.21)$$

thus leading to the single atom Hamiltonian

$$\hat{H}' = \frac{1}{2m} \hat{\mathbf{p}}^2 + V(\hat{\mathbf{r}}). \quad (2.22)$$

## 2.2. Band structure

The Bloch theorem states that the eigenfunctions of the Schrödinger equation

$$\left[ -\frac{\hbar^2}{2m} \nabla^2 + V(\mathbf{r}) \right] \Psi_{\mathbf{k}}^{(\mathbf{n})}(\mathbf{r}) = E_{\mathbf{k}}^{(\mathbf{n})} \Psi_{\mathbf{k}}^{(\mathbf{n})}(\mathbf{r}) \quad (2.23)$$

with a periodic potential  $V(\mathbf{r})$  has eigenfunctions of the form [50]

$$\Psi_{\mathbf{k}}^{(\mathbf{n})}(\mathbf{r}) = e^{i\mathbf{k} \cdot \mathbf{r}} \Phi_{\mathbf{k}}^{(\mathbf{n})}(\mathbf{r}), \quad (2.24)$$

where the Bloch functions  $\Phi_{\mathbf{k}}^{(\mathbf{n})}(\mathbf{r})$  have the same periodicity of  $V(\mathbf{r})$ ,  $\mathbf{n} = (n_x, n_y, n_z)$  is the collective band index, and  $\mathbf{k}$  is restricted to first Brillouin zone, i.e., its components are in the interval  $-\pi/a \leq k_i < \pi/a$ , with the lattice spacing  $a = \pi/k_L = \lambda/2$ .

In many interesting cases the depth of the potential  $V(\mathbf{r})$  is large enough to trap the atoms in its wells so that they move from one well to its neighbor by tunnel effect which is known as the tight-binding limit. As the Bloch functions are spatially delocalized, it is convenient to define a new set of wave functions which are localized around each potential well. These are the so called Wannier functions and are defined as [51]

$$\mathcal{U}^{(\mathbf{n})}(\mathbf{r} - \mathbf{r}_i) = \frac{1}{\sqrt{N_s}} \sum_{\mathbf{k}} e^{-i\mathbf{k} \cdot \mathbf{r}_i} \Psi_{\mathbf{k}}^{(\mathbf{n})}(\mathbf{r}), \quad (2.25)$$

where  $N_s$  is the total number of lattice sites,  $\mathbf{r}_i$  is the location of the  $i$ -th lattice site, and the sum in  $\mathbf{k}$  runs over the first Brillouin zone. From this definition it is possible to derive the orthonormality property

$$\begin{aligned} \int_{-\infty}^{\infty} d^3r \mathcal{U}^{(\mathbf{n})}(\mathbf{r} - \mathbf{r}_i)^* \mathcal{U}^{(\mathbf{n}')}(\mathbf{r} - \mathbf{r}_j) &= \frac{1}{N_s} \sum_{\mathbf{k}', \mathbf{k}} e^{i\mathbf{k}' \cdot \mathbf{r}_i - i\mathbf{k} \cdot \mathbf{r}_j} \int_{-\infty}^{\infty} d^3r \Psi_{\mathbf{k}'}^{(\mathbf{n}')}(\mathbf{r})^* \Psi_{\mathbf{k}}^{(\mathbf{n})}(\mathbf{r}) \\ &= \frac{\delta_{\mathbf{n}', \mathbf{n}}}{N_s} \sum_{\mathbf{k}} e^{i\mathbf{k} \cdot (\mathbf{r}_i - \mathbf{r}_j)} \\ &= \delta_{\mathbf{n}', \mathbf{n}} \delta_{i,j}, \end{aligned} \quad (2.26)$$

as well as the completeness property

$$\begin{aligned} \sum_{i, \mathbf{n}} \mathcal{U}^{(\mathbf{n})}(\mathbf{r}' - \mathbf{r}_i)^* \mathcal{U}^{(\mathbf{n})}(\mathbf{r} - \mathbf{r}_i) &= \frac{1}{N_s} \sum_{\mathbf{n}} \sum_{\mathbf{k}', \mathbf{k}} \Psi_{\mathbf{k}'}^{(\mathbf{n})}(\mathbf{r}')^* \Psi_{\mathbf{k}}^{(\mathbf{n})}(\mathbf{r}) \sum_i e^{i(\mathbf{k}' - \mathbf{k}) \cdot \mathbf{r}_i} \\ &= \sum_{\mathbf{n}} \sum_{\mathbf{k}} \Psi_{\mathbf{k}}^{(\mathbf{n})}(\mathbf{r}')^* \Psi_{\mathbf{k}}^{(\mathbf{n})}(\mathbf{r}) \\ &= \delta(\mathbf{r} - \mathbf{r}'). \end{aligned} \quad (2.27)$$

These conditions assure that any three-dimensional wavefunction can be expanded in terms of Wannier functions.

As the equation (2.23) with the periodic potential given by (2.21) can be solved by separation of variables, we can write its eigenfunctions and eigenvalues, respectively as

$$\Psi_{\mathbf{k}}^{(n)}(\mathbf{r}) = \psi_{k_x}^{(n_x)}(x)\psi_{k_y}^{(n_y)}(y)\psi_{k_z}^{(n_z)}(z), \quad (2.28)$$

$$E_{\mathbf{k}}^{(n)} = \varepsilon_{k_x}^{(n_x)} + \varepsilon_{k_y}^{(n_y)} + \varepsilon_{k_z}^{(n_z)}. \quad (2.29)$$

And analogously with the Bloch and Wannier functions

$$\Phi_{\mathbf{k}}^{(n)}(\mathbf{r}) = \phi_{k_x}^{(n_x)}(x)\phi_{k_y}^{(n_y)}(y)\phi_{k_z}^{(n_z)}(z), \quad (2.30)$$

$$\mathcal{U}^{(n)}(\mathbf{r} - \mathbf{r}_i) = u^{(n_x)}(x - x_i)u^{(n_y)}(y - y_i)u^{(n_z)}(z - z_i), \quad (2.31)$$

where  $\psi_k^{(n)}(x)$  are solutions of the one-dimensional Schrödinger equation

$$\left[ -\frac{\hbar^2}{2m} \frac{\partial^2}{\partial x^2} + V_0 \sin^2(k_L x) \right] \psi_k^{(n)}(x) = \varepsilon_k^{(n)} \psi_k^{(n)}(x), \quad (2.32)$$

with the one-dimensional Bloch and Wannier function defined as

$$\psi_k^{(n)}(x) = e^{ikx} \phi_k^{(n)}(x), \quad (2.33)$$

$$u^{(n)}(x - x_i) = \frac{1}{N_s^{1/6}} \sum_k e^{-ikx_i} \psi_k^{(n)}(x). \quad (2.34)$$

The one-dimensional Wannier functions also obey the orthonormality and completeness conditions

$$\int_{-\infty}^{\infty} dx u^{(n')}(x - x_i)^* u^{(n)}(x - x_j) = \delta_{i,j} \delta_{n,n'}, \quad (2.35)$$

$$\sum_{n,i} u^{(n)}(x' - x_i)^* u^{(n)}(x - x_i) = \delta(x - x'). \quad (2.36)$$

The Schrödinger equation (2.32) can be simplified by expressing it in terms the dimensionless quantities

$$x' = \frac{\pi}{a} x; \quad k' = \frac{a}{\pi} k; \quad V_0' = \frac{V_0}{E_R}; \quad \tilde{\varepsilon}^{(n)} = \frac{\varepsilon^{(n)}}{E_R}, \quad (2.37)$$

where the recoil energy is defined as

$$E_R = \frac{\hbar^2 k_L^2}{2m}. \quad (2.38)$$

Thus, the dimensionless Schrödinger equation (2.32) reads

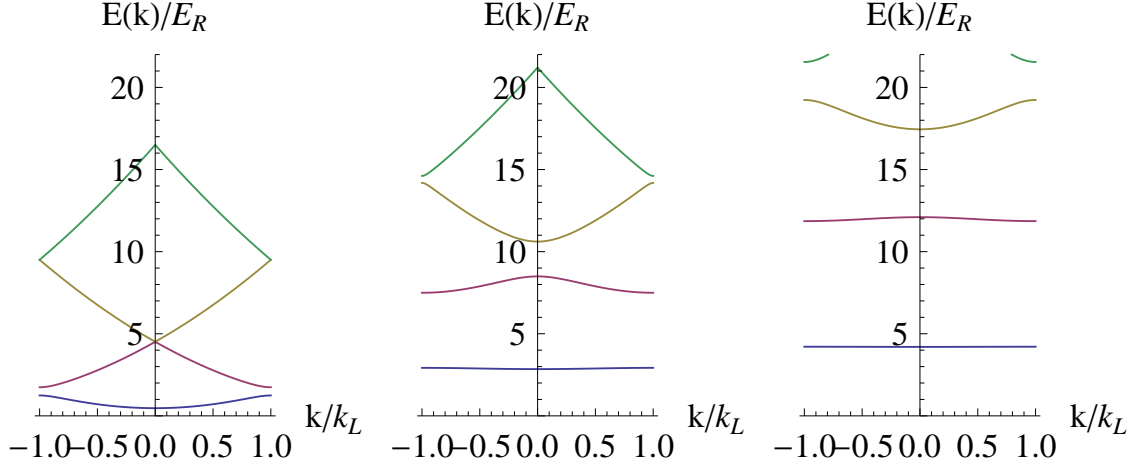


Figure 2.1.: First four Bloch bands for different values of  $V'_0$ . Left:  $V'_0 = 1$ . Middle:  $V'_0 = 10$ . Right:  $V'_0 = 20$ . Here we see that for high enough lattice potentials, each band energy can be considered as momentum independent.

$$\left[ -\frac{\partial^2}{\partial x'^2} + V'_0 \sin^2(x') \right] \psi_{k'}^{(n)}(x') = \tilde{\varepsilon}_{k'}^{(n)} \psi_{k'}^{(n)}(x'). \quad (2.39)$$

For the Bloch's function in dimensionless units we have

$$\left[ k'^2 - 2ik' \frac{\partial}{\partial x'} - \frac{\partial^2}{\partial x'^2} + V'_0 \sin^2(x') \right] \phi_{k'}^{(n)}(x') = \tilde{\varepsilon}_{k'}^{(n)} \phi_{k'}^{(n)}(x'). \quad (2.40)$$

Due to its periodicity, the Bloch function can be expanded in a Fourier series according to

$$\phi_{k'}^{(n)}(x') = \sum_{l=-\infty}^{\infty} c_{k',l}^{(n)} e^{2ilx'}. \quad (2.41)$$

Then Eq. (2.40) can be written in terms of the Fourier components

$$\left[ (k' + 2l)^2 + \frac{V'_0}{2} \right] c_{k',l}^{(n)} + \frac{V'_0}{4} (c_{k',l+1}^{(n)} + c_{k',l-1}^{(n)}) = \tilde{\varepsilon}_{k'}^{(n)} c_{k',l}^{(n)}. \quad (2.42)$$

This discrete form of the eigenvalue equation (2.42) makes it ideal for numerical diagonalization. The numerically calculated eigenvalues for different bands are depicted in 2.1. That figure illustrates the known property from condensed matter systems, that the spectrum becomes more and more flat as  $V'_0$  is increased. In addition it shows that energy gap between the Bloch bands increases with  $V'_0$ . This means for ultracold bosons in optical lattices, that the atoms can be considered as occupying only the lowest Bloch band which considerably simplifies the problem.

## 2.3. Bose-Hubbard Hamiltonian

An adequate description of many-body interacting systems consists in the inclusion of inter-particle potentials in the many-body Schrödinger equation. Another well known technique do deal with such systems is *second quantization* which greatly simplify the discussion of many-body interacting particles [52]. One advantage of this approach is that it automatically incorporates the particle statistics with no need for extra symmetrization or antisymmetrization for bosons and fermions, respectively. For the case of nonrelativistic interacting identical bosonic particles moving in the external potential  $V(\mathbf{r})$ , the second quantized Hamiltonian is

$$\begin{aligned}\hat{H} = & \int d^3r \hat{\Psi}^\dagger(\mathbf{r}) \left[ -\frac{\hbar^2}{2m} \nabla^2 + V(\mathbf{r}) - \mu' \right] \hat{\Psi}(\mathbf{r}) \\ & + \frac{1}{2} \int \int d^3\mathbf{r}_1 d^3\mathbf{r}_2 \hat{\Psi}^\dagger(\mathbf{r}_1) \hat{\Psi}^\dagger(\mathbf{r}_2) V_{\text{int}}(\mathbf{r}_1, \mathbf{r}_2) \hat{\Psi}(\mathbf{r}_1) \hat{\Psi}(\mathbf{r}_2),\end{aligned}\quad (2.43)$$

where  $\hat{\Psi}(\mathbf{r})$  and  $\hat{\Psi}^\dagger(\mathbf{r})$  are, respectively, the bosonic creation and annihilation field operators,  $V_{\text{int}}(\mathbf{r}_1, \mathbf{r}_2)$  is the interparticle potential,  $\mu'$  denotes the grand-canonical chemical potential. The field operators must obey the bosonic commutation rules

$$\left[ \hat{\Psi}(\mathbf{r}), \hat{\Psi}^\dagger(\mathbf{r}') \right] = \delta(\mathbf{r} - \mathbf{r}'), \quad \left[ \hat{\Psi}(\mathbf{r}), \hat{\Psi}(\mathbf{r}') \right] = 0, \quad \left[ \hat{\Psi}^\dagger(\mathbf{r}), \hat{\Psi}^\dagger(\mathbf{r}') \right] = 0. \quad (2.44)$$

For gases at low temperatures and densities, only two-body collisions have to be considered. In this limit, the interparticle potential can be taken as [11,47]

$$V_{\text{int}}(\mathbf{r}_1, \mathbf{r}_2) = \frac{4\pi a_{\text{BB}} \hbar^2}{m} \delta(\mathbf{r}_1 - \mathbf{r}_2), \quad (2.45)$$

where  $a_{\text{BB}}$  is the s-wave scattering length. The many-body Hamiltonian can then be simplified according to

$$\hat{H} = \int d^3r \left\{ \hat{\Psi}^\dagger(\mathbf{r}) \left[ -\frac{\hbar^2}{2m} \nabla^2 + V(\mathbf{r}) - \mu' \right] \hat{\Psi}(\mathbf{r}) + \frac{g}{2} \hat{\Psi}^\dagger(\mathbf{r}) \hat{\Psi}^\dagger(\mathbf{r}) \hat{\Psi}(\mathbf{r}) \hat{\Psi}(\mathbf{r}) \right\}, \quad (2.46)$$

where the coupling constant  $g = 4\pi a_{\text{BB}} \hbar^2 / m$  is introduced.

The field operators can be also expanded with respect to a complete set of functions in the single-particle Hilbert space. In particular, the Wannier functions corresponding to the periodic potential  $V(\mathbf{r})$  can be used as a basis for  $\hat{\Psi}(\mathbf{r})$  and  $\hat{\Psi}^\dagger(\mathbf{r})$ . However, as ultracold atoms in deep periodic potentials can be considered as occupying only the lowest Bloch band, only the Wannier functions  $\mathcal{U}^{(0)}(\mathbf{r})$  corresponding to the first Brillouin zone have to be considered. As these are the only relevant Wannier functions for the systems considered here, from now on, these functions will be written simply as  $\mathcal{U}(\mathbf{r})$ . In this way, the field operators can be expanded as

## 2. Optical Lattice Potentials

$$\hat{\Psi}(\mathbf{r}) = \sum_i \hat{a}_i \mathcal{U}(\mathbf{r} - \mathbf{r}_i), \quad (2.47)$$

$$\hat{\Psi}^\dagger(\mathbf{r}) = \sum_i \hat{a}_i^\dagger \mathcal{U}^*(\mathbf{r} - \mathbf{r}_i), \quad (2.48)$$

where the operators  $\hat{a}_i^\dagger$  and  $\hat{a}_i$  are the creation and annihilation operators of particles at a given lattice site, respectively. Using the orthonormality conditions, the following inverse relations can be derived

$$\hat{a}_i = \int_{-\infty}^{\infty} d^3r \mathcal{U}^*(\mathbf{r} - \mathbf{r}_i) \hat{\Psi}(\mathbf{r}), \quad (2.49)$$

$$\hat{a}_i^\dagger = \int_{-\infty}^{\infty} d^3r \mathcal{U}(\mathbf{r} - \mathbf{r}_i) \hat{\Psi}^\dagger(\mathbf{r}). \quad (2.50)$$

Substituting the definitions (2.49) and (2.50) in Eqs. (2.44) and using the orthonormality relations, we obtain the commutation relations for the lattice operator

$$[\hat{a}_i, \hat{a}_j^\dagger] = \delta_{ij}, \quad [\hat{a}_i, \hat{a}_j] = 0, \quad [\hat{a}_i^\dagger, \hat{a}_j^\dagger] = 0 \quad (2.51)$$

Now, substituting the definitions (2.47) and (2.48) into (2.46) and using again the orthonormality relations, we obtain the Bose-Hubbard Hamiltonian

$$\hat{H}_{\text{BH}} = -J \sum_{\langle ij \rangle} \hat{a}_i^\dagger \hat{a}_j + \frac{U}{2} \sum_i \hat{a}_i^\dagger \hat{a}_i^\dagger \hat{a}_i \hat{a}_i - \mu \sum_i \hat{a}_i^\dagger \hat{a}_i. \quad (2.52)$$

where the sum in  $\langle ij \rangle$  means that it must be carried over all nearest neighbors  $i$  and  $j$ . All other contributions due to the overlapping between non-nearest neighbor Wannier functions are neglectable and therefore discarded from the Bose-Hubbard Hamiltonian. Also from the same calculation, the following Hamiltonian parameters can be obtained

$$J = \int d^3r \mathcal{U}^*(\mathbf{r} - \mathbf{r}_i) \left[ -\frac{\hbar^2}{2m} \nabla^2 + V(\mathbf{r}) \right] \mathcal{U}(\mathbf{r} - \mathbf{r}_j), \quad (2.53)$$

$$U = g \int d^3r |\mathcal{U}(\mathbf{r})|^4, \quad (2.54)$$

$$\mu = \mu' - \int d^3r \mathcal{U}^*(\mathbf{r}) \left[ -\frac{\hbar^2}{2m} \nabla^2 + V(\mathbf{r}) \right] \mathcal{U}(\mathbf{r}). \quad (2.55)$$

Note that, due to discrete translational invariance, the hopping parameter  $J$  does not depend on which nearest neighboring points  $\mathbf{r}_i$  and  $\mathbf{r}_j$  are considered. These parameters have a clear physical meaning: the hopping parameter  $J$  is related to the probability of a given atom to jump from one lattice site to its neighbors by tunnel effect, the on-site interaction energy controls the strength of interparticle interactions of particle in the same lattice site, and the chemical potential  $\mu$  controls the number of particles in the systems in the grand-canonical ensemble.



### 2.3.1. Hamiltonian Parameters

As can be seen in Eqs. (2.53)-(2.55), a direct way for calculating the Bose-Hubbard parameters is through direct integration of the Wannier functions. For the hopping parameter and chemical potential, the definition (2.34) together with the equations (2.23)-(2.32) can be used for derivating alternative formulas. By applying (2.32) and (2.34) to (2.53), we get

$$\begin{aligned}
J &= \int d^3r \mathcal{U}^*(\mathbf{r} - \mathbf{r}_i) \left[ -\frac{\hbar^2}{2m} \nabla^2 + V(\mathbf{r}) \right] \mathcal{U}(\mathbf{r} - \mathbf{r}_j) \\
&= \int_{-\infty}^{\infty} dx u^*(x - a) \left[ -\frac{\hbar^2}{2m} \frac{\partial^2}{\partial x^2} + V_0 \sin^2(k_L x) \right] u(x) \\
&= \frac{1}{N_s^{1/3}} \sum_{k'k} e^{ika} \int_{-\infty}^{\infty} dx \phi_{k'}(x)^* \epsilon_k \phi_k(x).
\end{aligned}$$

Observe the  $J$  depends on the dimension of the lattice only through the pre-factor  $1/N_s^{1/3}$ .

Due to the orthonormality of  $\phi_k(x)$  this reduces to

$$J = \frac{1}{N_s^{1/3}} \sum_k e^{ika} \epsilon_k. \quad (2.56)$$

Analogously for the chemical potential we have

$$\mu = \mu' - \int d^3r \mathcal{U}^*(\mathbf{r}) \left[ -\frac{\hbar^2}{2m} \nabla^2 + V(\mathbf{r}) \right] \mathcal{U}(\mathbf{r}) \quad (2.57)$$

$$= \mu' - 3 \int_{-\infty}^{\infty} dx u^*(x) \left[ -\frac{\hbar^2}{2m} \frac{\partial^2}{\partial x^2} + V_0 \sin^2(k_L x) \right] u(x) \quad (2.58)$$

$$= \mu' - 3 \frac{1}{N_s^{1/3}} \sum_{k'k} \int_{-\infty}^{\infty} dx \phi_{k'}(x)^* \epsilon_k \phi_k(x). \quad (2.59)$$

This leads to the final formula

$$\mu = \mu' - \frac{3}{N_s^{1/3}} \sum_k \epsilon_k. \quad (2.60)$$

In particular, the hopping parameter  $J$  can be obtained in the limit  $V_0 \gg E_R$  from the exact result for the width of the lowest band in the 1d Mathieu-equation [53]

$$J = \frac{4}{\sqrt{\pi}} E_R \left( \frac{V_0}{E_R} \right)^{3/4} e^{-2\sqrt{V_0/E_R}}. \quad (2.61)$$

In addition to these results, we present here two methods used to calculate the Wannier function and the Bose-Hubbard parameters.

### Harmonic Approximation

The calculation of the Bose-Hubbard parameters using the harmonic approximation was carried out in Ref. [54]. In this approach, the periodic potential is approximated by a harmonic potential at the bottom of each well. The Wannier functions corresponding to a given lattice site are then considered as eigenfunctions of the Schrödinger equation with harmonic potential centered at this site. In this approximation, the equation for the one-dimensional Wannier function is

$$\left[ -\frac{\hbar^2}{2m} \frac{\partial^2}{\partial x^2} + V_0 k_L^2 x^2 \right] u(x) = \varepsilon u(x). \quad (2.62)$$

The ground-state of this equation gives the Wannier function corresponding to the first Bloch band

$$u(x) = \sqrt[4]{\frac{k_L \sqrt{2V_0 m}}{\hbar \pi}} \exp \left[ -\frac{k_L \sqrt{2V_0 m}}{2\hbar} x^2 \right] = \sqrt[4]{\frac{\pi \sqrt{V'_0}}{a^2}} \exp \left[ -\frac{\pi^2 \sqrt{V'_0}}{2} \left( \frac{x}{a} \right)^2 \right]. \quad (2.63)$$

From this harmonic approximation, all system parameters can be obtained. First, the on-site interaction parameter for the three-dimensional system is given by

$$U = g \int d^3r |\mathcal{U}(\mathbf{r})|^4 = g \left[ \int_{-\infty}^{\infty} dx |u(x)|^4 \right]^3. \quad (2.64)$$

By solving the resulting Gaussian integral and using the definition of the coupling constant  $g$ , we have

$$U = \sqrt{8\pi} \frac{E_R a_{\text{BB}}}{a} (V'_0)^{3/4}. \quad (2.65)$$

The hopping parameter is given by

$$J = \int d^3r \mathcal{U}^*(\mathbf{r} - \mathbf{r}_i) \left[ -\frac{\hbar^2}{2m} \nabla^2 + V(\mathbf{r}) \right] \mathcal{U}(\mathbf{r} - \mathbf{r}_j) = \int_{-\infty}^{\infty} dx u^*(x - a) \left[ -\frac{\hbar^2}{2m} \frac{\partial^2}{\partial x^2} + V_0 \sin^2(k_L x) \right] u(x). \quad (2.66)$$

A direct calculation of this integral leads to

$$J = -e^{-\frac{\pi^2}{4} \sqrt{\frac{V_0}{E_R}}} \left[ \frac{\hbar^2 \pi^2}{2ma^2} \left( \frac{1}{2} \sqrt{\frac{V_0}{E_R}} - \frac{\pi^2 V_0}{4E_R} \right) + \frac{V_0}{2} \left( e^{-\sqrt{\frac{E_R}{V_0}}} + 1 \right) \right]. \quad (2.67)$$

For deep lattices, i.e, for large  $V_0/E_R$ , the exponential function  $e^{-\sqrt{\frac{E_R}{V_0}}}$  can be approximated up to first order in  $\frac{E_R}{V_0}$ , thus leading to

$$J \approx V_0 \left( \frac{\pi^2}{4} - 1 \right) e^{-\frac{\pi^2}{4} \sqrt{\frac{V_0}{E_R}}} = E_R V'_0 \left( \frac{\pi^2}{4} - 1 \right) e^{-\frac{\pi^2}{4} \sqrt{V'_0}}. \quad (2.68)$$

The chemical potential is given by

$$\mu = \mu' - \int d^3r \mathcal{U}^*(\mathbf{r}) \left[ -\frac{\hbar^2}{2m} \nabla^2 + V(\mathbf{r}) \right] \mathcal{U}(\mathbf{r}) = \mu' - 3 \int_{-\infty}^{\infty} dx u^*(x) \left[ -\frac{\hbar^2}{2m} \frac{\partial^2}{\partial x^2} + V_0 \sin^2(k_L x) \right] u(x). \quad (2.69)$$

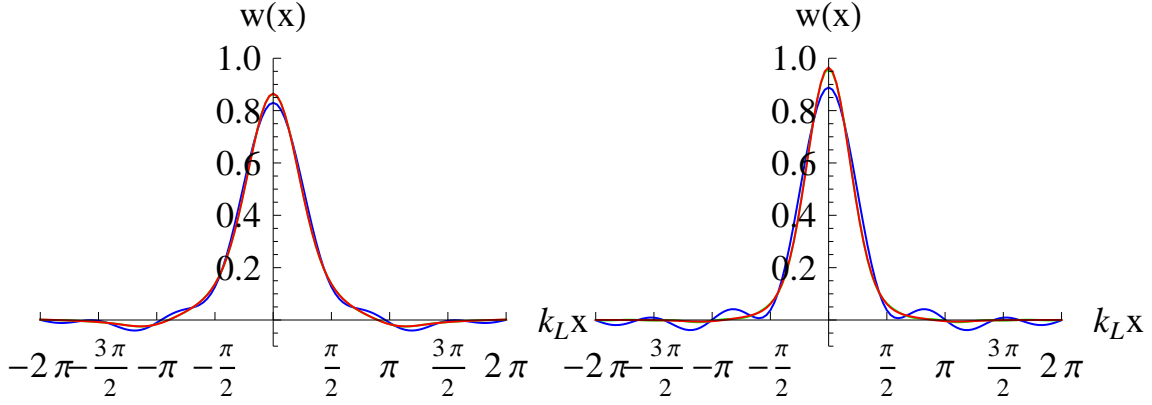


Figure 2.2.: Numerically calculated Wannier functions. Left:  $V_0 = 5E_R$ . Right:  $V_0 = 10E_R$ . Blue:  $l_{\max} = 1$ . Green:  $l_{\max} = 2$ . Red:  $l_{\max} = 4$ .

For large  $V_0/E_R$ , the solution of the above integral gives

$$\mu = \mu' - 3\sqrt{E_R V_0}. \quad (2.70)$$

### Numerical Calculations

The eigenvalue equation (2.42) can be written in matrix form

$$\begin{pmatrix} \ddots & -\frac{V'_0}{4} & & & & \\ -\frac{V'_0}{4} & g(-2) & -\frac{V'_0}{4} & & & \\ & -\frac{V'_0}{4} & g(-1) & -\frac{V'_0}{4} & & \\ & & -\frac{V'_0}{4} & g(0) & -\frac{V'_0}{4} & \\ & & & -\frac{V'_0}{4} & g(1) & -\frac{V'_0}{4} \\ 0 & & & -\frac{V'_0}{4} & g(2) & -\frac{V'_0}{4} \\ & & & & \ddots & \end{pmatrix} \begin{pmatrix} \vdots \\ c_{k',-2} \\ c_{k',-1} \\ c_{k',0} \\ c_{k',1} \\ c_{k',2} \\ \vdots \end{pmatrix} = \varepsilon_{k'} \begin{pmatrix} \vdots \\ c_{k',-2} \\ c_{k',-1} \\ c_{k',0} \\ c_{k',1} \\ c_{k',2} \\ \vdots \end{pmatrix}, \quad (2.71)$$

with  $g(l) = (k' + 2l)^2 + \frac{V'_0}{2}$ . In order to numerically diagonalize the infinity-dimensional system, it must be truncated so that  $l$  runs from  $-l_{\max}$  to  $l_{\max}$ . From Fig. 2.2, we can see that for  $l_{\max} = 4$ , we already have very good results for large potential depths  $V'_0 \geq 5$ . For all numerically calculated parameters presented here the value  $l_{\max} = 10$  is considered, in order to assure enough precision.

In Fig. 2.3, the Wannier functions calculated both numerically and using the harmonic approximation are shown. In Fig. 2.4, we can see the hopping parameter calculated from the approaches presented here. The figures 2.5 and 2.6, are, respectively, the corrections for the chemical potential and on-site energy calculated in the harmonic approximation and numerically. From these figures, we see that although the harmonic approximation gives a small relative error for both the on-site energy and the chemical potential, this is not true for the hopping parameter where the formula from Mathieu equation gives much better results. This means that in all analytical approximations the formula (2.61)

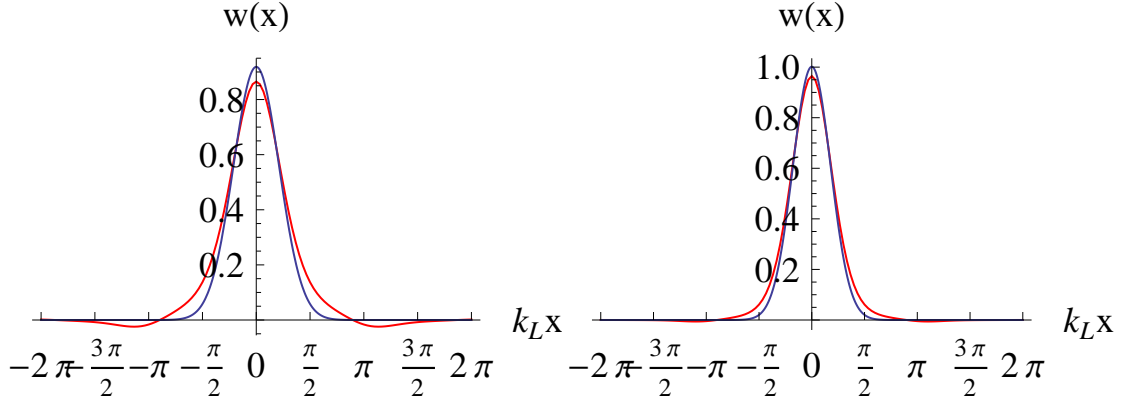


Figure 2.3.: Numerically calculated Wannier functions. Left:  $V_0 = 5E_R$ . Right:  $V_0 = 10E_R$ . Blue: Harmonic approximation. Red: Numerical calculation.

must be used instead of (2.68).

### 2.3.2. Corrections due to Laser Inhomogeneity

Due to an inhomogeneous intensity profile of Gaussian laser beams, the lattice potential has same deviations from its main periodic profile. Such deviations must then lead to corrections in the parameters of the Bose-Hubbard model. One obvious correction that can be seen in Eq. (2.15) comes from the additional site-dependent potential  $V_{\text{trap}}(\mathbf{r})$  which can be interpreted as a site-dependent shift in the chemical potential. In addition to this, we have the site-dependent coefficients  $V_{0x}(\mathbf{r})$ ,  $V_{0y}(\mathbf{r})$ , and  $V_{0z}(\mathbf{r})$  which can be seen as site-dependent potential depths. As the Wannier functions are strongly dependent on the potential  $V_0$ , such variations must also be reflected in the Bose-Hubbard parameters. In general the Wannier functions can be expressed by

$$\mathcal{U}_{\text{corr}}(\mathbf{r}) = u(x; V_{0x})u(y; V_{0y})u(z; V_{0z}), \quad (2.72)$$

where, for clearness, the  $V_0$ -dependency of the one-dimensional Wannier function is made explicit.

The inhomogeneous Bose-Hubbard model turns into

$$\hat{H}_{\text{BH}} = - \sum_{\langle ij \rangle} J(\mathbf{r}_i; \mathbf{r}_j) \hat{a}_i^\dagger \hat{a}_j + \frac{1}{2} \sum_i U(\mathbf{r}_i) \hat{a}_i^\dagger \hat{a}_i^\dagger \hat{a}_i \hat{a}_i - \sum_i \mu(\mathbf{r}_i) \hat{a}_i^\dagger \hat{a}_i, \quad (2.73)$$

Let us start with the chemical potential. In addition to the correction from  $V_{\text{trap}}(\mathbf{r})$ , we must consider the effect of  $\mathcal{U}_{\text{corr}}(\mathbf{r})$  which leads to

$$\begin{aligned} \mu(\mathbf{r}) &= \mu' + V_{\text{ext}}(\mathbf{r}) - \int d^3r \mathcal{U}^*(\mathbf{r}) \left[ -\frac{\hbar^2}{2m} \nabla^2 + V(\mathbf{r}) \right] \mathcal{U}(\mathbf{r}) \\ &= \mu' + V_{\text{ext}}(\mathbf{r}) - \sqrt{E_R} \left( \sqrt{V_{0x}(\mathbf{r})} + \sqrt{V_{0y}(\mathbf{r})} + \sqrt{V_{0z}(\mathbf{r})} \right) \\ &\approx \mu' - 3\sqrt{E_R V_0} + \frac{m\omega_L^2}{2} |\mathbf{r}|^2, \end{aligned} \quad (2.74)$$

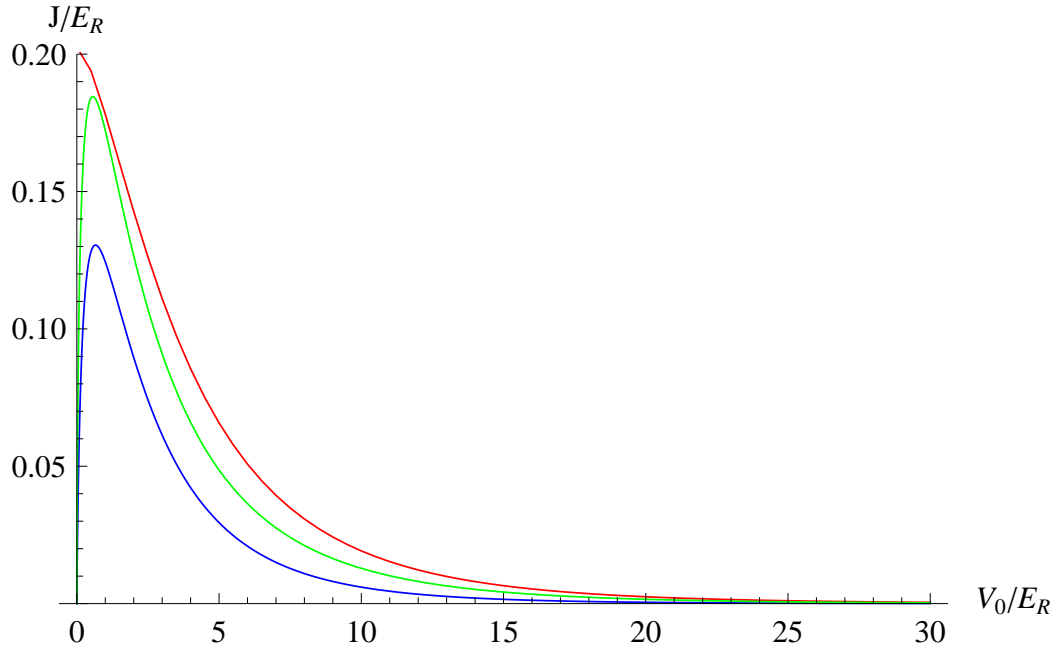


Figure 2.4.: Hopping parameter from: harmonic approximation (blue), Mathieu equation (Green), numerical calculation (red).

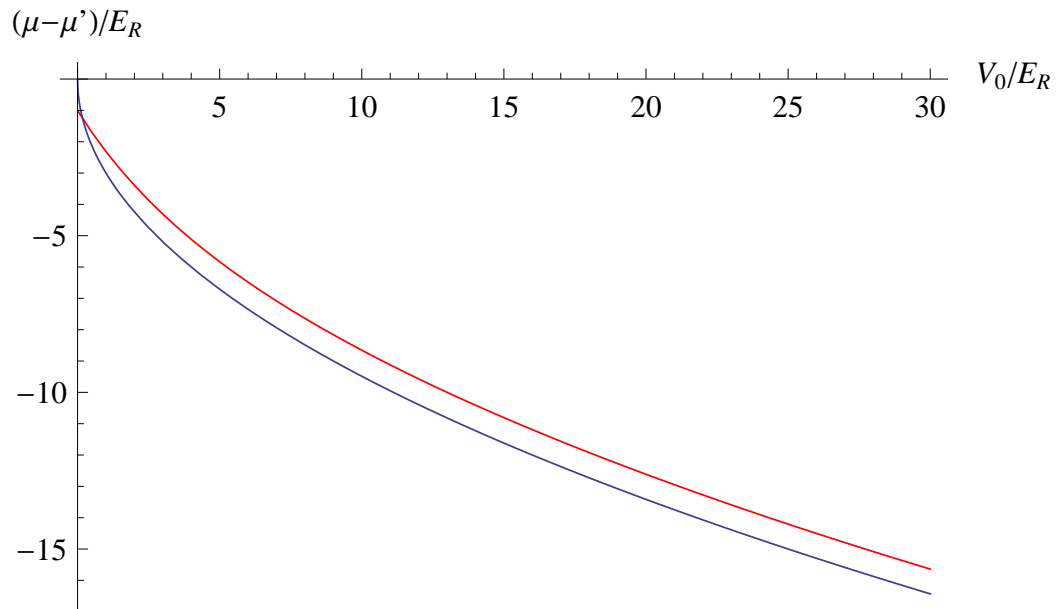


Figure 2.5.: Correction to chemical potential from: harmonic approximation (blue), numerical calculation (red).

## 2. Optical Lattice Potentials

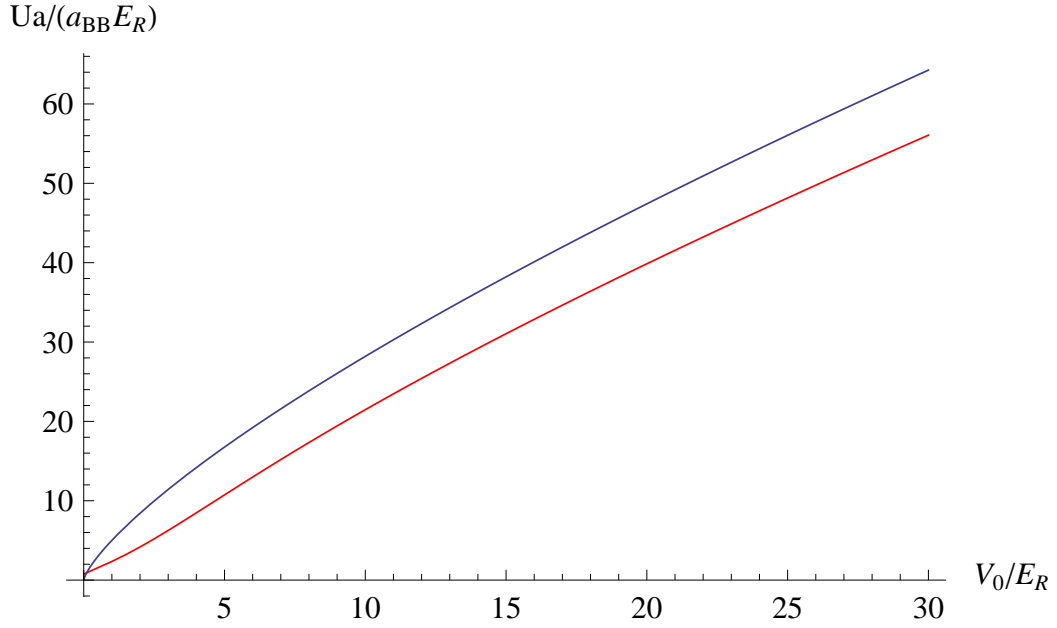


Figure 2.6.: On-site energy from: harmonic approximation (blue), numerical calculation (red).

where the trapping frequency  $\omega_R$  associated to the laser beams is [30]

$$\omega_R^2 = \frac{8V_0 - 4\sqrt{V_0/E_R}}{mw_0^2}. \quad (2.75)$$

In the following, we consider the corrections of the hopping parameter. By using formula (2.61), we get the direction-dependent hopping parameters

$$J(\mathbf{r} + a\mathbf{e}_x; \mathbf{r}) = J_x = \frac{4}{\sqrt{\pi}} E_R \left( \frac{V_{0x}}{E_R} \right)^{3/4} e^{-2\sqrt{V_{0x}/E_R}}, \quad (2.76)$$

$$J(\mathbf{r} + a\mathbf{e}_y; \mathbf{r}) = J_y = \frac{4}{\sqrt{\pi}} E_R \left( \frac{V_{0y}}{E_R} \right)^{3/4} e^{-2\sqrt{V_{0y}/E_R}}, \quad (2.77)$$

$$J(\mathbf{r} + a\mathbf{e}_z; \mathbf{r}) = J_z = \frac{4}{\sqrt{\pi}} E_R \left( \frac{V_{0z}}{E_R} \right)^{3/4} e^{-2\sqrt{V_{0z}/E_R}}, \quad (2.78)$$

where  $\mathbf{e}_i$  are the coordinate unit vectors. By using the approximations (2.17)–(2.19), we have

$$J_x \approx J_0 + \sigma(y^2 + z^2), \quad (2.79)$$

$$J_y \approx J_0 + \sigma(x^2 + z^2), \quad (2.80)$$

$$J_z \approx J_0 + \sigma(x^2 + y^2), \quad (2.81)$$

with the abbreviations

$$J_0 = \frac{4}{\sqrt{\pi}} E_R \left( \frac{V_0}{E_R} \right)^{3/4} e^{-2\sqrt{V_0/E_R}}, \quad (2.82)$$

$$\sigma = \frac{2}{w^2 \sqrt{\pi}} E_R \left[ 4 \left( \frac{V_0}{E_R} \right)^{5/4} - 3 \left( \frac{V_0}{E_R} \right)^{3/4} \right] e^{-2\sqrt{V_0/E_R}}. \quad (2.83)$$

Now, for the on-site energy we have

$$U(\mathbf{r}) = \sqrt{8\pi} \frac{E_R^{1/4} a_{\text{BB}}}{a} (V_{0x} V_{0y} V_{0z})^{1/4}. \quad (2.84)$$

By using the approximations (2.17)–(2.19), we have

$$U \approx U_0 \left( 1 - \frac{|\mathbf{r}|^2}{w_0^2} \right). \quad (2.85)$$

The limit of validity for the Homogeneous Bose-Hubbard Hamiltonian can now be extracted from Eqs. (2.74), (2.79), (2.80), (2.81), and (2.85). These equations show that as long as the region, at the center of the trap, is much smaller than the laser beam waist  $w$ , all system parameters can be considered as homogeneous. In Chapter 6, I show how spatially dependent chemical potential contributes to the observed damping of the condensate wave function in Ref. [1].





## 3. Quantum Phase Transitions

In this chapter, a general introduction to second-order phase transitions according to the modern classification of phase transitions is made. In particular, I address the symmetry breakdown mechanism which applies when the system passes from one more ordered to a less ordered phase of system. A discussion is also made about the role of the order parameter and concept of *universality* as well as its relation to the different critical exponents characterizing different systems. Special attention is given to quantum phase transitions which are transitions that can happen even in systems at zero temperature. Most of these discussions are made in the context of bosons in optical lattices so that the theory of second-order phase transitions is specifically applied to the Mott insulator-superfluid transition. Explicit calculation of the quantum phase diagram is performed by using mean-field theory and the properties of the two different phases are discussed.

### 3.1. Second-Order Quantum Phase Transitions

A common fact observed in nature is that matter in thermodynamical equilibrium exists in different phases. When a medium undergoes a transition from one phase to another, some of its properties are modified, often abruptly, as a result of the change in external conditions, such as temperature, pressure, or even external electric and magnetic fields. Some of these external conditions are quantified in terms of control parameters in the underlying system Hamiltonian. The values of the system parameters, at which the phase transition happens, define the phase boundary in the control parameter space. More precisely, phase transitions are defined as points in the control parameter space where the thermodynamical potential becomes non-analytic.

Such a non-analytical behavior of a thermodynamical potential seems, at first sight, to contradict statistical mechanics, as for any finite system, its partition function is a finite sum of analytical functions, and is therefore always analytic. This is not true, however, if the system's size together with its total number of particles is considered to be infinite, which is known as the *thermodynamical limit*. As macroscopic systems typically contain about  $10^{23}$  particles, the thermodynamic limit is considered to be a very good approximation.

The modern classification of phase transitions establishes two kinds of transitions depending on whether a thermodynamical potential varies continuously or not at the transition point. Transitions which involve latent heat are associated with a discontinuity in the thermodynamical potential and are called first-order phase transitions. On the other hand, if a transition does not involve any latent heat, then this thermodynamical potential is continuous and we have a second-order phase transition. Non-analytic properties of systems near a second-order phase transition are called *critical phenomena* [55–57]. The point in the phase diagram, where a second-order phase transition takes place, is called *critical point*.

### 3. Quantum Phase Transitions

In second-order phase transitions the symmetry present in one of the phases is reduced when the phase boundary is crossed and the other phase is reached. Due to this reduction of symmetry, an extra parameter is needed to describe the system in the less symmetrical phase. This extra parameter is called *order parameter*. The choice of the order parameter is often dictated by its utility and is usually taken in such a way that it vanishes in the symmetric phase and becomes non-zero in the non-symmetric one. Among many well-known examples of order parameters is the density in solid/liquid or liquid/gas transitions, and the net magnetization in ferromagnetic systems. Depending on the system considered, the order parameter may take the form of a complex number, a vector, or even a tensor.

An interesting feature of second-order phase transitions is that the lack of analyticity is also present in quantities which can be expressed as second derivatives of the free energy, such as the specific heat or the compressibility, as they usually exhibit a singular power law behavior at the vicinity of the transition point. In general, all non-analyticities of thermodynamical quantities with respect to one of the system parameters are described by a set of exponents in terms of a power law associated to these quantities. They are called *critical exponents* and are denoted by a list of Greek letters:  $\alpha, \beta, \gamma, \delta, \eta, \nu$  and for quantum systems we still have the so called dynamical critical exponent  $z$  [58].

Usually, the temperature is chosen to be the control parameter used to express the singularities. Here we consider a general parameter  $g$  which has the value  $g_c$  at the phase boundary. In the limit  $g \rightarrow g_c$ , any thermodynamic quantity can be decomposed into a regular part, which remains finite plus a singular part which absorbs all singularities of this quantity. This singular part is assumed to be proportional to some power of  $g - g_c$ .

The first four exponents are defined considering the singularities in the free-energy density  $f_s$ , the order parameter  $\psi$ , and the susceptibility  $\chi$  with respect to both  $g$  and the thermodynamic conjugate of the order parameter  $J$ , as follows [59]

$$f_s \sim |g - g_c|^{2-\alpha}, \quad (3.1)$$

$$\psi \sim |g - g_c|^\beta, \quad (3.2)$$

$$\chi \sim |g - g_c|^{-\gamma}, \quad (3.3)$$

$$\psi \sim J^{1/\delta}, \quad (3.4)$$

where for the first three relations we must consider  $J = 0$ , while the last one clearly refers to the case where  $J \neq 0$ . Observe that the equation (3.2) makes sense only when the phase boundary is approached from the ordered phase as in the disordered phase the order parameter should vanish identically. The other three equations are valid in both sides of the phase boundary.

The exponents  $\nu$  and  $z$  describe the singularities of the correlation length  $\xi$  and correlation time  $\tau_\xi$  at the vicinity of the phase boundary :

$$\xi \sim |g - g_c|^{-\nu}, \quad (3.5)$$

$$\tau_\xi \sim |g - g_c|^{-\nu z}. \quad (3.6)$$

And, finally, the parameter  $\eta$  relates to the power-law behavior of the correlation function at the phase

boundary, as follows

$$G(\mathbf{r}) \sim r^{-(d+z-2+\eta)}. \quad (3.7)$$

The early measures of critical exponents revealed the rather unexpected fact that many phase transitions occurring in apparently very different systems had actually the same critical exponents. This characteristic shared among many systems is known as *universality*. Such a peculiarity emerges in regimes in which the correlation length and all relevant distances are much larger than the microscopic scale, in other words, the main properties of the system near the critical point do not depend on its short-distance structure.

These critical exponents are actually not independent from one another. Instead, they are constrained by *scaling laws* for the system thermodynamic functions. These *laws* are usually derived from the *scaling hypothesis* [59] which states that, near the critical point, the correlation length  $\xi$  is the only relevant length of the system, in terms of which all other lengths can be measured. In the case of quantum systems, where time plays a very important role, the scaling hypothesis must be extended by considering that, together with the characteristic length  $\xi$ , we also have a characteristic time  $\tau_\xi$  which, is the only relevant time in terms of which all other times must be measured.

Comparing the dimensions of the above quantities and considering the scaling hypothesis we get the scaling laws [60], as follows

$$2 - \alpha = \nu(d + z) \quad (3.8)$$

$$\alpha + 2\beta + \gamma = 2 \quad (3.9)$$

$$\beta + \gamma = \beta\delta \quad (3.10)$$

$$\nu(2 - \eta) = \gamma. \quad (3.11)$$

Those relations reduce the number of independent critical exponents from seven to only three.

### 3.2. Quantum Phase Transitions in Bosonic Lattices

Unlike classical phase transitions, where the variation in the temperature induces the transition, quantum phase transitions can occur due to a competition between different control parameters in the system Hamiltonian. In the quantum case, the quantum fluctuations play the role of the thermal fluctuations in the classical case. This means that the quantum character of the critical fluctuations makes possible the occurrence of these phase transitions even at zero temperature.

As already discussed in Chapter 1, all low-temperature physics of spinless bosons loaded in optical lattices can be described by the single-band *Bose-Hubbard Hamiltonian*

$$\hat{H}_{BH} = - \sum_{i,i'} J_{ii'} \hat{a}_i^\dagger \hat{a}_{i'} + \frac{U}{2} \sum_i \hat{n}_i(\hat{n}_i - 1) - \sum_i \mu_i \hat{n}_i. \quad (3.12)$$

In the case of BEC, the order parameter is the macroscopic wave function of the condensate  $\Psi(\mathbf{r}) = \langle \hat{\Psi}(\mathbf{r}) \rangle$ . For the Bose-Hubbard Hamiltonian, the order parameter can be similarly defined as  $\psi_i = \langle \hat{a}_i \rangle$

### 3. Quantum Phase Transitions

which is simply  $\psi$  for a homogeneous system. In the ordered phase we have  $\psi = Ae^{i\theta}$ , with a well defined phase  $\theta$  while in the disordered phase we have  $\psi = 0$ . The phase  $\theta$  of the condensate wave function is *a priori* unknown, however, in order to attain the ordered phase, the system has to undergo a spontaneous symmetry breaking, i.e., the phase  $\theta$  has to pick a certain direction. In practice the resulting direction is decided by an infinitesimal external perturbation like a boundary condition.

When the system is not disturbed by an external perturbation, the different values of the phase  $\theta$  correspond to a global  $U(1)$  phase symmetry in the Bose-Hubbard Hamiltonian (3.12), and each microscopic configuration belongs to a set of configurations with exactly the same energy, where only the value of the phase  $\theta$  is modified. Now, according to Boltzmann's ergodic hypothesis, when a system is in equilibrium all system states with the same energy have exactly the same probability and will be equally populated, therefore yielding  $\psi = 0$ . This means that no ordered phase should ever occur.

The answer to this paradox lies in the fact that we are implicitly considering an infinite system, i.e., that we are working in the thermodynamical limit. The physical picture behind Boltzmann's ergodic hypothesis is that, as time progresses, the system goes from one state to the next, and will eventually visit all possible states. For a system with few degrees of freedom the transition rate between any two states is appreciable, and thus the system does visit all available states in a relatively short period of time. However, for large systems the situation can be very different as the time, which is necessary for the system to visit all microscopic configurations, may become infinitely large as we increase the system size. As a result, the system cannot explore the entire configuration space as Boltzmann assumed. Therefore, it is confined in a certain subspace which corresponds to  $\psi = Ae^{i\theta}$ . Thus, spontaneous symmetry breaking happens dynamically, i.e., it is a manifestation of *ergodicity breaking*.

In spite of these limitations, it doesn't mean that we cannot use the Boltzmann distribution anymore, actually all we have to do is to impose a constraint limiting the statistical sum to the configurations that the system can really explore. In 1932, John von Neumann [61] established that, in order to obtain the density matrix operator  $\hat{\rho}$  corresponding to any statistical ensemble, all we have to do is to find the Hermitean operator  $\hat{\rho}$  so that it maximizes the quantum mechanical entropy

$$S = -k_B \text{Tr} \hat{\rho} \ln(\hat{\rho}), \quad (3.13)$$

with the trace constraint  $\text{Tr} \hat{\rho} = 1$  and all additional constraints corresponding to the ensemble in which we are working, where  $k_B$  is the Boltzmann constant. In order to obtain the Boltzmann distribution one has to impose a constraint on the expectation value of the system energy  $E = \langle \hat{H}_{\text{BH}} \rangle$ , thus defining the canonical ensemble. The grand-canonical ensemble is obtained when we also include a constraint  $N = \sum_i \langle \hat{n}_i \rangle$  on the total number of particles in the system. The Lagrange parameters associated with these two constraints are the inverse of the absolute temperature  $1/T$  and the chemical potential  $\mu$ , respectively. This is equivalent to state that the grand-canonical distribution is a consequence of minimizing of the thermodynamical potential

$$\Gamma = \text{Tr} \hat{\rho} \hat{H}_{\text{BH}} + k_B T \text{Tr} \hat{\rho} \ln(\hat{\rho}), \quad (3.14)$$

where we redefined  $\mu_i$  according to  $\mu_i + \mu \rightarrow \mu_i$  so that it absorbs the chemical potential  $\mu$ . This

variational principle constitutes the starting point for an adequate approach towards second-order quantum phase transitions.

As already stated, in order to limit the statistical sum to the configurations that the system actually visits, we must still impose a constraint to the system so that its order parameter has a given fixed value. In the case of bosons in homogeneous optical lattices, we have the order parameters  $\psi = \langle \hat{a}_i \rangle$  and  $\psi^* = \langle \hat{a}_i^\dagger \rangle$  which leads to the introduction of Lagrange multipliers  $j$  and  $j^*$  in (3.14) and the free energy

$$F(j^*, j) = \Gamma + \text{Tr} \hat{\rho} \sum_i \left( j^* \hat{a}_i + j \hat{a}_i^\dagger \right). \quad (3.15)$$

The  $\psi$ -dependent effective thermodynamic potential is then called *effective potential*. This transformation is equivalent to modifying the Bose-Hubbard Hamiltonian in the following way

$$\hat{H}_{\text{BH}}(j^*, j) = \hat{H}_{\text{BH}} + \sum_i \left( j^* \hat{a}_i + j \hat{a}_i^\dagger \right). \quad (3.16)$$

By minimizing (3.15) with the constraint  $\text{Tr} \hat{\rho} = 1$ , we obtain the source-dependent density matrix

$$\hat{\rho}(j^*, j) = Z^{-1} e^{-\beta \hat{H}_{\text{BH}}(j^*, j)}, \quad (3.17)$$

where we define  $\beta = 1/k_B T$  and the partition function  $Z$  given by

$$Z(j^*, j) = \text{Tr} e^{-\beta \hat{H}_{\text{BH}}(j^*, j)}. \quad (3.18)$$

Substituting  $\hat{\rho}(j^*, j)$  into (3.15), we find the explicit form of the source-dependent free energy

$$F(j^*, j) = -\frac{1}{\beta} \ln Z(j^*, j). \quad (3.19)$$

The order parameter  $\psi$  as well as its complex conjugate  $\psi^*$  can be found by differentiating the free energy  $F(j^*, j)$  with respect to  $j^*$  and  $j$

$$\begin{aligned} \psi &= \frac{1}{N_s} \frac{\partial F}{\partial j^*}, \\ \psi^* &= \frac{1}{N_s} \frac{\partial F}{\partial j}, \end{aligned} \quad (3.20)$$

where  $N_s$  is the total number of lattice sites.

It is important to keep in mind that, in order to find the minimum of (3.14), we still have to minimize  $\Gamma$  with respect to  $\psi$ . This means that the value of  $\psi$  can be extracted from the equations

$$\frac{\partial \Gamma}{\partial \psi} = 0, \quad (3.21)$$

$$\frac{\partial \Gamma}{\partial \psi^*} = 0. \quad (3.22)$$

A direct consequence of the global phase invariance of  $\hat{H}_{\text{BH}}$  is that the effective potential  $\Gamma$  must also exhibit an invariance with respect to the order parameter phase. The independence on the phase

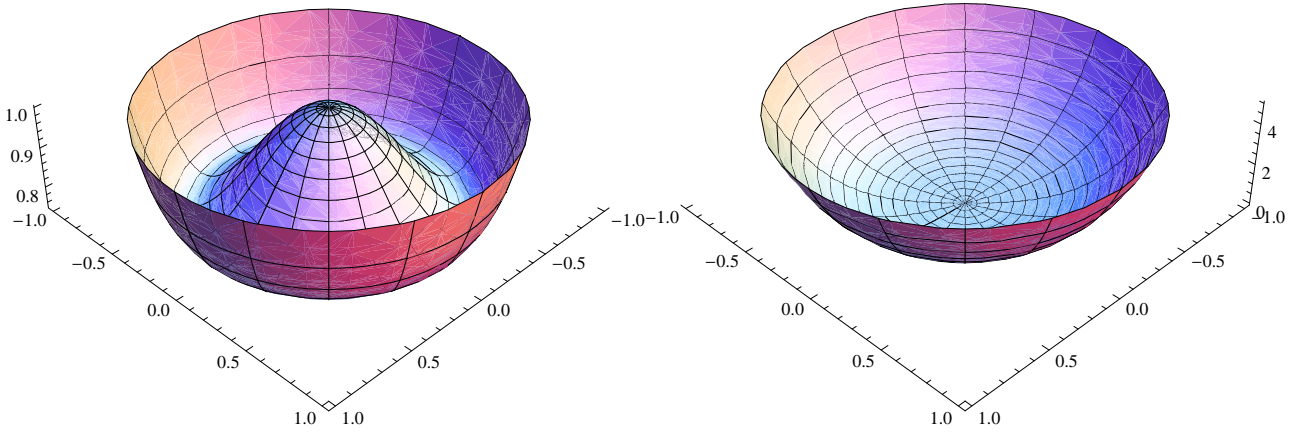


Figure 3.1.: Left: Mexican-hat potential typical of symmetry-broken phase. Right: potential with a single minimum at the origin which characterizes the symmetric phase.

of  $\psi$  implies that  $\Gamma$  has to be a function of  $|\psi|^2$ . This also implies that there is no unique solution for (3.21) with  $\psi \neq 0$ , as any particular solution of (3.21) can be multiplied by an arbitrary phase factor and still obeys this equation. As already discussed, this uncertainty in the phase of  $\psi$  characterizes a symmetry-broken phase. However, if we have only the trivial solution  $\psi = 0$ , then there is no ambiguity in defining the order parameter and, therefore, we have a symmetric phase.

Now, in order to know if a given set of control parameters in  $\hat{H}_{\text{HB}}$  leads to a symmetric or unsymmetrical phase, we must find out whether the minimum of  $\Gamma$  is attained for  $|\psi| = 0$  or  $|\psi| \neq 0$ . The solution to this problem was given by Lev Landau and is based on analyzing the terms in the respective expansion of  $\Gamma$  in a power series of  $|\psi|^2$

$$\Gamma = a_0 + a_2|\psi|^2 + a_4|\psi|^4 + \dots \quad (3.23)$$

Landau argued that second-order phase transitions could, in general, be fully explained by only considering the coefficients  $a_2$  and  $a_4$ . In the simplest case, where  $a_4 > 0$ , the second-order phase transition is characterized by the change in the sign of  $a_2$ . This comes from the fact that, if  $a_2 > 0$ , the only solution of (3.21) is  $\psi = 0$ , thus corresponding to a symmetric phase, while if  $a_2 < 0$ , the effective potential  $\Gamma$  has a Mexican hat shape as depicted in Fig. 3.1. In the latter case  $\Gamma$  has infinitely many minima with  $|\psi| \neq 0$  which differ only in phase.

The condition  $a_2 = 0$  defines the boundary line which separates the ordered and disordered phases in the control parameters space. At the vicinity of this boundary, the absolute value of the order parameter can be calculated by using (3.21) and (3.23), which leads to

$$|\psi| = \sqrt{-\frac{a_2}{2a_4}}. \quad (3.24)$$

Up to this point we focused our attention on the second-order phase transitions where the global  $U(1)$  phase symmetry of the system is broken by the emergence of a non-zero homogeneous order parameter. Although this approach is well suited for dealing with most second-order phase transitions, due to the

assumption of homogeneity, we cannot apply this effective potential method to systems which may exhibit spontaneous symmetry breaking with a site-dependent order parameter, i.e, systems where the translation symmetry is also broken. There are many well known cases of this kind of phase in the literature, perhaps the most famous of them being the anti-ferromagnetic phase in spin lattice systems, where the spins of any two neighbor lattice sites are antiparallely aligned to each other. An effect similar to antiferromagnetism can also take place in bosonic optical lattices if the hopping matrix elements in the Bose-Hubbard Hamiltonian could be tuned to become negative, as recently suggested in Ref. [62]. In such cases we may also have second-order phase transitions, but unlike the homogeneous case, the order parameter  $\psi_i = \langle \hat{a}_i \rangle$  can be also be site dependent. Therefore, in order to have a method capable of dealing also with site-dependent order parameters, we must introduce in our method site-dependent sources, which lead to a more general thermodynamic potential  $\Gamma(\psi_i^*, \psi_i)$ . Analogously to the homogeneous case, this is accomplished by using site-dependent sources  $j_i^*$  and  $j_i$ , which serve to impose the constraints  $\langle \hat{a}_i^\dagger \rangle = \psi_i^*$  and  $\langle \hat{a}_i \rangle = \psi_i$ , respectively.

An even more general thermodynamical potential can be defined if we explore the similarities between the quantum-mechanical evolution operator and the quantum-statistical density matrix. Considering  $\hbar = 1$ , we observe that the operator  $e^{-\beta \hat{H}}$  has the same form of the evolution operator  $e^{-it\hat{H}}$ . Thus, we can consider the operator  $e^{-\beta \hat{H}}$  as a quantum-evolution operator evolving in imaginary time from 0 to  $\beta$  by making the Wick rotation  $it \rightarrow \tau$ . Now, instead of considering only site-dependent source terms, we can have time-dependent as well as site-dependent terms by defining the general Hamiltonian

$$\hat{H}_{\text{BH}}(\tau) = \hat{H}_{\text{BH}} + \sum_i \left[ j_i^*(\tau) \hat{a}_i + j_i(\tau) \hat{a}_i^\dagger \right]. \quad (3.25)$$

The imaginary-time evolution operator therefore obeys a Schrödinger-like equation with  $\tau = it$ , i.e.,

$$-\frac{\partial \hat{U}(\tau, \tau_0)}{\partial \tau} = \hat{H}_{\text{BH}}(\tau) \hat{U}(\tau, \tau_0). \quad (3.26)$$

The solution of (3.26) can be written as

$$\hat{U}(\tau, \tau_0) = \hat{T} e^{-\int_{\tau_0}^{\tau} d\tau' \hat{H}_{\text{BH}}(\tau')}. \quad (3.27)$$

The source-dependent partition function is then defined by

$$Z[j_i^*(\tau), j_i(\tau)] = \text{Tr} \hat{U}(\beta, 0), \quad (3.28)$$

and analogous to the time-independent case we define the functional

$$F[j_i^*(\tau), j_i(\tau)] = -\frac{1}{\beta} \ln Z[j_i^*(\tau), j_i(\tau)]. \quad (3.29)$$

The use of this free-energy functional not only allows us to deal with more general phase transitions, but it also makes possible to represent most of the system quantities by means of functional derivatives

### 3. Quantum Phase Transitions

of  $F$  with respect to the sources. In particular, the space-time dependent order parameter is given by

$$\psi_i(\tau) = \beta \frac{\delta F}{\delta j_i^*(\tau)}. \quad (3.30)$$

Finally we are able to generalize the effective potential by means of a Legendre transformation. This gives us the effective action

$$\Gamma[\psi_i^*(\tau), \psi_i(\tau)] = F - \frac{1}{\beta} \sum_i \int_0^\beta d\tau [\psi_i^*(\tau) j_i(\tau) + \psi_i(\tau) j_i^*(\tau)]. \quad (3.31)$$

The physical value of the order-parameter is then obtained by minimizing  $\Gamma[\psi_i^*(\tau), \psi_i(\tau)]$  with respect to  $\psi_i(\tau)$  and  $\psi_i^*(\tau)$  leading to the equations of motion

$$\begin{aligned} \frac{\delta \Gamma\{\psi_i^*(\tau), \psi_i(\tau)\}}{\delta \psi_i(\tau)} &= 0, \\ \frac{\delta \Gamma\{\psi_i^*(\tau), \psi_i(\tau)\}}{\delta \psi_i^*(\tau)} &= 0. \end{aligned} \quad (3.32)$$

The effective action  $\Gamma[\psi_i^*(\tau), \psi_i(\tau)]$  is the central element in our analysis as it contains all information concerning the Bose-Hubbard Hamiltonian regardless of phase in which the system is.

### 3.3. Mean-Field Theory

In the mean-field theory, the central idea is to rewrite the field operator as a sum of its mean value with its fluctuations, i.e.,

$$\hat{a}_i = \langle \hat{a}_i \rangle + \delta \hat{a}_i \quad (3.33)$$

and then neglect all products of fluctuations  $\delta \hat{a}_i$  and  $\delta \hat{a}_i^\dagger$ , in the perturbation term, which in our case is the hopping term. Here we treat the homogeneous Bose-Hubbard Hamiltonian at  $T = 0$  with only nearest-interactions. In this way, we express the hopping term according to

$$\begin{aligned} -J \sum_{\langle i,j \rangle} \hat{a}_i^\dagger \hat{a}_j &= -J \sum_{\langle i,j \rangle} \left( \langle \hat{a}_i^\dagger \rangle + \delta \hat{a}_i^\dagger \right) \left( \langle \hat{a}_i \rangle + \delta \hat{a}_i \right) \\ &= -J \sum_{\langle i,j \rangle} \left( \langle \hat{a}_i^\dagger \rangle \hat{a}_i + \langle \hat{a}_i \rangle \hat{a}_i^\dagger - \langle \hat{a}_i^\dagger \rangle \langle \hat{a}_i \rangle + \delta \hat{a}_i^\dagger \delta \hat{a}_i \right) \end{aligned} \quad (3.34)$$

The mean-field approximation is achieved by neglecting *products of fluctuations*, i.e., neglecting the term  $\delta \hat{a}_i^\dagger \delta \hat{a}_i$  in Eq. (3.34), which results in



$$\begin{aligned}
-J \sum_{\langle i,j \rangle} \hat{a}_i^\dagger \hat{a}_j &\approx -J \sum_{\langle i,j \rangle} \left( \langle \hat{a}_i^\dagger \rangle \hat{a}_i + \langle \hat{a}_i \rangle \hat{a}_i^\dagger - \langle \hat{a}_i^\dagger \rangle \langle \hat{a}_i \rangle \right) \\
&= -Jz \sum_i \left( \psi^* \hat{a}_i + \psi \hat{a}_i^\dagger - |\psi|^2 \right).
\end{aligned} \tag{3.35}$$

In the last step, homogeneity of the system was assumed implying the expectation value  $\langle \hat{a}_i^\dagger \rangle = \psi$  to be independent of the lattice site  $i$ . Then the hopping term will reduce to a single sum over all lattice sites with  $z$  denoting the number of nearest-neighbor sites. By using the approximation (3.35), we obtain the mean-field Hamiltonian

$$\hat{H}_{\text{MF}} = -Jz \sum_i \left( \psi \hat{a}_i^\dagger + \psi^* \hat{a}_i - \psi^* \psi \right) + \frac{U}{2} \sum_i \hat{n}_i (\hat{n}_i - 1) - \mu \sum_i \hat{n}_i. \tag{3.36}$$

Here we can observe that imposing the conditions

$$\psi^* = \langle \hat{a}_i^\dagger \rangle \quad ; \quad \psi = \langle \hat{a}_i \rangle \tag{3.37}$$

to the ground state of  $\hat{H}_{\text{MF}}$  is equivalent to minimize the ground-state energy  $E_{\text{MF}}$  as follows

$$\frac{\partial E_{\text{MF}}}{\partial \psi} = 0 \quad ; \quad \frac{\partial E_{\text{MF}}}{\partial \psi^*} = 0. \tag{3.38}$$

Our statement that  $\psi$  is site independent lies on the assumption that the translational symmetry is never broken, as the order parameter is the same on every site. This approximation simplifies considerably the calculation of quantities related to our system due to fact that now our problem is reduced to the analysis of independent identical Hamiltonians defined at each site of our lattice. Notice also that  $\hat{H}_{\text{MF}}$  does not possess the explicit  $U(1)$  symmetric present in  $\hat{H}_{\text{BH}}$ . In order to recover this symmetry, we must apply to the order parameter the same phase transformation applied in the operators. This is necessary in order to allow for the possibility of symmetry-broken phases, while symmetric phases will appear at the special value  $\psi = 0$ .

Due to this phase invariance the energy  $E_{\text{MF}}$  must be a function of only  $|\psi|^2$  which can be calculated perturbatively producing the Landau series

$$\frac{E_{\text{MF}}(|\psi|^2)}{N_s} = a_0 + a_2 |\psi|^2 + \frac{1}{2!} a_4 |\psi|^4 + \dots, \tag{3.39}$$

where  $N_s$  is the total number of sites and  $a_0$  is the ground state of  $\hat{H}_{\text{BH}}$  for case  $J = 0$ , while the coefficients  $a_2$  and  $a_4$  can be calculated using Rayleigh-Schrödinger perturbation theory.

The first step to calculate the Landau coefficients is to find the ground state of the on-site Hamiltonian

$$\hat{H}_0 = \frac{U}{2} \hat{n}(\hat{n} - 1) - \mu \hat{n}, \tag{3.40}$$

here, as all sites are equivalent, we ignored the site indices. As this Hamiltonian involves only the number operator  $\hat{n}$ , its eigenstates are the states containing integer number of bosons per lattice site,

### 3. Quantum Phase Transitions

and its eigenvalues are given by

$$\epsilon_n = \frac{U}{2}n(n-1) - \mu n. \quad (3.41)$$

By comparing these different eigenvalues we can express the integer  $n$  which minimizes  $\epsilon_n$  by

$$n(\mu/U) = 1 + \lfloor \mu/U \rfloor, \quad (3.42)$$

where  $\lfloor \mu/U \rfloor$  is the largest integer less than or equal to  $x$ .

Now we can use Rayleigh-Schrödinger perturbation theory and obtain

$$a_0 = \epsilon_n \quad (3.43)$$

$$a_2 = (Jz)^2 \left( \frac{n+1}{\epsilon_n - \epsilon_{n+1}} + \frac{n}{\epsilon_n - \epsilon_{n-1}} \right) + Jz, \quad (3.44)$$

$$a_4 = 4(Jz)^4 \left\{ \frac{(n+2)(n+1)}{(\epsilon_n - \epsilon_{n+1})^2 (\epsilon_n - \epsilon_{n+2})} + \frac{n(n-1)}{(\epsilon_n - \epsilon_{n-1})^2 (\epsilon_n - \epsilon_{n-2})} \right. \\ \left. - \left[ \frac{n+1}{(\epsilon_n - \epsilon_{n+1})^2} + \frac{n}{(\epsilon_n - \epsilon_{n-1})^2} \right] \left( \frac{n+1}{\epsilon_n - \epsilon_{n+1}} + \frac{n}{\epsilon_n - \epsilon_{n-1}} \right) \right\}. \quad (3.45)$$

As expected, we have  $a_4 > 0$ , while  $a_2$  goes from positive to negative values as we increase the hopping parameter, therefore evidencing the transition of  $E_{\text{MF}}(|\psi|^2)$  from convex potential to a Mexican hat potential and demonstrating the existence of a second-order phase transition at least at the mean-field level. In the quantum phase diagram, the points where  $a_2$  changes its sign define the boundary separating the ordered from the non-ordered phase. The explicit solution of the equation  $a_2 = 0$ , then gives the phase boundary

$$\frac{Jz}{U} = \frac{(n - \mu/U)(\mu/U - n + 1)}{1 + \mu/U}. \quad (3.46)$$

This formula enables us to construct the phase diagram as depicted Fig. 3.2. There we see a series of lobes each one corresponding to an occupation number  $n$ . According to the mean-field theory, inside the regions enclosed by each lobe, the particle density  $\rho$  is constant. This implies that the compressibility  $\partial\rho/\partial\mu$  vanishes everywhere inside these regions, i.e., they are Mott insulating phases. Outside these regions the order parameter becomes nonzero, which means that the system possesses a macroscopic wave function, i.e, we have a Bose-Einstein condensate.

The existence such a wave function implies that a fraction of the system can move throughout the lattice with no viscosity at all [40], in other words, it implies that the system is in a superfluid phase.

Inside the superfluid phase but still close to the phase boundary, the mean-field energy can be explicitly minimized by using equation (3.39), which gives

$$|\psi_{\text{MF}}|^2 = -\frac{2a_2}{a_4}. \quad (3.47)$$

This quantity is called condensate density, as it measures the density of particles sharing the condensate wave function. This quantity enables to finally evaluate the ground-state energy

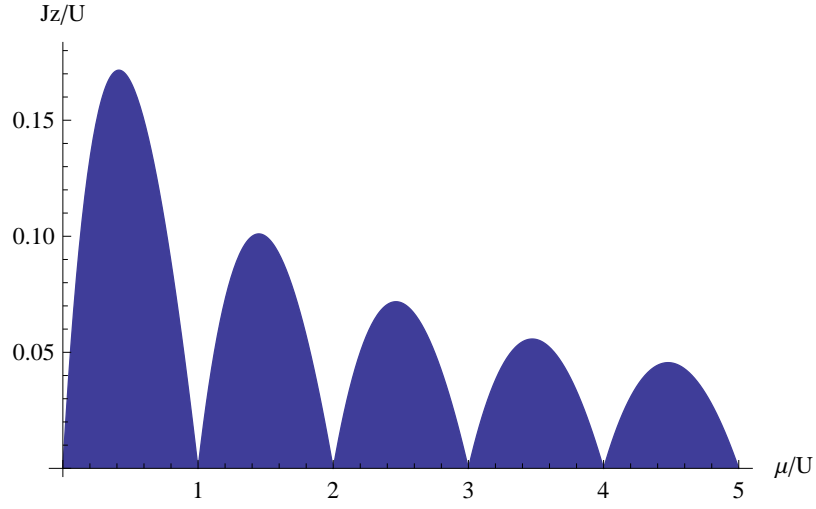


Figure 3.2.: Mean-field quantum phase diagram for the Bose-Hubbard model. The filled regions are the successive Mott lobes corresponding to integer occupation numbers.

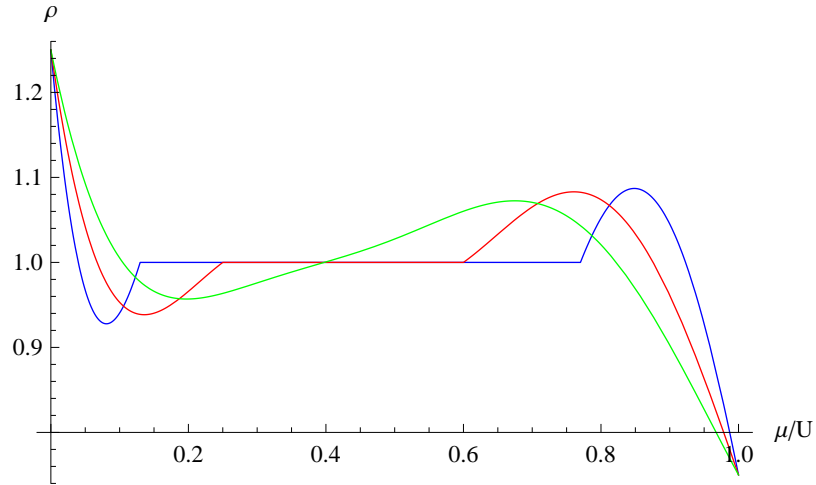


Figure 3.3.: Total particle density. The blue, red, and green lines correspond to  $\frac{Jz}{U} = 0.1$ ,  $\frac{Jz}{U} = 0.15$ , and  $\frac{Jz}{U} = 0.2$ , respectively.

### 3. Quantum Phase Transitions

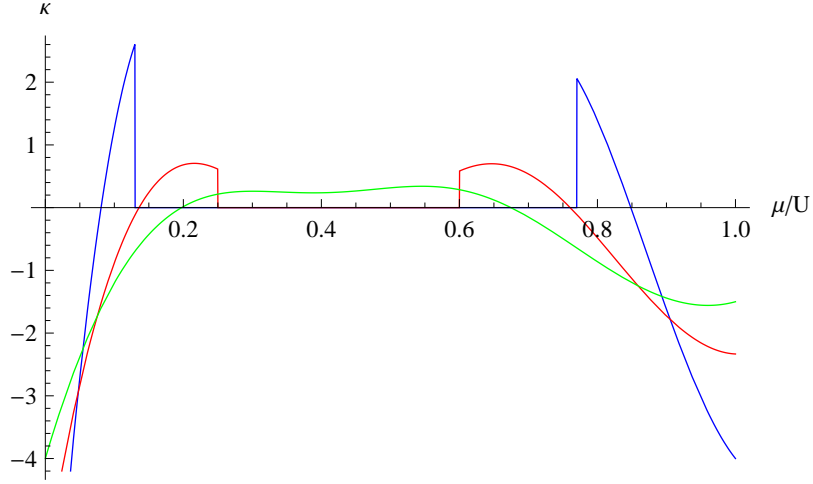


Figure 3.4.: Compressibility as defined in (3.54). The blue, red, and green lines correspond to  $\frac{Jz}{U} = 0.1$ ,  $\frac{Jz}{U} = 0.15$ , and  $\frac{Jz}{U} = 0.2$ , respectively. For regions far from the lobe tip, there is an unphysical negative compressibility which is a weakness of this mean-field theory.

$$E_0 = E_{\text{MF}}(|\psi|^2)/N_s \approx a_0 - \frac{a_2^2}{a_4}. \quad (3.48)$$

This theory allows us to calculate the so-called thermodynamical exponents  $\alpha$ ,  $\beta$ ,  $\gamma$ , and  $\delta$ , giving the result

$$\alpha = 0 \quad (3.49)$$

$$\beta = \frac{1}{2} \quad (3.50)$$

$$\gamma = 1 \quad (3.51)$$

$$\delta = 3. \quad (3.52)$$

Indeed these are the critical exponents of the universality class corresponding to a system in dimension higher  $d \geq 3$  and with an order parameter with  $U(1)$  symmetry. The remaining critical exponents can only be calculated by allowing space as well as imaginary-time dependent order parameters. In Chapter 4, this possibility will be considered in the context of our effective action formalism.

The total density of particles and  $\rho$  as well as the compressibility  $\kappa$  can now be easily calculated from this mean-field theory

$$\rho = -\frac{\partial E_0}{\partial \mu}, \quad (3.53)$$

$$\kappa = -\frac{\partial^2 E_0}{\partial \mu^2}. \quad (3.54)$$

The figures 3.3 and 3.4 show some of the crucial weaknesses of this mean-field theory. Observe that for the regions far from the lobe tip, there is an unphysical negative compressibility. In general the

mean-field theory gives very bad if not contradictory results inside the superfluid phase.

In the next chapters we will see how these problems are fixed by using the effective potential and effective action methods.



## 4. Bosonic Lattices at Finite Temperature

In this chapter, a perturbation theory is developed by taking advantage of a diagrammatic notation specially developed to deal with bosons in optical lattices. The calculation of the effective action, which is defined through a Legendre transformation of the free energy, leads to an automatic resummation of the hopping expansion. This allows the description of the system properties in both the Mott-insulator and the superfluid phase. By using a set of diagrammatic rules, the effective action is calculated up to second hopping order.

We treat the Bose-Hubbard model as belonging to a more general class of Hamiltonians which can be written as a sum of a hopping term and a local term

$$\hat{H} = \hat{H}_h + \hat{H}_l, \quad (4.1)$$

with the respective terms being defined by

$$\hat{H}_l = \sum_i f_i(\hat{n}_i), \quad (4.2)$$

$$\hat{H}_h = - \sum_{ii'} J_{ii'} \hat{a}_i^\dagger \hat{a}_{i'}. \quad (4.3)$$

The Bose-Hubbard Hamiltonian is recovered if we choose  $f_i(x) = U(x^2 - x)/2 - \mu x$  and  $J_{ij} = J$  if  $ij$  are nearest neighbors lattice sites while  $J_{ij} = 0$  otherwise.

In order to calculate the expectation values of physical quantities, we use the so-called Green's functions

$$G^{(n,m)}(\tau_1, i_1; \dots; \tau_n, i_n | \tau'_1, i'_1; \dots; \tau'_m, i'_m) = Z^{-1} \text{Tr} \left\{ e^{-\beta \hat{H}} \hat{T} \left[ \hat{a}_{i_1}(\tau_1) \dots \hat{a}_{i_n}(\tau_n) \hat{a}_{i'_1}^\dagger(\tau'_1) \dots \hat{a}_{i'_m}^\dagger(\tau'_m) \right] \right\} \quad (4.4)$$

where the partition function is  $Z = \text{Tr} e^{-\beta \hat{H}}$  and a time-dependent Heisenberg operator is defined from the Schrödinger operator  $\hat{O}_S$  as  $\hat{O}(\tau) = e^{\tau \hat{H}} \hat{O}_S e^{-\tau \hat{H}}$ .

In order to facilitate the calculation of  $G^{(n,m)}$ , we define a new time-dependent Hamiltonian by adding to it a time-dependent source term, according to

$$\hat{H}(\tau) = \hat{H} + \hat{H}_s(\tau), \quad (4.5)$$

where

$$\hat{H}_s(\tau) = \sum_i \left[ j_i^*(\tau) \hat{a}_i + j_i(\tau) \hat{a}_i^\dagger \right]. \quad (4.6)$$

#### 4. Bosonic Lattices at Finite Temperature

The partition function for  $\hat{H}(\tau)$  is then given by the functional

$$Z[j^*, j] = \text{Tr} \hat{U}(\beta, 0), \quad (4.7)$$

where the imaginary-time evolution operator  $\hat{U}(\tau, \tau_0)$  obeys the evolution equation

$$-\frac{\partial}{\partial \tau} \hat{U}(\tau, \tau_0) = \hat{H}(\tau) \hat{U}(\tau, \tau_0) \quad (4.8)$$

with the initial condition  $\hat{U}(\tau_0; \tau_0) = \hat{1}$ . In the following, we show that all Green functions can be obtained from functional derivatives of  $Z[j^*, j]$  with respect to  $j^*$  and  $j$ . To this end note that equation (4.8) together with its initial condition can be rewritten in the integral form

$$\hat{U}(\tau, \tau_0) = \hat{1} - \int_{\tau_0}^{\tau} \hat{H}(\tau') \hat{U}(\tau', \tau_0) d\tau', \quad (4.9)$$

which can be solved iteratively leading to the Born series

$$\hat{U}(\tau, \tau_0) = \hat{1} - \int_{\tau_0}^{\tau} d\tau_1 \hat{H}(\tau_1) + \int_{\tau_0}^{\tau} d\tau_1 \int_{\tau_0}^{\tau_1} d\tau_2 \hat{H}(\tau_2) \hat{H}(\tau_1) \quad (4.10)$$

$$- \int_{\tau_0}^{\tau} d\tau_1 \int_{\tau_0}^{\tau_1} d\tau_2 \int_{\tau_0}^{\tau_2} d\tau_3 \hat{H}(\tau_3) \hat{H}(\tau_2) \hat{H}(\tau_1) + \dots \quad (4.11)$$

Using the time-ordering operator we have

$$\begin{aligned} \hat{U}(\tau, \tau_0) &= \hat{1} - \int_{\tau_0}^{\tau} d\tau_1 \hat{H}(\tau_1) + \frac{1}{2!} \int_{\tau_0}^{\tau} d\tau_1 \int_{\tau_0}^{\tau_1} d\tau_2 \hat{T} [\hat{H}(\tau_2) \hat{H}(\tau_1)] \\ &\quad - \frac{1}{3!} \int_{\tau_0}^{\tau} d\tau_1 \int_{\tau_0}^{\tau_1} d\tau_2 \int_{\tau_0}^{\tau_2} d\tau_3 \hat{T} [\hat{H}(\tau_3) \hat{H}(\tau_2) \hat{H}(\tau_1)] + \dots \end{aligned} \quad (4.12)$$

This series can be summarized by the formula

$$\hat{U}(\tau, \tau_0) = \hat{T} e^{-\int_{\tau_0}^{\tau} \hat{H}(\tau') d\tau'}. \quad (4.13)$$

It is also useful to observe the semi-group property of the imaginary-time evolution operator

$$\hat{U}(\tau, \tau_0) = \hat{U}(\tau, \tau') \hat{U}(\tau', \tau_0), \text{ if } \tau \geq \tau' \geq \tau_0. \quad (4.14)$$

This semi-group property allows us rewrite the evolution operator by isolating a subinterval from  $\tau - \Delta$  to  $\tau + \Delta$ , with  $\Delta > 0$ , i.e.,

$$\hat{U}(\beta, 0) = \hat{U}(\beta, \tau + \Delta) \hat{U}(\tau + \Delta, \tau - \Delta) \hat{U}(\tau - \Delta, 0). \quad (4.15)$$

The functional derivative of  $\hat{U}(\beta, 0)$  with respect to  $j_i^*(\tau)$  can be expressed as

$$\frac{\delta}{\delta j_i^*(\tau)} \hat{U}(\beta, 0) = \hat{U}(\beta, \tau + \Delta) \frac{\delta \hat{U}(\tau + \Delta, \tau - \Delta)}{\delta j_i^*(\tau)} \hat{U}(\tau - \Delta, 0). \quad (4.16)$$



Using equation (4.12), we see that

$$\frac{\delta \hat{U}(\tau + \Delta, \tau - \Delta)}{\delta j_i^*(\tau)} = -\hat{a}_i + \int_{\tau-\Delta}^{\tau+\Delta} d\tau_1 \left[ \Theta(\tau - \tau_1) \hat{a}_i \hat{H}(\tau_1) + \Theta(\tau_1 - \tau) \hat{H}(\tau_1) \hat{a}_i \right] - \dots \quad (4.17)$$

By substituting (4.17) into (4.16) and taking the limit  $\Delta \rightarrow 0$  we obtain

$$\frac{\delta \hat{U}(\beta, 0)}{\delta j_i^*(\tau)} = -\hat{U}(\beta, \tau) \hat{a}_i \hat{U}(\tau, 0) = -\hat{U}(\beta, 0) \hat{a}_i(\tau), \quad (4.18)$$

where  $\hat{a}_i(\tau) = \hat{U}^{-1}(\tau, 0) \hat{a}_i \hat{U}(\tau, 0)$ . Observe that we get back to the definition of Heisenberg operators in (4.4) by setting  $j_i^*(\tau) = j_i(\tau) = 0$ .

By taking more functional derivatives of (4.18) with respect to the source fields, we finally obtain the formula

$$\frac{\delta^{(n+m)} \hat{U}(\beta, 0)}{\delta j_{i_1}^*(\tau_1) \dots \delta j_{i_n}^*(\tau_n) \delta j_{i'_1}(\tau'_1) \dots \delta j_{i'_m}(\tau'_m)} = \hat{U}(\beta, 0) \hat{T} \left[ \hat{a}_{i_1}(\tau_1) \dots \hat{a}_{i_n}(\tau_n) \hat{a}_{i'_1}^\dagger(\tau'_1) \dots \hat{a}_{i'_m}^\dagger(\tau'_m) \right]. \quad (4.19)$$

The trace of this equation finally leads us to the formula for Green's functions as functional derivatives of the generating functional  $Z[j^*, j]$

$$G^{(n,m)}(\tau_1, i_1; \dots; \tau_n, i_n | \tau'_1, i'_1; \dots; \tau'_m, i'_m) = Z[j^*, j]^{-1} \frac{\delta^{(n+m)} Z[j^*, j]}{\delta j_{i_1}^*(\tau_1) \dots \delta j_{i_n}^*(\tau_n) \delta j_{i'_1}(\tau'_1) \dots \delta j_{i'_m}(\tau'_m)} \Big|_{j^*=j=0}. \quad (4.20)$$

## 4.1. Perturbation Theory

In order to calculate  $\hat{U}(\tau, 0)$  as a power series of the hopping matrix element  $J_{ij}$ , we split the full imaginary-time dependent Hamiltonian  $\hat{H}(\tau)$  into an unperturbed part  $\hat{H}_0(\tau) = \hat{H}_1 + \hat{H}_s(\tau)$  plus the hopping-dependent perturbation  $\hat{H}_h$ , i.e.,

$$\hat{H}(\tau) = \hat{H}_0(\tau) + \hat{H}_h. \quad (4.21)$$

The imaginary-time dependent evolution operator can now be factorized as an unperturbed part times an interaction part

$$\hat{U}(\tau; 0) = \hat{U}_0(\tau; 0) \hat{U}_I(\tau; 0), \quad (4.22)$$

where the unperturbed evolution operator obeys the following evolution equation:

$$-\frac{\partial}{\partial \tau} \hat{U}_0(\tau; 0) = \hat{H}_0(\tau) \hat{U}_0(\tau; 0), \quad (4.23)$$

which analogously to Eq. (4.13) has the solution

$$\hat{U}_0(\tau; \tau_0) = \hat{T} e^{-\int_{\tau_0}^{\tau} \hat{H}_0(\tau') d\tau'}. \quad (4.24)$$

#### 4. Bosonic Lattices at Finite Temperature

Using (4.8) and (4.23) we deduce the evolution equation for the interaction part of evolution operator

$$-\frac{\partial}{\partial \tau} \hat{U}_I(\tau; 0) = \hat{H}_h^I(\tau) \hat{U}_I(\tau; 0), \quad (4.25)$$

where

$$\hat{H}_h^I(\tau) = \hat{U}_0^{-1}(\tau; 0) \hat{H}_h \hat{U}_0(\tau; 0). \quad (4.26)$$

Here we can repeat the same iterative procedure as in (4.13) and obtain the solution for (4.25) as

$$\hat{U}_I(\tau; 0) = \hat{T} e^{-\int_0^\tau d\tau' \hat{H}_h^I(\tau')}. \quad (4.27)$$

The full partition function (4.7) can now, with (4.22) and (4.27), written as

$$Z[j^*, j] = \text{Tr} \left[ \hat{U}_0(\beta; 0) \hat{T} e^{-\int_0^\beta d\tau' \hat{H}_h^I(\tau')} \right] \quad (4.28)$$

Thus, using the (4.3) and (4.19), we can express  $Z[j^*, j]$  in terms of functional derivatives of the unperturbed partition function  $Z_0[j^*, j]$  via

$$Z[j^*, j] = e^{\sum_{ij} J_{ij} \int_0^\beta d\tau \frac{\delta^2}{\delta j_i^*(\tau) \delta j_j(\tau)}} Z_0[j^*, j], \quad (4.29)$$

where we have

$$Z_0[j^*, j] = \text{Tr} \left[ \hat{U}_0(\beta, 0) \right]. \quad (4.30)$$

## 4.2. Lattice Diagrammatics

Let us now consider the unperturbed partition function in more detail. For  $J_{ij} = 0$ , the system splits into independent lattice sites in such a way that the partition function can be factorized as

$$Z_0[j^*, j] = \prod_i Z_i[j^*, j]. \quad (4.31)$$

In practice, in order to avoid the annoying  $\beta^{-1}$  prefactor appearing in equations (3.29) and (3.31), we use instead, in our diagrammatic calculations, the functional

$$W[j^*, j] = \ln Z[j^*, j] = -\beta F[j^*, j]. \quad (4.32)$$

For a reason that will become clear later we can also call  $W[j^*, j]$  the generating functional of the connected Green's functions  $G_c$ , while the partition function  $Z[j^*, j]$  can be also be named the generating functional of the full Green's function  $G$ . The functional  $W$  can also be represented as a power of the sources  $j$  and  $j^*$  as follows

$$\begin{aligned}
W[j^*, j] = & W^{(0)} + \sum_{ii'} \int_0^\beta d\tau \int_0^\beta d\tau' W_{ii'}^{(2)}(\tau; \tau') j_i^*(\tau) j_i(\tau') \\
& + \frac{1}{2!^2} \sum_{i_1 i_2, i'_1 i'_2} \int_0^\beta d\tau_1 \int_0^\beta d\tau_2 \int_0^\beta d\tau'_1 \int_0^\beta d\tau'_2 W_{i_1 i_2, i'_1 i'_2}^{(4)}(\tau_1, \tau_2; \tau'_1, \tau'_2) j_{i_1}^*(\tau_1) j_{i_2}^*(\tau_2) j_{i'_1}(\tau'_1) j_{i'_2}(\tau'_2) + \dots
\end{aligned} \tag{4.33}$$

For the case  $J_{ij} = 0$ , the Eq. (4.31) implies that

$$W_0[j^*, j] = \sum_i W_i[j_i^*, j_i], \tag{4.34}$$

where each of these local terms can be expanded in a power of the sources  $j^*$  and  $j$

$$\begin{aligned}
W_{0i}[j^*, j] = & W_{0i}^{(0)} + \int_0^\beta d\tau \int_0^\beta d\tau' W_{0i}^{(2)}(\tau; \tau') j_i^*(\tau) j_i(\tau') \\
& + \frac{1}{2!^2} \int_0^\beta d\tau_1 \int_0^\beta d\tau_2 \int_0^\beta d\tau'_1 \int_0^\beta d\tau'_2 W_{0i}^{(4)}(\tau_1, \tau_2; \tau'_1, \tau'_2) j_i^*(\tau_1) j_i^*(\tau_2) j_i(\tau'_1) j_i(\tau'_2) + \dots,
\end{aligned} \tag{4.35}$$

where the functions  $W_{0i}^{(2n)}(\tau_i, \dots, \tau_n; \tau'_1, \dots, \tau'_n)$  are the so called local  $2n$ -point correlation functions.

### 4.3. Diagrammatic Representation

Now, by using a diagrammatic notation similar to the one in Ref. [63], we represent diagrammatically the local correlation functions as

$$W_{0i}^{(2n)}(\tau_i, \dots, \tau_n; \tau'_1, \dots, \tau'_n) = \begin{array}{c} \tau'_1 \\ \tau'_2 \\ \vdots \\ \tau'_n \end{array} \begin{array}{c} \nearrow \\ \nearrow \\ \vdots \\ \nearrow \end{array} \bullet_i \begin{array}{c} \nwarrow \\ \nwarrow \\ \vdots \\ \nwarrow \end{array} \begin{array}{c} \tau_1 \\ \tau_2 \\ \vdots \\ \tau_n \end{array}, \tag{4.36}$$

where the central point as well as its label stands for a given lattice site while the external legs are labeled with the respective time variables.

Similarly the functional  $W_0[j^*, j]$  can be represented as a sum of 1-vertex diagrams

$$W_0[j^*, j] = \bullet + \begin{array}{c} \nearrow \\ \nearrow \end{array} \bullet \begin{array}{c} \nwarrow \\ \nwarrow \end{array} + \frac{1}{2!^2} \begin{array}{c} \nearrow \nearrow \\ \nwarrow \nwarrow \end{array} \bullet \begin{array}{c} \nwarrow \nwarrow \\ \nearrow \nearrow \end{array} + \frac{1}{3!^2} \begin{array}{c} \nearrow \nearrow \nearrow \\ \nwarrow \nwarrow \nwarrow \end{array} \bullet \begin{array}{c} \nwarrow \nwarrow \nwarrow \\ \nearrow \nearrow \nearrow \end{array} + \dots, \tag{4.37}$$

where each diagram corresponds to a term in the series (4.35). Unlike (4.36), it is not necessary to include the imaginary-time indices attached to the legs nor the site index  $i$  attached to the central point of a diagram, as these are only dummy indices. Nevertheless, we must keep in mind that an unlabeled point means a sum running over all lattices sites while unlabeled inward (outward) lines mean a multiplication by  $j$  ( $j^*$ ) and integration from 0 to  $\beta$  in imaginary time. This leads to an exact correspondence between the terms in (4.35) and (4.37). Observe that each diagram has a symmetry factor  $\frac{1}{n!^2}$ , where  $n!^2$  is the number of permutations of inward and outward lines.

#### 4. Bosonic Lattices at Finite Temperature

The unperturbed partition function is by definition given by  $Z_0 = e^{-\beta F^{(0)}}$ . Here, in order to simplify our notation we represent the  $l$ -th term in (4.37) by  $D_l$ . Thus, the unperturbed partition function becomes

$$Z_0 = e^{\sum_{l=0}^{\infty} D_l} = \prod_{l=0}^{\infty} e^{D_l} = \prod_{l=0}^{\infty} \sum_{n_l=0}^{\infty} \frac{1}{n_l!} D_l^{n_l}, \quad (4.38)$$

This means that  $Z^{(0)}$  is composed by sums of all possible products of powers  $D_l^{n_l}$  of  $D_l$  multiplied by the symmetry factor  $\frac{1}{n_l!}$ . Such products of diagrams are also named disconnected diagrams. The unperturbed partition function can then be diagrammatically expressed as

$$Z^{(0)}\{j^*, j\} = e \cdot \left\{ \begin{array}{l} \text{---} \bullet \text{---} + \frac{1}{2!} \begin{array}{c} \text{---} \bullet \text{---} \\ \text{---} \bullet \text{---} \end{array} + \frac{1}{2!^2} \begin{array}{c} \text{---} \bullet \text{---} \\ \text{---} \bullet \text{---} \end{array} + \frac{1}{2!^2} \begin{array}{c} \text{---} \bullet \text{---} \\ \text{---} \bullet \text{---} \end{array} + \\ \frac{1}{3!} \begin{array}{c} \text{---} \bullet \text{---} \\ \text{---} \bullet \text{---} \\ \text{---} \bullet \text{---} \end{array} + \frac{1}{3!^2} \begin{array}{c} \text{---} \bullet \text{---} \\ \text{---} \bullet \text{---} \\ \text{---} \bullet \text{---} \end{array} + \dots \end{array} \right\}, \quad (4.39)$$

According to (4.29), we can obtain the  $n$ -th order hopping correction to the full partition function by applying  $n$  times the operator  $\sum_{ii'} J_{ii'} \int_0^\beta d\tau \frac{\delta^2}{\delta j_i^*(\tau) \delta j_{i'}(\tau)}$  to  $Z^{(0)}$  and multiplying the result by  $\frac{1}{n!}$ . We translate diagrammatically the effect of the functional derivatives  $\frac{\delta}{\delta j_i(\tau)}$  or  $\frac{\delta}{\delta j_i^*(\tau)}$  on a local diagram  $D_l$  as the introduction of the index  $i$  to the central point of the diagram and of the time variable  $\tau$  to its inward or outward lines, respectively. Similarly the effect of the full operator  $\sum_{ii'} J_{ii'} \int_0^\beta \frac{\delta^2}{\delta j_i^*(\tau) \delta j_{i'}(\tau)}$  acting on a product of diagrams is to generate a sum of all products of diagrams which are generated by joining an inward line of a diagram to the outward of another disconnected diagram. This process creates other kinds of diagrams which contain vertices connected by internal lines.

Now we can diagrammatically represent the full partition function to any desired order in the sources, as well as in the hopping elements  $J_{ij}$ . For example, up to 2nd order in the currents  $j^*$  and  $j$ , and first order in  $J_{ii'}$ , we have

$$Z\{j^*, j\} = e \cdot \left\{ \begin{array}{l} \text{---} \bullet \text{---} + \frac{1}{2!} \begin{array}{c} \text{---} \bullet \text{---} \\ \text{---} \bullet \text{---} \end{array} + \frac{1}{2!^2} \begin{array}{c} \text{---} \bullet \text{---} \\ \text{---} \bullet \text{---} \end{array} + \text{---} \bullet \text{---} \bullet \text{---} + \\ \text{---} \bullet \text{---} \bullet \text{---} + \frac{1}{2!} \begin{array}{c} \text{---} \bullet \text{---} \\ \text{---} \bullet \text{---} \end{array} + \frac{1}{2!} \begin{array}{c} \text{---} \bullet \text{---} \\ \text{---} \bullet \text{---} \end{array} + \dots \end{array} \right\}. \quad (4.40)$$

An interesting property of the series above is that its logarithm contains only connected diagrams as consequence of the so-called *linked-cluster theorem* [64]. That is the reason why we call  $W[j^*, j]$  the generating functional of connected diagrams whose expansion is given by

$$W\{j^*, j\} = \bullet + \text{---} \bullet \text{---} + \frac{1}{2!^2} \begin{array}{c} \text{---} \bullet \text{---} \\ \text{---} \bullet \text{---} \end{array} + \text{---} \bullet \text{---} \bullet \text{---} + \frac{1}{2!} \begin{array}{c} \text{---} \bullet \text{---} \\ \text{---} \bullet \text{---} \end{array} + \frac{1}{2!} \begin{array}{c} \text{---} \bullet \text{---} \\ \text{---} \bullet \text{---} \end{array} + \dots, \quad (4.41)$$

Now we summarize the diagrammatic rules for calculating  $Z[j^*, j]$  and  $W[j^*, j]$  as follows:

- The generator of disconnected diagram  $Z$  is obtained from the generator of connected diagrams

by  $Z = e^W$ .

- The functional  $W$  is composed by a sum of diagrams each one multiplied by a symmetry factor. Each diagram has  $n_v$  vertices,  $n_l$  external lines evenly divided in outward and inward lines, and  $n_i$  internal lines connecting all  $n_v$  vertices into one single piece. We also denote  $n_{v_l}$  the number of vertices in a diagram which are connected with lines.
- The perturbation theory is based on two expansions, one with respect to the sources  $j^*$  and  $j$ , and another with respect to the hopping matrix elements. The order of a diagram with respect to the sources  $j$  and  $j^*$  is given by the number of inward and outward lines in this diagram. The order of a diagram with respect to the hopping matrix  $J_{ij}$  is given by the number of internal lines in a diagram. Therefore, in order to compute the term of  $n$ -th order in the sources and  $m$ -th order in the hopping matrix, we must sum up all diagrams containing  $n$  external lines and  $m$  internal lines multiplied by their respective symmetry factor.
- The symmetry factor of a diagram can be calculated following the steps
  1. Take  $\frac{1}{n_i!}$
  2. Multiply by  $\frac{1}{n_{v_i}!}$  for each kind of vertex present in the diagram.
  3. For each vertex multiply with  $\frac{1}{n_{j_i}!n_{j_i^*}!}$ , where  $n_{j_i}$  and  $n_{j_i^*}$  are respectively the number of external lines going inward and outward the diagram, respectively.
  4. Multiply by the number of ways of joining the diagram vertices so that we obtain different topologies.

Now for sake of illustration let us calculate the symmetry factor for the diagram


(4.42)

Following the rules presented above, we have

1. Two internal lines:  $\frac{1}{2!} \dots$
2. One four-line and one two-line vertex:  $\frac{1}{2!} \times \frac{1}{1!} \times \frac{1}{1!} \dots$
3. One inward line and one outward line connected to the lower vertex:  $\frac{1}{2!} \times \frac{1}{1!} \times \frac{1}{1!} \times \frac{1}{1!} \times \frac{1}{1!} \dots$
4. The two internal lines can be connected to the vertices in two different ways:  $\frac{1}{2!} \times \frac{1}{1!} \times \frac{1}{1!} \times \frac{1}{1!} \times \frac{1}{1!} \times 2 = 1$

## 4.4. Effective Action and 1-Particle Irreducible Diagrams

In the previous section, we have shown that the diagrammatic representation remarkably simplifies the calculation of the system partition function. It shows that real computational effort is actually concentrated in the connected  $n$ -point functions. However, this diagrammatic approach allows us to

#### 4. Bosonic Lattices at Finite Temperature

simplify even further our calculations by using the so called 1-particle irreducible (1PI) diagrams. A 1PI diagram is defined as any connected diagram which cannot be separated into two different pieces by simply cutting one of its internal lines.

As the first example, let us take the two-point function which is also denoted as the Green function and plays a crucial role in the theory of critical phenomena as discussed in Chapter 3. By following the diagrammatic rules from the previous section, we can represent the Green function by

$$W_{ii'}(\tau; \tau') = \begin{array}{c} i'; \tau' \rightarrow \text{diagram} \rightarrow i; \tau = \delta_{ii'} \rightarrow \text{diagram} + \text{diagram} + \text{diagram} + \text{diagram} \\ + \delta_{ii'} \rightarrow \text{diagram} + \text{diagram} + \text{diagram} + \text{diagram} + \dots \end{array} \quad (4.43)$$

The 1PI Green function is defined as the sum of all 1PI diagrams in (4.43), i.e.,

$$W_{ii'}^{(1PI)}(\tau; \tau') = \begin{array}{c} i'; \tau' \rightarrow \text{diagram} \rightarrow i; \tau = \delta_{ii'} \rightarrow \text{diagram} + \delta_{ii'} \rightarrow \text{diagram} + \text{diagram} + \dots \end{array} \quad (4.44)$$

The full Green's function (4.43) can then be reconstructed by combining the 1PI Green's function in (4.44) with the hopping matrix. This can be diagrammatically represented as

$$i'; \tau' \rightarrow \text{diagram} \rightarrow i; \tau = \begin{array}{c} i'; \tau' \rightarrow \text{diagram} \rightarrow i; \tau \\ + i'; \tau' \rightarrow \text{diagram} \rightarrow \text{diagram} \rightarrow i; \tau \\ + i'; \tau' \rightarrow \text{diagram} \rightarrow \text{diagram} \rightarrow \text{diagram} \rightarrow i; \tau + \dots \end{array} \quad (4.45)$$

In general all  $n$ -point functions can be constructed out of 1PI diagrams. For example, for the 4-point function, we have

$$W_{i_1 i_2; i'_1 i'_2}^{(4)}(\tau_1, \tau_2; \tau'_1, \tau'_2) = \begin{array}{c} i'_2; \tau'_2 \rightarrow \text{diagram} \rightarrow i_2; \tau_2 \\ i'_1; \tau'_1 \rightarrow \text{diagram} \rightarrow i_1; \tau_1 \end{array} = \begin{array}{c} i'_2; \tau'_2 \rightarrow \text{diagram} \rightarrow i_2; \tau_2 \\ i'_1; \tau'_1 \rightarrow \text{diagram} \rightarrow i_1; \tau_1 \end{array} \quad (4.46)$$

Now, in addition to the generating functionals  $Z$  and  $W$  of the disconnected Green's functions and connected Green's function, we can also define the generating functional of the 1PI functions by a Legendre transformation of  $W$ :

$$-\beta \Gamma[\psi_i^*(\tau), \psi_i(\tau)] = W + \sum_i \int_0^\beta d\tau [\psi_i^*(\tau) j_i(\tau) + \psi_i(\tau) j_i^*(\tau)]. \quad (4.47)$$

Here the  $\beta$  factor in front of the first term is used in order to identify this generator with the effective action in (3.31).

The effective action also can be expressed as a power series of the fields  $\psi_i(\tau)$  and  $\psi_i^\dagger(\tau)$ , according to

$$\begin{aligned}
 -\beta\Gamma[\psi^*, \psi] = & \Gamma^{(0)} + \sum_{ii'} \int_0^\beta d\tau \int_0^\beta d\tau' \Gamma_{ii'}^{(2)}(\tau, \tau') \psi_i^*(\tau) \psi_{i'}(\tau') \\
 & + \frac{1}{2!^2} \sum_{i_1 i_2, i'_1 i'_2} \int_0^\beta d\tau_1 \int_0^\beta d\tau_2 \int_0^\beta d\tau'_1 \int_0^\beta d\tau'_2 \Gamma_{i_1 i_2, i'_1 i'_2}^{(4)}(\tau_1, \tau_2; \tau'_1, \tau'_2) \psi_{i_1}^*(\tau_1) \psi_{i_2}^*(\tau_2) \psi_{i'_1}(\tau'_1) \psi_{i'_2}(\tau'_2) + \dots
 \end{aligned} \tag{4.48}$$

By performing the Legendre transformation of (4.35) order by order in the fields  $\psi^*$  and  $\psi$ , we get the respective coefficients of (4.48)

$$\begin{aligned}
 \Gamma^{(0)} &= W^{(0)}, \\
 \Gamma_{ii'}^{(2)}(\tau, \tau') &= - \left[ W^{(2)} \right]_{ii'}^{-1}(\tau, \tau'), \\
 \Gamma_{i_1 i_2, i'_1 i'_2}^{(4)}(\tau_1, \tau_2; \tau'_1, \tau'_2) &= \sum_{i''_1 i''_2, i'''_1 i'''_2} \int_0^\beta d\tau''_1 \int_0^\beta d\tau''_2 \int_0^\beta d\tau'''_1 \int_0^\beta d\tau'''_2 W_{i''_1 i''_2, i'''_1 i'''_2}^{(4)}(\tau''_1, \tau''_2; \tau'''_1, \tau'''_2) \\
 &\quad \times \left[ W^{(2)} \right]_{i_1 i''_1}^{-1}(\tau_1, \tau''_1) \left[ W^{(2)} \right]_{i_2 i''_2}^{-1}(\tau_2, \tau''_2) \left[ W^{(2)} \right]_{i'_1 i'''_1}^{-1}(\tau'_1, \tau'''_1) \left[ W^{(2)} \right]_{i'_2 i'''_2}^{-1}(\tau'_2, \tau'''_2).
 \end{aligned} \tag{4.49}$$

These functions can now be diagrammatically expressed as

$$\Gamma_{ii'}^{(2)} = \text{diagram: a circle with two external legs, one labeled } i'; \tau' \text{ and the other } i; \tau \tag{4.50}$$

$$\Gamma_{i_1 i_2, i'_1 i'_2}^{(4)}(\tau_1, \tau_2; \tau'_1, \tau'_2) = \text{diagram: a circle with four external legs, labeled } i'_2; \tau'_2, i_2; \tau_2, i'_1; \tau'_1, \text{ and } i_1; \tau_1 \tag{4.51}$$

In general, these  $n$ -point diagrams are also named  $n$ -point amputated diagrams, as two-point function  $W_{ii'}^{(2)}(\tau, \tau')$  must still be attached to its legs in order to generate the  $n$ -point connected function, as depicted in (4.46) for the case of 4-point functions.

Now we can have our final formula for the effective action in terms of only 1PI diagrams

$$-\beta\Gamma = \Gamma^{(0)} + \text{diagram: a circle with two external legs} + \frac{1}{2!^2} \text{diagram: a circle with four external legs} + \frac{1}{3!^2} \text{diagram: a circle with six external legs} + \dots \tag{4.52}$$

The explicit calculation of these 1PI will be shown in the following sections.

## 4.5. Matsubara Representation

Due to the time invariance of the systems considered in this thesis, our calculations can be even more simplified if, instead of using the imaginary-time as an independent variable, we work in frequency space. As our imaginary-time variable runs from 0 to  $\beta$ , we must perform a so-called Matsubara transformation in all our functions. For an arbitrary single-variable function  $g(\tau)$ , such as the source

#### 4. Bosonic Lattices at Finite Temperature

field  $j_i(\tau)$  or the order order-parameter field  $\psi_i(\tau)$ , this transformation has the form

$$f(\omega_n) = \int_0^\beta d\tau e^{i\omega^{(l)}\tau} f(\tau), \quad (4.53)$$

where the discrete variable  $\omega^{(l)} = (2\pi/\beta)l$  are known as Matsubara frequencies. Analogously, for an arbitrary multivariable function  $M(\tau_1, \dots, \tau_n; \tau'_1, \dots, \tau'_n)$  like  $W^{(2n)}$  and  $\Gamma^{(2n)}$ , the Matsubara transformation reads

$$M(\omega_1, \dots, \omega_n; \omega'_1, \dots, \omega'_n) = \int_0^\beta d\tau_1 \dots \int_0^\beta d\tau_n \int_0^\beta d\tau'_1 \dots \int_0^\beta d\tau'_n e^{i(\omega_1\tau_1 + \dots + \omega_n\tau_n - \omega'_1\tau'_1 - \dots - \omega'_n\tau'_n)} M(\tau_1, \dots, \tau_n; \tau'_1, \dots, \tau'_n),$$

where we dropped here the upper  $l$  indices in order to simplify the notation.

The inverse Matsubara transformations are given by

$$f(\tau) = \frac{1}{\beta} \sum_{\omega} e^{-i\omega\tau} f(\omega), \quad (4.54)$$

$$M(\tau_1, \dots, \tau_n; \tau'_1, \dots, \tau'_n) = \frac{1}{\beta^{2n}} \sum_{\omega_1 \dots \omega_n} \sum_{\omega'_1 \dots \omega'_n} e^{-i(\omega_1\tau_1 + \dots + \omega_n\tau_n - \omega'_1\tau'_1 - \dots - \omega'_n\tau'_n)} M(\omega_1, \dots, \omega_n; \omega'_1, \dots, \omega'_n). \quad (4.55)$$

Now we can express all our functionals in Matsubara space. For example, by substituting (4.54) and (4.55) into (4.56) and (4.48), we have

$$W[j^*, j] = W^{(0)} + \frac{1}{\beta^2} \sum_{ii'} \sum_{\omega\omega'} W_{ii'}^{(2)}(\omega, \omega') j_i^*(\omega) j_i(\omega') + \frac{1}{2!^2} \frac{1}{\beta^4} \sum_{i_1 i_2, i'_1 i'_2} \sum_{\omega_1 \omega_2; \omega'_1 \omega'_2} W_{i_1 i_2; i'_1 i'_2}^{(4)}(\omega_1, \omega_2; \omega'_1, \omega'_2) j_{i_1}^*(\omega_1) j_{i_2}^*(\omega_2) j_{i'_1}(\omega'_1) j_{i'_2}(\omega'_2) + \dots \quad (4.56)$$

$$-\beta\Gamma[\psi^*, \psi] = \Gamma^{(0)} + \frac{1}{\beta^2} \sum_{ii'} \sum_{\omega\omega'} \Gamma_{ii'}^{(2)}(\omega, \omega') \psi_i^*(\omega) \psi_i(\omega') + \frac{1}{2!^2} \frac{1}{\beta^4} \sum_{i_1 i_2, i'_1 i'_2} \sum_{\omega_1 \omega_2; \omega'_1 \omega'_2} \Gamma_{i_1 i_2; i'_1 i'_2}^{(4)}(\omega_1, \omega_2; \omega'_1, \omega'_2) \psi_{i_1}^*(\omega_1) \psi_{i_2}^*(\omega_2) \psi_{i'_1}(\omega'_1) \psi_{i'_2}(\omega'_2) + \dots \quad (4.57)$$

Observe that functionals (4.56) and (4.57) are very similar to (4.33) and (4.48). In fact they differ only by the substitutions



$$\tau_n \rightarrow \omega_n, \quad (4.58)$$

$$\int_0^\beta d\tau_n \rightarrow \frac{1}{\beta} \sum_{\omega_n}. \quad (4.59)$$

This means that all diagrammatic rules previously discussed here also apply to Matsubara space if we consider the substitutions (4.58) and (4.59).

Another advantage of using the Matsubara representation is that all  $n$ -point functions are invariant under the transformation

$$\begin{aligned} f_i(n) &\rightarrow f_i(n) + in\omega, \\ \omega_n &\rightarrow \omega_n + \omega. \end{aligned} \quad (4.60)$$

## 4.6. Zeroth-Hopping Order Effective Action

The starting point in our calculations is to find the effective action for  $J_{ij} = 0$ . In this case the system is split into independent lattice sites and, therefore, its effective action can be represented as

$$\Gamma[\psi^*, \psi] = \sum_i \Gamma_i(\psi_i^*, \psi_i), \quad (4.61)$$

where the local actions  $\Gamma_i$  are given by

$$\begin{aligned} -\beta\Gamma_i(\psi_i^*, \psi_i) &= \Gamma_{0i}^{(0)} + \int_0^\beta d\tau \int_0^\beta d\tau' \Gamma_{0i}^{(2)}(\tau, \tau') \psi_i^*(\tau) \psi_i(\tau') + \\ &+ \frac{1}{2!^2} \int_0^\beta d\tau_1 \int_0^\beta d\tau_2 \int_0^\beta d\tau'_1 \int_0^\beta d\tau'_2 \Gamma_{0i}^{(4)}(\tau_1, \tau_2; \tau'_1, \tau'_2) \psi_i^*(\tau_1) \psi_i^*(\tau_2) \psi_i(\tau'_1) \psi_i(\tau'_2) + \dots \end{aligned} \quad (4.62)$$

This series can also be diagrammatically represented as

$$-\beta\Gamma_{0i} = \Gamma_{0i}^{(0)} + \text{---}\bullet_i\text{---} + \frac{1}{2!^2} \text{---}\bullet_i\text{---} + \frac{1}{3!^2} \text{---}\bullet_i\text{---} + \dots \quad (4.63)$$

Here  $-\beta\Gamma_i(\psi_i^*, \psi_i)$  is the Legendre transform of  $W_i(j_i^*, j_i)$ . This means that the term  $\Gamma_{0i}^{(0)}$  appearing in its expansion must be equal to  $W_{0i}^{(0)}$  which, therefore

$$\Gamma_{0i}^{(0)} = \ln \sum_{n=0}^{\infty} e^{-\beta f_i(n)}. \quad (4.64)$$

If someone is interested only in the zero-temperature, must observe that in this limit we have

$$-\beta^{-1}\Gamma_{0i}^{(0)} \rightarrow f_i(n). \quad (4.65)$$

#### 4. Bosonic Lattices at Finite Temperature

The next term to be considered is  $\Gamma_{0i}^{(2)}$ . According to (4.49), it can be obtained by inverting

$$W_{0i}^{(2)}(\tau, \tau') = \frac{1}{Z_0} \text{Tr} \left\{ e^{-\beta \hat{H}_0 \hat{T}} \left[ \hat{a}_i^\dagger(\tau') \hat{a}_i(\tau) \right] \right\}. \quad (4.66)$$

The direct evaluation yields

$$W_{0i}^{(2)}(\tau, \tau') = \frac{1}{Z_0} \sum_{n=0}^{\infty} e^{-\beta f_i(n)} \left\{ \theta(\tau - \tau')(n+1) e^{(\tau - \tau')[f_i(n) - f_i(n+1)]} + \theta(\tau' - \tau) n e^{(\tau' - \tau)[f_i(n) - f_i(n+1)]} \right\}, \quad (4.67)$$

which is given, in the Matsubara representation, by

$$W_{0i}^{(2)}(\omega, \omega') = \beta \delta_{\omega, \omega'} g_i(\omega), \quad (4.68)$$

where  $\delta_{\omega, \omega'}$  is the Kronecker delta symbol and

$$g_i(\omega) = \frac{1}{Z_{0i}} \sum_{n=0}^{\infty} (n+1) \frac{e^{-\beta f_i(n+1)} - e^{-\beta f_i(n)}}{i\omega + f_i(n) - f_i(n+1)}. \quad (4.69)$$

Now the inverse must obey the equation

$$\frac{1}{\beta} \sum_{\omega''} W_{0i}^{(2)}(\omega, \omega'') \Gamma_{0i}^{(2)}(\omega'', \omega') = \frac{1}{\beta} \sum_{\omega''} \Gamma_{0i}^{(2)}(\omega, \omega'') W_{0i}^{(2)}(\omega'', \omega') = -\beta \delta_{\omega \omega'}. \quad (4.70)$$

The diagonal form of  $W_{0i}^{(2)}$  in the Matsubara representation makes its inversion very simple, thus giving

$$\Gamma_{0i}^{(2)}(\omega, \omega') = -\beta \delta_{\omega, \omega'} Z_0 \left[ \sum_{n=0}^{\infty} (n+1) \frac{e^{-\beta f_i(n+1)} - e^{-\beta f_i(n)}}{i\omega + f_i(n) - f_i(n+1)} \right]^{-1}. \quad (4.71)$$

In order to get the zero-temperature limit of  $\Gamma_{0i}^{(2)}(\omega, \omega')$ , we must at first observe that the Matsubara sums and Kronecker deltas transform in this limit into frequency integrals and Dirac deltas, respectively, according to

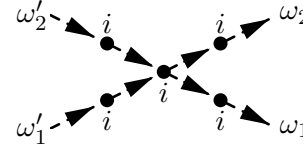
$$\frac{1}{\beta} \sum_{\omega} \rightarrow \frac{1}{2\pi} \int d\omega, \quad (4.72)$$

$$\beta \delta_{\omega, \omega'} \rightarrow 2\pi \delta(\omega - \omega'). \quad (4.73)$$

Therefore the zero-temperature limit of  $\Gamma_{0i}^{(2)}(\omega, \omega')$  reads

$$\Gamma_{0i}^{(2)}(\omega, \omega') \rightarrow -2\pi \delta(\omega - \omega') \left[ \frac{n}{i\omega + f_i(n-1) - f_i(n)} - \frac{n+1}{i\omega + f_i(n) - f_i(n+1)} \right]^{-1}. \quad (4.74)$$

Now we must calculate the term  $\Gamma_{0i}^{(4)}$ , in order to construct our Ginzburg-Landau expansion. Its diagrammatic representation is

$$\Gamma_{0i}^{(4)}(\omega_1, \omega_2; \omega'_1, \omega'_2) =$$

(4.75)

This representation shows that  $\Gamma_{0i}^{(4)}$  can be constructed from  $W^{(4)}$  and  $\Gamma^{(2)}$  according to

$$\Gamma_{0i}^{(4)}(\omega_1, \omega_2; \omega'_1, \omega'_2) = \frac{1}{\beta^4} \sum_{\omega''_1 \omega''_2 \omega'''_1 \omega'''_2} W_{0i}^{(4)}(\omega''_1, \omega''_2; \omega'''_1, \omega'''_2) \Gamma_{0i}^{(2)}(\omega_1; \omega''_1) \Gamma_{0i}^{(2)}(\omega_2; \omega''_2) \Gamma_{0i}^{(2)}(\omega'_1; \omega'''_1) \Gamma_{0i}^{(2)}(\omega'_2; \omega'''_2). \quad (4.76)$$

This means that we must calculate first the explicit form of  $W_{0i}^{(4)}$ , in order to obtain an explicit formula for  $\Gamma_{0i}^{(4)}$ .

In the imaginary-time representation  $W_{0i}^{(4)}$  reads

$$W_{0i}^{(4)}(\tau_1, \tau_2; \tau'_1, \tau'_2) = G_{0i}^{(4)}(\tau_1, \tau_2; \tau'_1, \tau'_2) - W_{0i}^{(2)}(\tau_1; \tau'_1) W_{0i}^{(2)}(\tau_2; \tau'_2) - W_{0i}^{(2)}(\tau_1; \tau'_2) W_{0i}^{(2)}(\tau_2; \tau'_1), \quad (4.77)$$

where  $G_{0i}^{(4)}(\tau_1, \tau_2; \tau'_1, \tau'_2)$  explicitly reads

$$\begin{aligned} G_{0i}^{(4)}(\tau_1, \tau_2; \tau'_1, \tau'_2) &= \frac{1}{Z_{0i}} \text{Tr} \left\{ e^{-\beta \hat{H}_0} \hat{T} \left[ \hat{a}_i(\tau_1) \hat{a}_i(\tau_2) \hat{a}_i^\dagger(\tau'_1) \hat{a}_i^\dagger(\tau'_2) \right] \right\} = \frac{1}{Z_{0i}} \sum_{n=0}^{\infty} e^{-\beta f_i(n)} \\ &\times \left\{ \theta(\tau_1 - \tau_2) \theta(\tau_2 - \tau'_1) \theta(\tau'_1 - \tau'_2) (n+1)(n+2) \right. \\ &\times e^{\tau_1[f_i(n) - f_i(n+1)]} e^{\tau_2[f_i(n+1) - f_i(n+2)]} e^{\tau'_1[f_i(n+2) - f_i(n+1)]} e^{\tau'_2[f_i(n+1) - f_i(n)]} \\ &+ \theta(\tau_1 - \tau'_1) \theta(\tau'_1 - \tau_2) \theta(\tau_2 - \tau'_2) (n+1)^2 \\ &\times e^{\tau_1[f_i(n) - f_i(n+1)]} e^{\tau'_1[f_i(n+1) - f_i(n)]} e^{\tau_2[f_i(n) - f_i(n+1)]} e^{\tau'_2[f_i(n+1) - f_i(n)]} \\ &+ \theta(\tau'_1 - \tau_1) \theta(\tau_1 - \tau_2) \theta(\tau_2 - \tau'_2) n(n+1) \\ &\times e^{\tau'_1[f_i(n) - f_i(n-1)]} e^{\tau_1[f_i(n-1) - f_i(n)]} e^{\tau_2[f_i(n) - f_i(n+1)]} e^{\tau'_2[f_i(n+1) - f_i(n)]} \\ &+ \theta(\tau'_1 - \tau'_2) \theta(\tau'_2 - \tau'_1) \theta(\tau_1 - \tau_2) n(n-1) \\ &\times e^{\tau'_1[f_i(n) - f_i(n-1)]} e^{\tau'_2[f_i(n-1) - f_i(n-2)]} e^{\tau_1[f_i(n-2) - f_i(n-1)]} e^{\tau_2[f_i(n-1) - f_i(n)]} \\ &+ \theta(\tau'_1 - \tau_1) \theta(\tau_1 - \tau'_2) \theta(\tau'_2 - \tau_2) n^2 \\ &\times e^{\tau'_1[f_i(n) - f_i(n-1)]} e^{\tau_1[f_i(n-1) - f_i(n)]} e^{\tau'_2[f_i(n) - f_i(n-1)]} e^{\tau_2[f_i(n-1) - f_i(n)]} \\ &+ \theta(\tau_1 - \tau'_1) \theta(\tau'_1 - \tau'_2) \theta(\tau'_2 - \tau_2) n(n+1) \\ &\times e^{\tau_1[f_i(n) - f_i(n+1)]} e^{\tau'_1[f_i(n+1) - f_i(n)]} e^{\tau'_2[f_i(n) - f_i(n-1)]} e^{\tau_2[f_i(n-1) - f_i(n)]} \\ &\left. + \begin{array}{l} \tau_1 \leftrightarrow \tau_2 \\ \tau'_1 \leftrightarrow \tau'_2 \end{array} \right\}, \quad (4.78) \end{aligned}$$

where the last line denotes the remaining permutations of  $\tau_1$  with  $\tau_2$  and of  $\tau'_1$  with  $\tau'_2$ .

Now we have to calculate  $G_{0i}^{(4)}$  in the Matsubara representation. In principle, it would be a very long calculation as we should calculate a total of 6 four-fold integrals, each one corresponding to a single term in (4.78). However, due to time-translation invariance of the considered system, we have

#### 4. Bosonic Lattices at Finite Temperature

to calculate only 3 three-fold integrals. In Appendix A, it is shown that we actually can set one of the imaginary-time variables equal to zero and integrate the other variables so that  $G_{0i}^{(4)}$  is given, in the Matsubara representation, by

$$G_{0i}^{(4)}(\omega_1, \omega_2; \omega'_1, \omega'_2) = \beta \delta_{\omega'_1 + \omega'_2, \omega_1 + \omega_2} \int_0^\beta d\tau_1 \int_0^\beta d\tau_2 \int_0^\beta d\tau'_1 e^{-i(\omega_1 \tau_1 + \omega_2 \tau_2 - \omega'_1 \tau'_1)} G_{0i}^{(4)}(\tau_1, \tau_2; \tau'_1, 0). \quad (4.79)$$

By inserting the formula (4.78) for  $G_{0i}^{(4)}$ , we get

$$\begin{aligned} G_{0i}^{(4)}(\omega_1, \omega_2; \omega'_1, \omega'_2) &= \frac{\beta}{Z_{0i}} \delta_{\omega'_1 + \omega'_2, \omega_1 + \omega_2} \\ &\times \sum_{n=0}^{\infty} e^{-\beta f_i(n)} \{ (n+1)^2 I [i\omega_2 + f_i(n) - f_i(n+1), -i\omega'_1 + f_i(n+1) - f_i(n), i\omega_1 + f_i(n) - f_i(n+1)] \\ &\quad + (n+1)(n+2) I [i\omega_2 + f_i(n) - f_i(n+1), i\omega_1 + f_i(n+1) - f_i(n+2), -i\omega'_1 + f_i(n+2) - f_i(n+1)] \\ &\quad + n(n+1) I [-i\omega'_1 + f_i(n) - f_i(n-1), i\omega_2 + f_i(n-1) - f_i(n), i\omega_1 + f_i(n) - f_i(n+1)] \\ &\quad + \omega'_1 \leftrightarrow \omega_1 \}, \end{aligned} \quad (4.80)$$

$$(4.81)$$

where the function  $I(x_3, x_2, x_1)$  represents the integral

$$I(x_3, x_2, x_1) = \int_0^\beta d\tau_3 \int_0^{\tau_3} d\tau_2 \int_0^{\tau_2} d\tau_1 e^{x_3 \tau_3 + x_2 \tau_2 + x_1 \tau_1}. \quad (4.82)$$

The direct calculation of this integral gives

$$\begin{aligned}
& I \left[ i\omega_2 + f_i(n) - f_i(n+1), -i\omega'_1 + f_i(n+1) - f_i(n), i\omega_1 + f_i(n) - f_i(n+1) \right] \\
&= \frac{e^{-\beta[f_i(n+1)-f_i(n)]} - 1}{[f_i(n+1) - f_i(n+2) + i\omega_1][f_i(n) - f_i(n+1) + i\omega_2][f_i(n+2) - f_i(n+1) - i\omega'_1]} \\
&- \frac{e^{-\beta[f_i(n+2)-f_i(n)]} - 1}{[f_i(n+1) - f_i(n+2) + i\omega_1][f_i(n) - f_i(n+2) + i\omega_1 + i\omega_2][f_i(n+2) - f_i(n+1) - i\omega'_1]} \\
&+ \frac{\beta\delta_{\omega_1, \omega'_1} e^{-\beta[f_i(n+1)-f_i(n)]}}{[f_i(n+2) - f_i(n+1) - i\omega'_1][f_i(n) - f_i(n+1) + i\omega_2]} \\
&- \frac{e^{-\beta[f_i(n+1)-f_i(n)]} - 1}{[f_i(n+2) - f_i(n+1) - i\omega'_1][f_i(n) - f_i(n+1) + i\omega_1 + i\omega_2 - i\omega'_1][f_i(n) - f_i(n+1) + i\omega_2]}, \\
& I \left[ -i\omega'_1 + f_i(n) - f_i(n-1), i\omega_2 + f_i(n-1) - f_i(n), i\omega_1 + f_i(n) - f_i(n+1) \right]
\end{aligned} \tag{4.83}$$

$$\begin{aligned}
&= \frac{e^{-\beta[f_i(n-1)-f_i(n)]} - 1}{[f_i(n) - f_i(n+1) + i\omega_1][f_i(n-1) - f_i(n) + i\omega_2][f_i(n) - f_i(n-1) - i\omega'_1]} \\
&- \frac{e^{-\beta[f_i(n-1)-f_i(n)]} - 1}{[f_i(n) - f_i(n+1) + i\omega_1][f_i(n-1) - f_i(n+1) + i\omega_1 + i\omega_2][f_i(n) - f_i(n-1) - i\omega'_1]} \\
&+ \frac{\beta\delta_{\omega_2, \omega'_1}}{[f_i(n) - f_i(n+1) + i\omega_1][f_i(n-1) - f_i(n) + i\omega_2]} \\
&- \frac{e^{-\beta[f_i(n+1)-f_i(n)]} - 1}{[f_i(n) - f_i(n+1) + i\omega_1][f_i(n-1) - f_i(n+1) + i\omega_1 + i\omega_2][f_i(n) - f_i(n+1) + i\omega_1 + i\omega_2 - i\omega'_1]}, \\
& I \left[ i\omega_2 + f_i(n) - f_i(n+1), -i\omega'_1 + f_i(n+1) - f_i(n), i\omega_1 + f_i(n) - f_i(n+1) \right]
\end{aligned} \tag{4.84}$$

$$\begin{aligned}
&= \frac{e^{-\beta[f_i(n+1)-f_i(n)]} - 1}{[f_i(n) - f_i(n+1) + i\omega_1][f_i(n) - f_i(n+1) + i\omega_2][f_i(n+1) - f_i(n) - i\omega'_1]} \\
&- \frac{\beta\delta_{\omega_2, \omega'_1}}{[f_i(n) - f_i(n+1) + i\omega_1][f_i(n+1) - f_i(n) - i\omega'_1]} + \frac{\beta\delta_{\omega_2, \omega'_1} e^{-\beta[f_i(n+1)-f_i(n)]}}{[f_i(n) - f_i(n+1) + i\omega_1][f_i(n) - f_i(n+1) + i\omega_2]} \\
&- \frac{e^{-\beta[f_i(n+1)-f_i(n)]} - 1}{[f_i(n) - f_i(n+1) + i\omega_1][f_i(n) - f_i(n+1) + i\omega_1 + i\omega_2 - i\omega'_1][f_i(n) - f_i(n+1) + i\omega_2]}.
\end{aligned} \tag{4.85}$$

By substituting these results into (4.81) and simplifying the terms with the help of the condition  $\omega'_1 + \omega'_2 = \omega_1 + \omega_2$ , we get

$$\begin{aligned}
 G_{0i}^{(4)}(\omega_1, \omega_2; \omega'_1, \omega'_2) = & \frac{\beta^2}{Z_{0i}} \left( \delta_{\omega_1, \omega'_1} \delta_{\omega_2, \omega'_2} + \delta_{\omega_1, \omega'_2} \delta_{\omega_2, \omega'_1} \right) \\
 & \times \sum_{n=0}^{\infty} e^{-\beta f_i(n)} \left[ \frac{n+1}{f_i(n+1) - f_i(n) - i\omega_2} + \frac{n}{f_i(n-1) - f_i(n) + i\omega_2} \right] \\
 & \times \left[ \frac{n+1}{f_i(n+1) - f_i(n) - i\omega_1} + \frac{n}{f_i(n-1) - f_i(n) + i\omega_1} \right] \\
 & + \frac{\beta}{Z_{0i}} \delta_{\omega'_1 + \omega'_2, \omega_1 + \omega_2} \sum_{n=0}^{\infty} e^{-\beta f_i(n)} \\
 & \times \left( \frac{(n+2)(n+1)}{[f_i(n+1) - f_i(n) - i\omega'_2][f_i(n+2) - f_i(n) - i\omega'_1 - i\omega'_2][f_i(n+1) - f_i(n) - i\omega_1]} \right. \\
 & \quad \left. + \frac{n(n-1)}{[f_i(n-1) - f_i(n) + i\omega_2][f_i(n-1) - f_i(n) + i\omega'_1][f_i(n-2) - f_i(n) + i\omega_1 + i\omega_2]} \right. \\
 & \quad \left. - \left\{ \frac{n+1}{[f_i(n+1) - f_i(n) - i\omega_1][f_i(n+1) - f_i(n) + i\omega'_1]} + \frac{n}{[f_i(n-1) - f_i(n) + i\omega_1][f_i(n-1) - f_i(n) + i\omega'_1]} \right\} \right. \\
 & \quad \left. \times \left\{ \frac{n+1}{f_i(n+1) - f_i(n) - i\omega'_2} + \frac{n}{f_i(n-1) - f_i(n) + i\omega_2} \right\} + \frac{\omega'_1 \leftrightarrow \omega'_2}{\omega_1 \leftrightarrow \omega_2} \right). \tag{4.86}
 \end{aligned}$$

This leads to the final expression for  $W_{0i}^{(4)}$

$$\begin{aligned}
 W_{0i}^{(4)}(\omega_1, \omega_2; \omega'_1, \omega'_2) = & \frac{\beta^2}{Z_{0i}} \left( \delta_{\omega_1, \omega'_1} \delta_{\omega_2, \omega'_2} + \delta_{\omega_1, \omega'_2} \delta_{\omega_2, \omega'_1} \right) \\
 & \times \left\{ \sum_{n=0}^{\infty} e^{-\beta f_i(n)} \left[ \frac{n+1}{f_i(n+1) - f_i(n) - i\omega_2} + \frac{n}{f_i(n-1) - f_i(n) + i\omega_2} \right] \right. \\
 & \times \left[ \frac{n+1}{f_i(n+1) - f_i(n) - i\omega_1} + \frac{n}{f_i(n-1) - f_i(n) + i\omega_1} \right] \\
 & - \frac{1}{Z_{0i}} \sum_{m,n=0}^{\infty} e^{-\beta[f_i(n)+f_i(m)]} \left[ \frac{n+1}{f_i(n+1) - f_i(n) - i\omega_2} + \frac{n}{f_i(n-1) - f_i(n) + i\omega_2} \right] \\
 & \times \left[ \frac{m+1}{f_i(m+1) - f_i(m) - i\omega_1} + \frac{m}{f_i(m-1) - f_i(m) + i\omega_1} \right] \Big\} \\
 & + \frac{\beta}{Z_{0i}} \delta_{\omega'_1 + \omega'_2, \omega_1 + \omega_2} \sum_{n=0}^{\infty} e^{-\beta f_i(n)} \left( \frac{(n+2)(n+1)}{[f_i(n+1) - f_i(n) - i\omega'_2][f_i(n+2) - f_i(n) - i\omega'_1 - i\omega'_2][f_i(n+1) - f_i(n) - i\omega_1]} \right. \\
 & \quad \left. + \frac{n(n-1)}{[f_i(n-1) - f_i(n) + i\omega_2][f_i(n-1) - f_i(n) + i\omega'_1][f_i(n-2) - f_i(n) + i\omega_1 + i\omega_2]} \right. \\
 & \quad \left. - \left\{ \frac{n+1}{[f_i(n+1) - f_i(n) - i\omega_1][f_i(n+1) - f_i(n) - i\omega'_1]} + \frac{n}{[f_i(n-1) - f_i(n) + i\omega_1][f_i(n-1) - f_i(n) + i\omega'_1]} \right\} \right. \\
 & \quad \left. \times \left\{ \frac{n+1}{f_i(n+1) - f_i(n) - i\omega'_2} + \frac{n}{f_i(n-1) - f_i(n) + i\omega_2} \right\} + \frac{\omega'_1 \leftrightarrow \omega'_2}{\omega_1 \leftrightarrow \omega_2} \right). \tag{4.87}
 \end{aligned}$$

Finally we can construct  $\Gamma_{0i}^{(4)}$  in following way

$$\Gamma_{0i}^{(4)}(\omega_1, \omega_2; \omega'_1, \omega'_2) = \frac{W_{0i}^{(4)}(\omega_1, \omega_2; \omega'_1, \omega'_2)}{g(\omega_1)g(\omega'_1)g(\omega_2)g(\omega'_2)}. \quad (4.88)$$

The zero-temperature of  $\Gamma_{0i}^{(4)}(\omega_1, \omega_2; \omega'_1, \omega'_2)$  can be obtained by observing that

$$\begin{aligned} & W_{0i}^{(4)}(\omega_1, \omega_2; \omega'_1, \omega'_2) \rightarrow \\ & + 2\pi\delta(\omega'_1 + \omega'_2 - \omega_1 - \omega_2) \left( \frac{(n+2)(n+1)}{[f_i(n+1) - f_i(n) - i\omega'_2][f_i(n+2) - f_i(n) - i\omega'_1 - i\omega'_2][f_i(n+1) - f_i(n) - i\omega_1]} \right. \\ & \quad \left. + \frac{n(n-1)}{[f_i(n-1) - f_i(n) + i\omega_2][f_i(n-1) - f_i(n) + i\omega'_1][f_i(n-2) - f_i(n) + i\omega_1 + i\omega_2]} \right. \\ & \quad \left. - \left\{ \frac{n+1}{[f_i(n+1) - f_i(n) - i\omega_1][f_i(n+1) - f_i(n) - i\omega'_1]} + \frac{n}{[f_i(n-1) - f_i(n) + i\omega_1][f_i(n-1) - f_i(n) + i\omega'_1]} \right\} \right. \\ & \quad \left. \times \left\{ \frac{n+1}{f_i(n+1) - f_i(n) - i\omega'_2} + \frac{n}{f_i(n-1) - f_i(n) + i\omega_2} \right\} + \frac{\omega'_1 \leftrightarrow \omega'_2}{\omega_1 \leftrightarrow \omega_2} \right), \end{aligned} \quad (4.89)$$

while for  $g_i(\omega)$  we have

$$g_i(\omega) \rightarrow \frac{n}{i\omega + f_i(n-1) - f_i(n)} - \frac{n+1}{i\omega + f_i(n) - f_i(n+1)}. \quad (4.90)$$

This completes all the terms necessary for our Ginzburg-Landau theory.

## 4.7. First-hopping order effective action

Now, by observing the diagrammatic expansions, we see that  $W_{ii'}^{(1PI)(2)}(\tau, \tau')$  is the only 1PI function which has a first-order hopping contribution. It means that at first-hopping order only  $\Gamma^{(2)}$  has to be corrected. From equation (4.49), it can be obtained by inverting  $W_{ii'}^{(2)}(\tau, \tau')$ , which up to first order is given by

$$W_{ii'}(\tau; \tau') = \delta_{ii'} \begin{array}{c} i \\ \bullet \\ \xrightarrow{\omega'} \end{array} \begin{array}{c} \bullet \\ \xrightarrow{\omega} \end{array} \omega + \begin{array}{c} i' \\ \bullet \\ \xrightarrow{\omega'} \end{array} \begin{array}{c} \bullet \\ \xrightarrow{\omega} \end{array} \begin{array}{c} i \\ \bullet \\ \xrightarrow{\omega} \end{array} \omega + \dots \quad (4.91)$$

Order by order inversion of (4.91) leads to

$$\Gamma_{ij}^{(2)}(\omega; \omega') = \delta_{ij} \begin{array}{c} \omega' \\ \bullet \\ \xrightarrow{\omega} \end{array} \begin{array}{c} \bullet \\ \xrightarrow{\omega} \end{array} \omega + \beta\delta_{\omega, \omega'} J_{ij} + \dots \quad (4.92)$$

Thus, by using the result for  $\Gamma_{0i}^{(2)}$  in (4.71), we can explicitly write (4.92) up to first-hopping order in the Matsubara space

$$\Gamma_{ij}^{(2)}(\omega, \omega') \approx \beta\delta_{\omega, \omega'} J_{ij} - \beta\delta_{\omega, \omega'} \delta_{ij} Z_0 \left[ \sum_{n=0}^{\infty} (n+1) \frac{e^{-\beta f_i(n+1)} - e^{-\beta f_i(n)}}{i\omega + f_i(n) - f_i(n+1)} \right]^{-1}. \quad (4.93)$$

This means that up to first hopping order, the effective action has a very simple form

$$\Gamma[\psi^*, \psi] \approx -\frac{1}{\beta^2} \sum_{\omega} \sum_{ij} J_{ij} \psi_i^*(\omega) \psi_j(\omega) + \Gamma_0[\psi^*, \psi]. \quad (4.94)$$

## 4.8. Second-hopping order effective action

Now we will calculate the second-order correction to  $\Gamma^{(2)}$ . This correction is given by



$$(4.95)$$

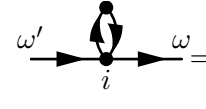
In order to calculate this diagram, we must first calculate the second-order correction to  $W^{(2)}$  which can be represented as



$$(4.96)$$

Now we can make use of the transformation (4.60) so that we can set  $\omega = \omega' = 0$  in  $W_{0i}^{(4)}$  and later make the transformation  $f_i(n) \rightarrow f_i(n) - in\omega$ .

According to our diagrammatic rules, this diagram can be constructed from  $W_{0i}^{(4)}$  and  $W_{0i}^{(2)}$ , according to



$$= \frac{1}{\beta} \sum_j J_{ij}^2 \sum_{\omega''} W_{0i}^{(4)}(\omega'', \omega'; \omega'', \omega) g_j(\omega'') \quad (4.97)$$

where  $W_{0i}^{(4)}(\omega, 0; \omega, 0)$  is obtained from (4.87) and can be rewritten as



$$\begin{aligned}
\frac{Z^{(0)}}{\beta} W_{0i}^{(4)}(\omega, 0; \omega, 0) &= \beta \delta_{\omega, 0} \left\{ \sum_{n=0}^{\infty} e^{-\beta f_i(n)} \left[ \frac{n+1}{f_i(n+1) - f_i(n) - i\omega} + \frac{n}{f_i(n-1) - f_i(n) + i\omega} \right]^2 \right. \\
&\quad \left. - \frac{1}{Z^{(0)}} \left( \sum_{n=0}^{\infty} e^{-\beta f_i(n)} \left[ \frac{n+1}{f_i(n+1) - f_i(n) - i\omega} + \frac{n}{f_i(n-1) - f_i(n) + i\omega} \right] \right)^2 \right\} \\
&\quad + \beta \left\{ \sum_{n=0}^{\infty} e^{-\beta f_i(n)} \left[ \frac{n+1}{f_i(n+1) - f_i(n) - i\omega} + \frac{n}{f_i(n-1) - f_i(n) + i\omega} \right] \right. \\
&\quad \times \left[ \frac{n+1}{f_i(n+1) - f_i(n)} + \frac{n}{f_i(n-1) - f_i(n)} \right] \\
&\quad - \frac{1}{Z^{(0)}} \left( \sum_{m,n=0}^{\infty} e^{-\beta[f_i(n)+f_i(m)]} \left[ \frac{n+1}{f_i(n+1) - f_i(n) - i\omega} + \frac{n}{f_i(n-1) - f_i(n) + i\omega} \right] \right. \\
&\quad \times \left. \left[ \frac{m+1}{f_i(m+1) - f_i(m)} + \frac{m}{f_i(m-1) - f_i(m)} \right] \right) \left. \right\} \\
&\quad + \sum_{n=0}^{\infty} \frac{i [e^{-\beta f_i(n+1)} - e^{-\beta f_i(n)}]}{\omega - i [f_i(n) - f_i(n+1)]} \left\{ (n+2)(n+1) \left[ \frac{1}{f_i(n+2) - f_i(n+1)} + \frac{1}{f_i(n) - f_i(n+1)} \right]^2 \right. \\
&\quad + n(n+1) \left[ \frac{1}{f_i(n) - f_i(n-1)} + \frac{1}{f_i(n) - f_i(n+1)} \right]^2 \left. \right\} \\
&\quad - \sum_{n=0}^{\infty} \frac{i [e^{-\beta f_i(n+2)} - e^{-\beta f_i(n)}]}{\omega - i [f_i(n) - f_i(n+2)]} (n+2)(n+1) \left[ \frac{1}{f_i(n+1) - f_i(n+2)} + \frac{1}{f_i(n+1) - f_i(n)} \right]^2 \\
&\quad + \sum_{n=0}^{\infty} \frac{e^{-\beta f_i(n+1)} - e^{-\beta f_i(n)}}{\{\omega - i [f_i(n) - f_i(n+1)]\}^2} \left[ \frac{(n+2)(n+1)}{f_i(n+2) - f_i(n+1)} + \frac{n(n+1)}{f_i(n) - f_i(n-1)} + 2 \frac{(n+1)^2}{f_i(n) - f_i(n+1)} \right].
\end{aligned} \tag{4.98}$$

This form of writing  $W_{0i}^{(4)}(\omega, 0; \omega, 0)$  is particularly useful, as it can be used to obtain (4.97) with the help of the formulas in Appendix B. For the special case of homogeneous systems, i.e., if  $f_i(n) = f(n)$ ,  $W_{0i}^{(4)}(\omega, 0; \omega, 0) = W_0^{(4)}(\omega, 0; \omega, 0)$ , and  $g_i(\omega) = g(\omega)$ , we have

$$\begin{aligned}
 \frac{(Z^{(0)})^2}{\beta} \sum_{\omega} W_0^{(4)}(\omega, 0; \omega, 0) g(\omega) = & -\beta \left\{ \sum_{n=0}^{\infty} e^{-\beta f(n)} b(n)^2 - \frac{1}{Z^{(0)}} \left[ \sum_{n=0}^{\infty} e^{-\beta f(n)} b(n) \right]^2 \right\} \sum_{n=0}^{\infty} e^{-\beta f(n)} b(n) \\
 & + \beta \sum_{m \neq n} (n+1)(m+1) [a(n) + b(n)] \frac{e^{-\beta[f(n)+f(m+1)]} - e^{-\beta[f(m)+f(n+1)]}}{\{[f(n) - f(n+1)] - [f(m) - f(m+1)]\}^2} \\
 & + \beta^2 \sum_{m \neq n} \frac{(n+1)(m+1)}{[f(n) - f(n+1)] - [f(m) - f(m+1)]} \left\{ e^{-\beta[f(m)+f(n+1)]} a(n) + e^{-\beta[f(n)+f(m+1)]} b(n) \right\} \\
 & + \frac{\beta^2}{Z^{(0)}} \left[ \sum_{n=0}^{\infty} e^{-\beta f(n)} b(n) \right] \sum_{m \neq n} (m+1)(n+1) \frac{e^{-\beta[f(n)+f(m+1)]} - e^{-\beta[f(m)+f(n+1)]}}{[f(m) - f(m+1)] - [f(n) - f(n+1)]} \\
 & + \beta \sum_{m \neq n} (m+1)c(n) \frac{e^{-\beta[f(m)+f(n+1)]} - e^{-\beta[f(n)+f(m+1)]}}{[f(m) - f(m+1)] - [f(n) - f(n+1)]} \\
 & + \beta \sum_{m, n=0}^{\infty} (m+1)d(n) \frac{e^{-\beta[f(m)+f(n+2)]} - e^{-\beta[f(n)+f(m+1)]}}{[f(m) - f(m+1)] - [f(n) - f(n+2)]} \\
 & + \frac{\beta^3}{2} \sum_{n=0}^{\infty} e^{-\beta[f(n+1)+f(n)]} (n+1)^2 [a(n) - b(n)] \\
 & + \frac{\beta^3}{Z^{(0)}} \left[ \sum_{n=0}^{\infty} e^{-\beta f(n)} b(n) \right] \left[ \sum_{n=0}^{\infty} (n+1)^2 e^{-\beta[f(n+1)+f(n)]} \right] \\
 & - \beta^2 \sum_{n=0}^{\infty} e^{-\beta[f(n+1)+f(n)]} (n+1)c(n),
 \end{aligned} \tag{4.99}$$

where

$$\begin{aligned}
 a(n) &= \frac{n+2}{f(n+2) - f(n+1)} + \frac{n+1}{f(n) - f(n+1)} \\
 b(n) &= \frac{n}{f(n) - f(n-1)} + \frac{n+1}{f(n) - f(n+1)} \\
 c(n) &= (n+2)(n+1) \left[ \frac{1}{f(n+2) - f(n+1)} + \frac{1}{f(n) - f(n+1)} \right]^2 \\
 &\quad + n(n+1) \left[ \frac{1}{f(n) - f(n-1)} + \frac{1}{f(n) - f(n+1)} \right]^2 \\
 d(n) &= -(n+2)(n+1) \left[ \frac{1}{f(n+1) - f(n+2)} + \frac{1}{f(n+1) - f(n)} \right]^2.
 \end{aligned} \tag{4.100}$$

Now, by applying the transformation  $f_i(n) \rightarrow f_i(n) - in\omega$ , we can obtain the final result for the second-order correction to  $\Gamma^{(2)}$





## 5. Homogeneous Lattices

Having developed our field-theoretical approach for the general Hamiltonian in the previous chapter, we can now apply it to the specific case of the homogeneous Bose-Hubbard Hamiltonian in  $D$ -dimensional cubic optical lattices. To this end, we must make following identifications

$$f_i(n) = \frac{U}{2}(n^2 - n) - \mu n, \quad (5.1)$$

$$J_{ij} = \begin{cases} J, & \text{if } i \text{ and } j \text{ are nearest neighbors} \\ 0, & \text{otherwise.} \end{cases} \quad (5.2)$$

### 5.1. Quasi-Momentum Representation

The discrete translation symmetry in the homogeneous case allows us to further simplify our formalism by performing a discrete Fourier transformation to our fields, thus leading to the quasi-momentum representation

$$\psi(\mathbf{k}) = \sum_i e^{-i\mathbf{k} \cdot \mathbf{r}_i} \psi_i, \quad (5.3)$$

where  $\mathbf{r}_i$  denotes the location of the  $i$ -th lattice site and components  $k_\alpha$  of quasi-momentum  $\mathbf{k}$  are restricted to the first Brillouin zone. Analogously all site-dependent functions are transformed according to

$$M(\mathbf{k}_1, \dots, \mathbf{k}_n; \mathbf{k}'_1, \dots, \mathbf{k}'_n) = \sum_{i_1, \dots, i_n; i'_1, \dots, i'_n} e^{-i(\mathbf{k}_1 \cdot \mathbf{r}_{i_1} + \dots + \mathbf{k}_n \cdot \mathbf{r}_{i_n} - \mathbf{k}'_1 \cdot \mathbf{r}_{i'_1} - \dots - \mathbf{k}'_n \cdot \mathbf{r}_{i'_n})} M_{i_1, \dots, i_n; i'_1, \dots, i'_n}. \quad (5.4)$$

The inverse transformations read

$$\psi_i = \left(\frac{a}{2\pi}\right)^D \int d^D \mathbf{k} e^{i\mathbf{k} \cdot \mathbf{r}_i} \psi(\mathbf{k}), \quad (5.5)$$

$$M_{i_1, \dots, i_n; i'_1, \dots, i'_n} = \left(\frac{a}{2\pi}\right)^{2Dn} \int d^D \mathbf{k}_1 \dots \int d^D \mathbf{k}_n \int d^D \mathbf{k}'_1 \dots \int d^D \mathbf{k}'_n e^{i(\mathbf{k}_1 \cdot \mathbf{r}_{i_1} + \dots + \mathbf{k}_n \cdot \mathbf{r}_{i_n} - \mathbf{k}'_1 \cdot \mathbf{r}_{i'_1} - \dots - \mathbf{k}'_n \cdot \mathbf{r}_{i'_n})} \times M(\mathbf{k}_1, \dots, \mathbf{k}_n; \mathbf{k}'_1, \dots, \mathbf{k}'_n). \quad (5.6)$$

These transformations can be checked by using the formula

## 5. Homogeneous Lattices

$$\sum_i e^{-i\mathbf{k}\cdot\mathbf{r}_i} = \left(\frac{2\pi}{a}\right)^D \delta(\mathbf{k}). \quad (5.7)$$

This formula enables us to relate  $\delta(\mathbf{k} = \mathbf{0})$  and the total number of lattice sites  $N_s$  according to

$$\delta(\mathbf{k} = \mathbf{0}) = \left(\frac{a}{2\pi}\right)^D N_s. \quad (5.8)$$

By combining this discrete Fourier transformation with the Matsubara transformation, we can rewrite the effective action in (4.48) and (4.57) according to

$$\begin{aligned} -\beta\Gamma[\psi^*, \psi] &= \Gamma^{(0)} + \frac{1}{\beta^2} \left(\frac{a}{2\pi}\right)^{2D} \sum_{\omega\omega'} \int d^D\mathbf{k} \int d^D\mathbf{k}' \Gamma^{(2)}(\mathbf{k}, \omega; \mathbf{k}', \omega') \psi^*(\mathbf{k}, \omega) \psi(\mathbf{k}', \omega') \\ &+ \frac{1}{2!^2} \frac{1}{\beta^4} \left(\frac{a}{2\pi}\right)^{4D} \sum_{\omega_1\omega_2; \omega'_1\omega'_2} \int d^D\mathbf{k}_1 \int d^D\mathbf{k}_2 \int d^D\mathbf{k}'_1 \int d^D\mathbf{k}'_2 \Gamma^{(4)}(\mathbf{k}_1, \omega_1, \mathbf{k}_2, \omega_2; \mathbf{k}'_1, \omega'_1, \mathbf{k}'_2, \omega'_2) \\ &\times \psi^*(\mathbf{k}_1, \omega_1) \psi^*(\mathbf{k}_2, \omega_2) \psi(\mathbf{k}'_1, \omega'_1) \psi(\mathbf{k}'_2, \omega'_2) + \dots \end{aligned} \quad (5.9)$$

From (4.92) and (4.95) we know the 2-point 1PI Green's function up to second hopping order

$$\Gamma_{ij}^{(2)}(\omega; \omega') = \delta_{ij} \begin{array}{c} \omega' \text{---} \bullet \text{---} \omega \\ i \end{array} + \beta\delta_{\omega, \omega'} J_{ij} + \delta_{ij} \begin{array}{c} \omega' \text{---} \bullet \text{---} \omega \\ i \text{---} \text{loop} \end{array} + \dots \quad (5.10)$$

From (4.71) and (4.101), we see that for homogeneous lattices, both diagrams in (5.10) are site independent. Thus, using (5.4) and (5.10), we have

$$\Gamma^{(2)}(\mathbf{k}, \omega; \mathbf{k}', \omega') = \left(\frac{2\pi}{a}\right)^D \delta(\mathbf{k} - \mathbf{k}') \left[ \begin{array}{c} \omega' \text{---} \bullet \text{---} \omega \\ i \end{array} + \beta\delta_{\omega, \omega'} J(\mathbf{k}) + \begin{array}{c} \omega' \text{---} \bullet \text{---} \omega \\ i \text{---} \text{loop} \end{array} + \dots \right] \quad (5.11)$$

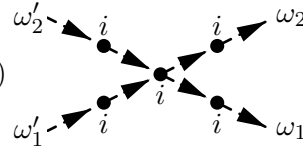
with the Fourier transformed hopping

$$J(\mathbf{k}) = 2J \sum_{\alpha} \cos(k_{\alpha}a). \quad (5.12)$$

For the 4-point 1PI function, we know only its zeroth-order contribution

$$\Gamma_{i_1 i_2; i'_1 i'_2}^{(4)}(\omega_1, \omega_2; \omega'_1, \omega'_2) = \delta_{i_1 i_2} \delta_{i'_1 i'_2} \delta_{i_1 i'_1} \begin{array}{c} \omega'_2 \text{---} \bullet \text{---} \omega_2 \\ \omega'_1 \text{---} \bullet \text{---} \omega_1 \\ i \end{array} + \dots \quad (5.13)$$

From (4.87) and (4.88), we observe that the diagram in (5.13) is also site independent. By using (5.4) and (5.13), we get

$$\Gamma^{(4)}(\mathbf{k}_1, \omega_1, \mathbf{k}_2, \omega_2; \mathbf{k}'_1, \omega'_1, \mathbf{k}'_2, \omega'_2) = \left(\frac{a}{2\pi}\right)^D \delta(\mathbf{k}_1 + \mathbf{k}_2 - \mathbf{k}'_1 - \mathbf{k}'_2) + \dots \quad (5.14)$$


## 5.2. Static Properties

In the homogeneous optical lattices discussed here, the spatial and temporal translation symmetry of the Bose-Hubbard Hamiltonian is preserved in its equilibrium state. Therefore, in order to calculate many of their equilibrium properties it is enough to consider the effective action for an order parameter which is homogeneous in both space and imaginary time, i.e.

$$\psi_i(\tau) = \psi_{\text{eq}}. \quad (5.15)$$

This can be expressed in the quasi-momentum Matsubara representation according to

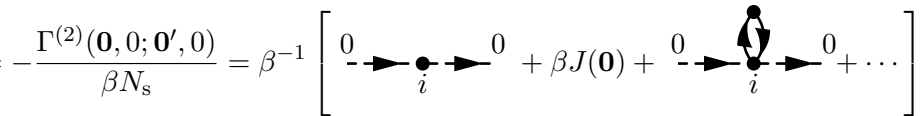
$$\psi_{\text{eq}}(\mathbf{k}, \omega) = \beta \left(\frac{2\pi}{a}\right)^D \delta_{\omega,0} \delta(\mathbf{k}) \psi_{\text{eq}}. \quad (5.16)$$

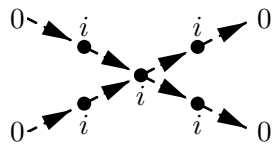
For homogeneous order parameters, it is usual to work with the so called effective potential [39,40] which is defined as the effective action per lattice site:  $\Gamma_{\text{pot}} = \Gamma/N_s$ . Considering this definition and substituting (5.16) into (5.9), we obtain the Landau expansion

$$\Gamma_{\text{pot}}(\psi^*, \psi) = a_0 + a_2 |\psi|^2 + \frac{1}{2!^2} a_4 |\psi|^4 + \dots, \quad (5.17)$$

with the coefficients given by

$$a_0 = -\beta^{-1} \ln \sum_{n=0}^{\infty} e^{-\beta f_i(n)}, \quad (5.18)$$

$$a_2 = -\frac{\Gamma^{(2)}(\mathbf{0}, 0; \mathbf{0}', 0)}{\beta N_s} = \beta^{-1} \left[ \text{diagram 1} + \beta J(\mathbf{0}) + \text{diagram 2} + \dots \right], \quad (5.19)$$


$$a_4 = \frac{\Gamma^{(4)}(\mathbf{0}, 0, 0, 0; \mathbf{0}, 0, 0, 0)}{\beta N_s 2!^2} = \frac{1}{\beta 2!^2} \left[ \text{diagram 3} + \dots \right] \quad (5.20)$$


### 5.2.1. First Hopping Order

According to the discussion in Chapter 4, we must first check whether the condition  $a_4 > 0$  is satisfied. It can be directly calculated from Eqs. (4.87), (4.88), and (5.20). The positivity of  $a_4$  can be seen from Fig. 5.1. Once this condition is satisfied, the phase boundary separating the Mott insulator and the superfluid phases is given by the condition  $a_2 = 0$ .

In the first hopping order approximation, the phase boundary is obtained by ignoring second and higher hopping order in (5.19) and imposing the condition  $a_2 = 0$  on the system parameters, which

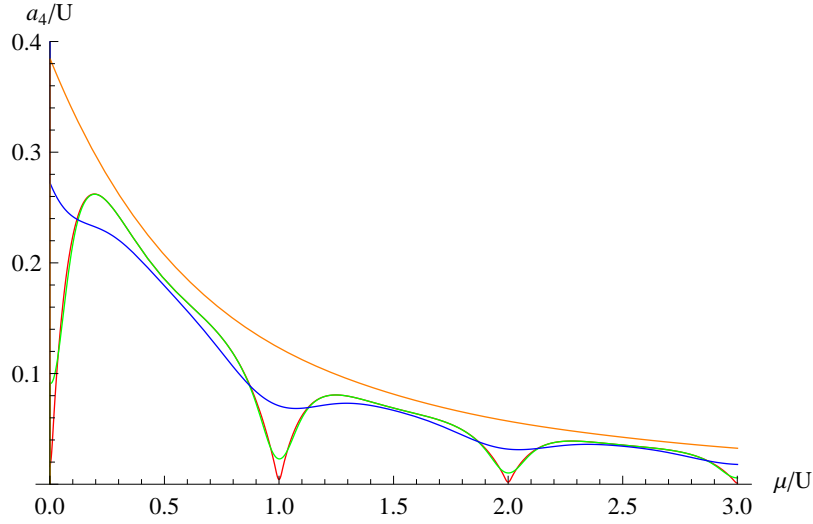


Figure 5.1.: Coefficient  $a_4$  at different temperatures. Red:  $\beta \rightarrow \infty$ . Green:  $\beta = 50/U$ . Blue:  $\beta = 10/U$ . Orange:  $\beta = 3/U$ . The positivity of this quantity makes possible the determination of the phase of the system by looking at the sign of  $a_2$ .

explicitly reads

$$J_c z = -\beta^{-1} \overset{0}{\underset{i}{\longrightarrow}} \bullet \overset{0}{\longrightarrow}, \quad (5.21)$$

where  $z = 2D$  is the lattice coordination number and  $Jz = J(\mathbf{0})$ . By using Eq. (4.71), we obtain the explicit formula for the critical value of the hopping parameter

$$J_c z = Z_0 \left[ \sum_{n=0}^{\infty} \frac{e^{-\beta f_i(n+1)} - e^{-\beta f_i(n)}}{f_i(n) - f_i(n+1)} \right]^{-1}. \quad (5.22)$$

In Fig. 5.2, we have a plot of the quantum-phase diagram for different temperatures in the first hopping order approximation, obtained using Eq. (5.22).

The equilibrium value for the condensate density in the ordered phase is then given by

$$|\psi_{\text{eq}}|^2 = -\frac{2a_2}{a_4}. \quad (5.23)$$

Substituting back into (5.17), the effective potential becomes

$$\Gamma_{\text{pot}} \approx a_0 - \frac{a_2^2}{a_4}. \quad (5.24)$$

By evaluating the derivatives of  $\Gamma_{\text{pot}}$ , many of the thermodynamical quantities can be obtained. For instance, the particle density is given by

$$\rho = -\frac{\partial \Gamma_{\text{pot}}}{\partial \mu} \quad (5.25)$$

and, correspondingly, the compressibility  $\kappa = \partial \rho / \partial \mu$  follows from



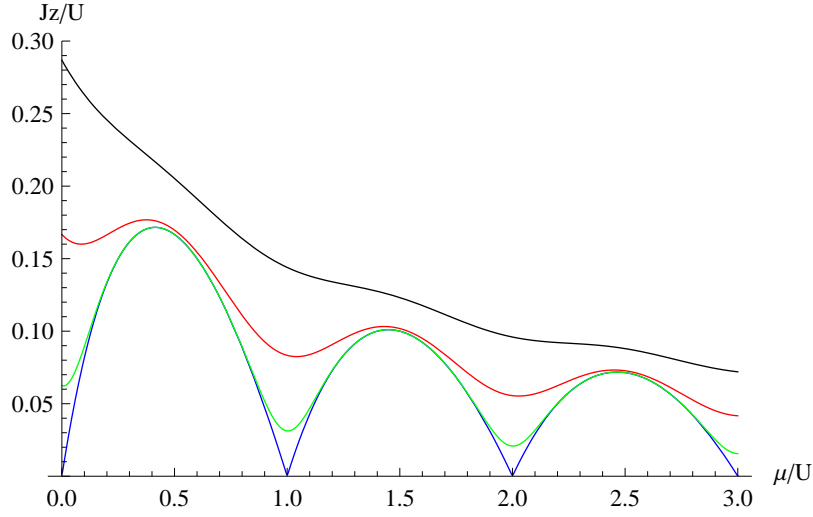


Figure 5.2.: Quantum phase diagram in the first hopping order approximation. Each line separating the Mott insulator from the superfluid phase corresponds to a different temperature. Blue:  $\beta \rightarrow \infty$ . Green:  $\beta = 30/U$ . Red:  $\beta = 10/U$ . Black:  $\beta = 5/U$ .

$$\kappa = -\frac{\partial^2 \Gamma_{\text{pot}}}{\partial \mu^2}. \quad (5.26)$$

In Fig. 5.3, these quantities are plotted for different values of temperature and hopping parameter.

By taking the zero temperature limit in Eq. (5.22), i.e., by making  $\beta \rightarrow \infty$ , we recover the mean-field formula (3.46). This, however, does not imply the equivalence between the mean-field theory and the first hopping order effective potential. In fact, at zero temperature, the results obtained from the effective potential have a wider range of validity than the ones from mean-field theory as illustrated in the Fig. 5.4. While the mean-field theory predicts unphysical results like negative compressibility far from the boundary, the effective potential leads to a monotonically increasing particle density with respect to  $\mu$  and therefore to an always positive compressibility.

### 5.2.2. Second Hopping Order

As the effective potential approach at first hopping order reproduces the same MI-SF phase boundary from mean-field theory, the first non-trivial result for the quantum phase diagram is obtained only at second order level. In order to facilitate the calculations at second hopping order, it is useful to isolate the hopping dependency of the diagrams in Eq. (5.11) according to

$$\begin{array}{c} 0 \\ \text{---} \rightarrow \bullet \rightarrow 0 \\ i \end{array} = \beta \alpha_0, \quad (5.27)$$

$$\begin{array}{c} 0 \\ \text{---} \rightarrow \text{---} \bullet \text{---} \rightarrow 0 \\ i \end{array} = J^2 z \beta \alpha_2. \quad (5.28)$$

In this way, the condition  $a_2 = 0$ , imposed to the system parameters, is equivalent to

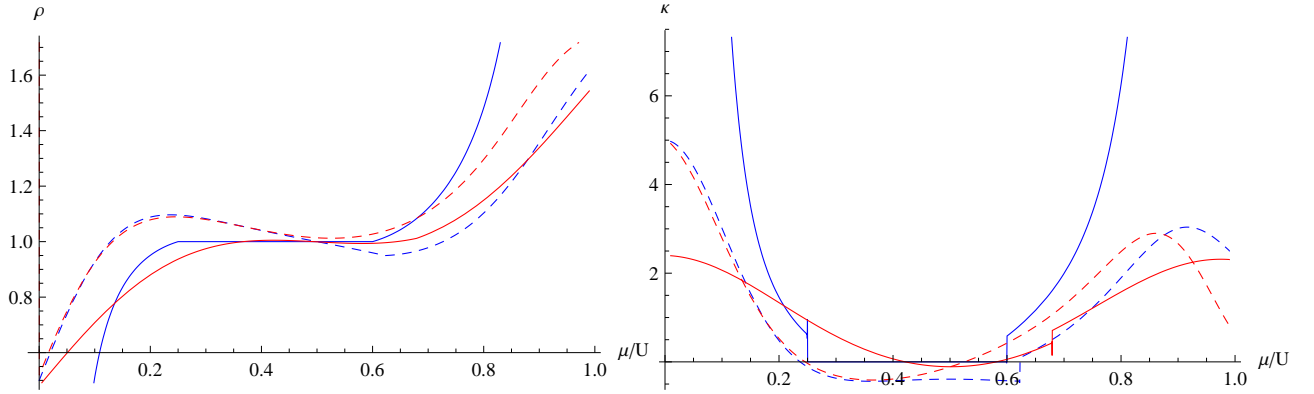


Figure 5.3.: Total particle density (left) and compressibility (right) for different values of temperature and hopping parameter. The blue and red lines correspond to  $\frac{Jz}{U} = 0.15$  and  $\frac{Jz}{U} = 0.18$ , respectively. Dashed and continuous lines correspond to  $\beta \rightarrow \infty$  and  $\beta = 10/U$ , respectively.

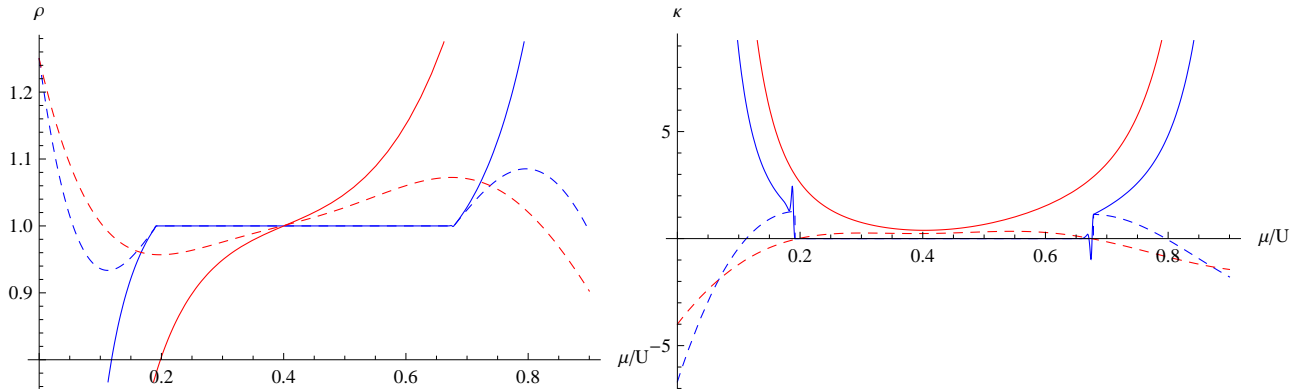


Figure 5.4.: Total particle density (left) and compressibility (right) at zero temperature. The blue and red lines correspond to  $\frac{Jz}{U} = 0.13$  and  $\frac{Jz}{U} = 0.2$ , respectively. Dashed and continuous lines are obtained using mean-field theory and effective potential, respectively.

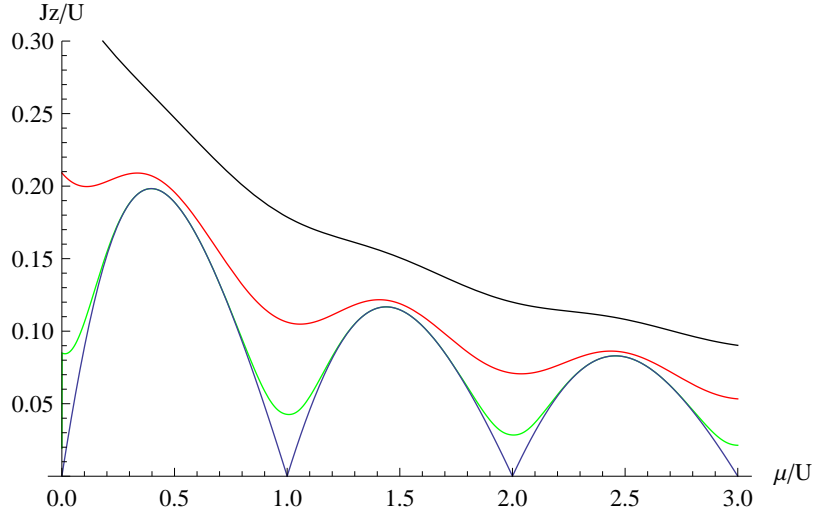


Figure 5.5.: Quantum phase diagram in the second hopping order approximation. Each line separating the Mott insulator from the superfluid phase corresponds to a different temperature. Blue:  $\beta \rightarrow \infty$ . Green:  $\beta = 30/U$ . Red:  $\beta = 10/U$ . Black:  $\beta = 5/U$ .

$$\alpha_0 + J_c z + J_c^2 z \alpha_2 = 0. \quad (5.29)$$

This second-degree algebraic equation has two solutions. In fact, this approach always leads to algebraic equations whose degree depends on the order of the hopping expansion considered. These equations can have, in principle, many real roots depending on its degree. However, as these expansions are valid only for small values of the hopping parameter, only the solution corresponding to the smallest value of  $J_c$  must be considered as physical. All other solutions must be discarded as they are artificially introduced. Therefore, the critical value of the hopping parameter at second hopping order reads

$$J_c z = -\frac{z}{2\alpha_2} \left( 1 - \sqrt{1 - 4\alpha_0\alpha_2/z} \right). \quad (5.30)$$

In this formula we can observe that in the limit  $z \rightarrow \infty$ , the critical hopping reproduces the mean-field result (3.46). This comes from the fact that the mean-field theory becomes exact as the system dimension tends to infinity [36].

In Fig. 5.5, we have a plot of the quantum-phase diagram for different temperatures in the second hopping order approximation, obtained using Eq. (5.30).

In Fig. 5.6, the results from our effective potential method [39] are compared, for the first MI-SF lobe, with the mean-field phase-boundary [28,36], with third-order strong-coupling expansion [37], and with numerical data obtained by using the density-matrix renormalization-group technique [32] for one dimension as well as quantum Monte Carlo simulations [34,35] for two and three dimensions. In this figure, we see that our effective potential method provides very accurate results for the first MI-SF lobe in comparison with Monte Carlo data. This indicates that our method also gives essentially exact results for any MI-SF lobe in more than one dimension, where no Monte Carlo simulations have been yet performed systematically.

For  $d = 1$ , the quantum phase boundary of the Bose-Hubbard model is more complicated as it is a

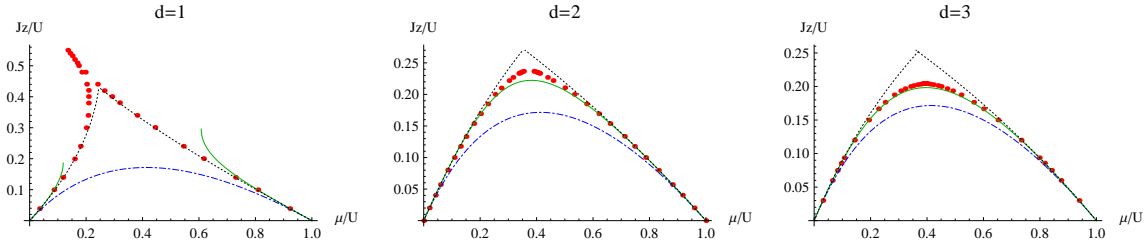


Figure 5.6.: Quantum phase diagram of the first MI-SF lobe ( $n = 1$ ) at zero temperature. Solid green lines are results from our effective potential method [39], dot-dashed blue lines are from mean-field theory [28], dotted black lines are from third-order strong-coupling expansion [37], and red dots are numerical data. For the one-dimensional case the data stem from density-matrix renormalization-group calculations [33], while the data for two and three dimension are obtained from quantum Monte Carlo simulations [34,35].

Kosterlitz-Thouless type of phase transition [65,36]. This nonanalytic behavior is reproduced in Fig. 5.6 quite well by both the precise density-matrix renormalization-group results and strong-coupling expansion [38]. However, our effective potential method cannot deal with this. In fact, it leads to a finite interval of the chemical potential where no real solution for the phase boundary exists. This finding is insofar consistent as the effective action approach is expected to be applicable only for small values of the hopping parameter  $J$ .

In Fig. 5.7, we can clearly observe how the phase boundary predicted by our method approaches the mean-field phase boundary as the dimension  $d$  of the system increases which is consistent with the fact that at large dimensions the mean-field results become exact [36]. Such an agreement with the mean-field for  $d \rightarrow \infty$  can also be checked directly in (3.46) and (5.30).

Finally, we observe that so far our method yields a phase boundary for  $d = 3$  dimensions which turns out to be analytical at the lobe tip. This finding is consistent with the theory of critical phenomena as a quantum phase transition in  $d$  spatial dimensions belongs effectively to the universality class of a standard phase transition in  $d + 1$  dimensions [28,36,37]. In contrast to that, the strong-coupling expansion of Ref. [37] leads in each order to a pronounced artificial cusp at the lobe tip. At present, it remains open to resolve the analytical structure of lobe tips via QMC simulations [34]. This is certainly demanding as the lobe tip is the most sensible region of the Mott lobe with respect to finite-size scalings. The analytic structure of our effective action approach makes it ideal for dealing with experimental situations where the MI-SF phase boundary is crossed at fixed particle number density.

## 5.3. Dynamical Properties

### 5.3.1. Superfluid Density

By relaxing the condition of spacial homogeneity of the order parameter, we are able to determine many other quantities as, for instance, the superfluid density of the system. The superfluid density is defined as the effective fluid density that remains at rest when the entire system is moved at constant velocity [66,67]. As is well known in quantum mechanics, such a uniform velocity corresponds to imposing twisted boundary conditions. Equivalently, we introduce Peierls phase factors

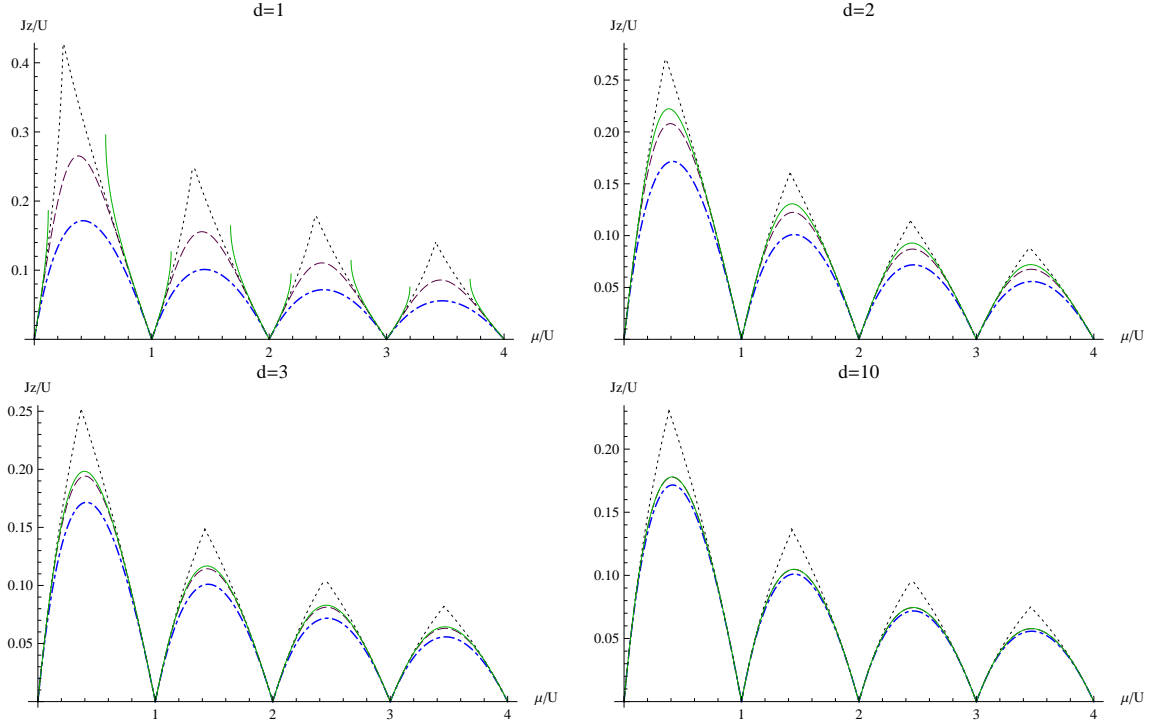


Figure 5.7.: Quantum phase diagram of MI-SF lobes at zero temperatures for different dimensions. Solid green lines are results from our effective potential method, dot-dashed blue lines are from mean-field theory, and dotted black lines are from third-order strong-coupling expansion [37]. The nonphysical ten-dimensional case is included to show that our method converges to the mean-field theory [28] in the limit  $d \rightarrow \infty$ , as is expected on general grounds [36].

$$\hat{a}_i \rightarrow \hat{a}_i e^{i(\mathbf{r}_i \cdot \boldsymbol{\phi})/L} \quad (5.31)$$

in the Bose-Hubbard Hamiltonian. Here  $\boldsymbol{\phi}$  is related to the velocity of the system according to  $\mathbf{v} = \boldsymbol{\phi}/m^*L$ , where  $m^* = 1/(2J)$  is the effective particle mass, and  $L$  is the extent of the system in the direction of  $\mathbf{v}$ . In the effective action, Eq. (5.31) has the same effect as the transformation

$$\psi_i(\tau) \rightarrow \psi_i(\tau) e^{i(\mathbf{r}_i \cdot \boldsymbol{\phi})/L} \quad (5.32)$$

in the effective action  $\Gamma[\psi^*, \psi]$ , where we denote  $\Gamma(\boldsymbol{\phi})$  the effective action transformed by the phase  $\boldsymbol{\phi}$ .

Equating the kinetic energy of the superfluid with the difference  $\Gamma(\boldsymbol{\phi}) - \Gamma(0)$ , the superfluid density is defined as [66,67]

$$\rho_s = \lim_{|\boldsymbol{\phi}| \rightarrow 0} \frac{2m^*L^2}{N_s |a\boldsymbol{\phi}|^2} [\Gamma(\boldsymbol{\phi}) - \Gamma(0)]. \quad (5.33)$$

Let us consider the first hopping order effective action in Eq. (4.94). The equilibrium order parameter in Matsubara space is given by

$$\psi_i(\omega) = \beta \delta_{\omega,0} \psi_{\text{eq}}, \quad (5.34)$$

where  $\psi_{\text{eq}}$  is given in Eq. (5.23). By making the transformation (5.32) and substituting into (5.33) we have

$$\rho_s = \lim_{|\boldsymbol{\phi}| \rightarrow 0} \frac{2m^*L^2}{N_s |a\boldsymbol{\phi}|^2} |\psi_{\text{eq}}|^2 \sum_{ij} J_{ij} \left[ 1 - e^{-i(\mathbf{r}_i - \mathbf{r}_j) \cdot \boldsymbol{\phi}/L} \right]. \quad (5.35)$$

Now, by choosing the direction of  $\boldsymbol{\phi}$  along one of the lattice vectors and  $J_{ij}$  according to (5.2), we have

$$\rho_s = \lim_{\phi \rightarrow 0} \frac{L^2}{(a\phi)^2} |\psi_{\text{eq}}|^2 [2 - 2 \cos(a\phi/L)] = |\psi_{\text{eq}}|^2. \quad (5.36)$$

This interesting result shows that, at first hopping order, both the condensate density and the superfluid density coincide. Therefore, for small values of the hopping parameter we can always assume a numerical equivalence between these two quantities.

An expected feature of bosonic lattices, is the increase of the condensate density as the system parameters go deeper in the superfluid phase. As we see in Fig. 5.8, the mean-field theory predicts again unphysical results as the system goes far from the phase boundary while the effective potential predicts the correct monotonic increase of  $|\psi_{\text{eq}}|^2$  with respect to the hopping parameter.

### 5.3.2. Excitation Spectra

The excitation spectra of a system is the set of relations between the frequency  $\omega$  and the momentum  $\mathbf{k}$  associated with its excitations. For a given excitation, the function  $\omega(\mathbf{k})$  relating its frequency and momentum is known as dispersion relation. The dispersion relations of excitations in both BEC [68,69] and optical lattices [70,71] have been experimentally investigated using Bragg spectroscopy [20,70] and modulation of the lattice potential [16]. Theoretical studies of the excitation spectra of optical lattices

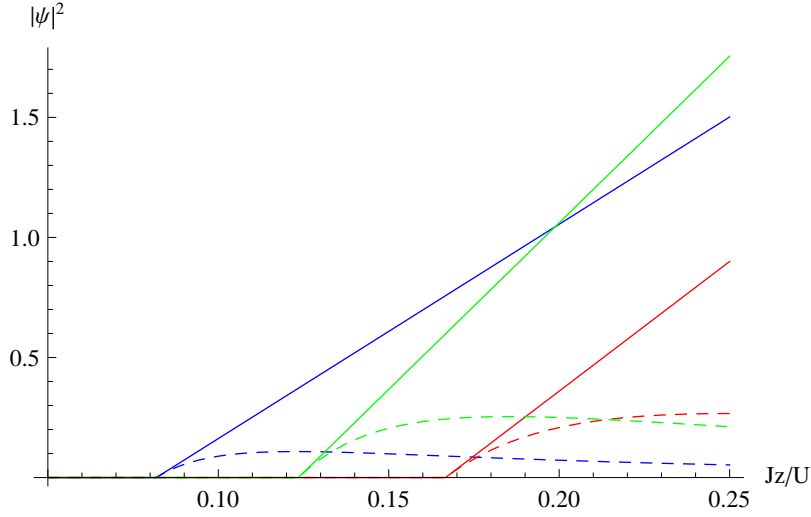


Figure 5.8.: Condensate and superfluid density. The blue, green, and red lines correspond to  $\mu/U = 0.1$ ,  $\mu/U = 0.2$ , and  $\mu/U = 0.5$ , respectively. Dashed and continuous lines are obtained using mean-field theory and effective potential, respectively.

were performed using the lattice Gross-Pitaevskii equation [72], slave-bosons approach [73], random-phase approximation [74], and the Keldysh formalism [45,46]. Here, will be discussed the different excitations appearing in both the Mott-insulator and superfluid phases and spectra corresponding to each excitation will be calculated.

In our approach, these excitations are treated as linear perturbations  $\delta\psi$  to the equilibrium value  $\psi_{\text{eq}}$  of the order parameter field. In order to obtain the linearized equations of motion for  $\delta\psi$ , we must make the substitution  $\psi \rightarrow \psi_{\text{eq}} + \delta\psi$  in our effective action and consider only the terms up to second order in  $\delta\psi$ . However, as the excitation spectra is related in the real-time dynamics of the system near equilibrium, we must transform this effective action from imaginary to real time. In the linear approximation the transition from imaginary to real time can be done by performing the following transformations [52,75,76]

$$\frac{1}{\beta} \sum_{\omega} \rightarrow \frac{1}{2\pi} \int_{-\infty}^{\infty} d\omega, \quad (5.37)$$

$$\omega \rightarrow -i\omega \quad (5.38)$$

in the effective action, where the frequency  $\omega$  must now be treated as a continuous variable. Here a remark must be made: as the transformation  $\omega \rightarrow -i\omega$  works only for 2-point functions [52,75,76], it can be used only for effective actions which are of second order in the fields  $\delta\psi_i(t)$ . If we were interested in higher-order corrections, it would be necessary to reformulate the entire formalism from the beginning in real time.

### Spectra in the Mott-Insulator Phase

In the MI phase, the equilibrium value of the order-parameter field is  $\psi_{\text{eq}} = 0$ . Therefore, the effective action for the excitations can be obtained by substituting  $\psi \rightarrow \delta\psi$  into (5.9), expanding it up to second

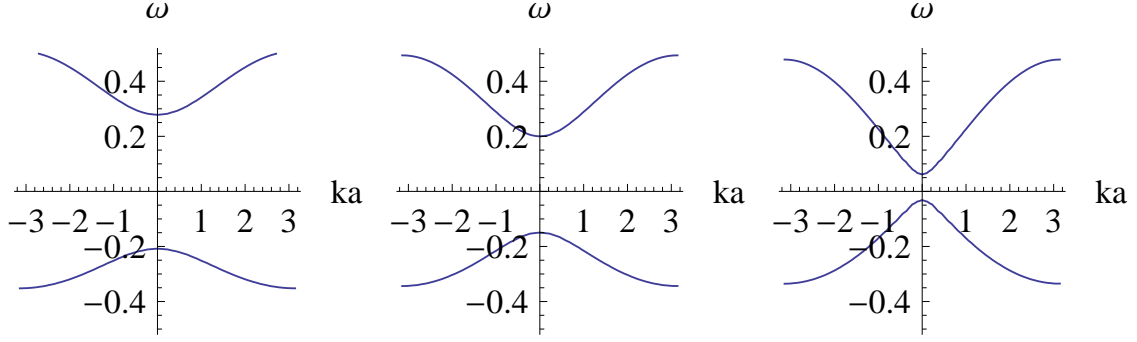


Figure 5.9.: Excitation spectra of a cubic lattice in the Mott-insulator phase with  $\beta = 30/U$  and  $\mu = 0.4U$  and different values of the hopping parameter. Left:  $Jz = 0.13U$ . Middle:  $Jz = 0.15U$ . Right:  $Jz = 0.17U$ .

order in  $\delta\psi$ , and making the transformations (5.37) and (5.38). This finally yields

$$\Gamma_{\text{real}}[\delta\psi^*, \delta\psi] = -\beta^{-1}\Gamma^{(0)} + \frac{1}{2\pi} \left(\frac{a}{2\pi}\right)^{2D} \int d\omega \int d^D \mathbf{k} \xi_0(\mathbf{k}, \omega) |\delta\psi(\mathbf{k}, \omega)|^2, \quad (5.39)$$

where the function  $\xi_0$  is given by

$$\begin{aligned} \xi_0(\mathbf{k}, \omega) &= -\beta^{-1}\Gamma^{(2)}(\mathbf{k}, -i\omega; \mathbf{k}, -i\omega) \\ &= -J(\mathbf{k}) + Z_0 \left[ \sum_{n=0}^{\infty} (n+1) \frac{e^{-\beta f_i(n+1)} - e^{-\beta f_i(n)}}{\omega + f_i(n) - f_i(n+1)} \right]^{-1}. \end{aligned} \quad (5.40)$$

By extremalizing (5.39), we obtain the equation of motion

$$\xi_0(\mathbf{k}, \omega) \delta\psi(\mathbf{k}, \omega) = 0, \quad (5.41)$$

which has nontrivial solutions only if

$$\xi_0(\mathbf{k}, \omega) = 0. \quad (5.42)$$

This is the equation which relates the frequencies and momenta of the excitations in the system and defines the dispersion relations  $\omega(\mathbf{k})$  for each of these excitations. The MI phase is characterized by the existence of gaps in the dispersion relations of all excitations, i.e., for all excitations we must have  $|\omega(\mathbf{0})| > 0$ . In fact, since the phase boundary is defined by  $\xi_0(\mathbf{0}, 0) = 0$ , the gap of at least one excitation must vanish as the phase boundary is approached from the MI phase. The numerical solution of (5.42) can be seen in Fig. 5.9 for a cubic lattice at finite temperature in the MI phase. There we can observe how the gaps become smaller as we approach the MI-SF phase boundary.

Now, by observing that  $\xi_0(\mathbf{k}, \omega)$  in Eq. (5.40) is invariant under the transformations



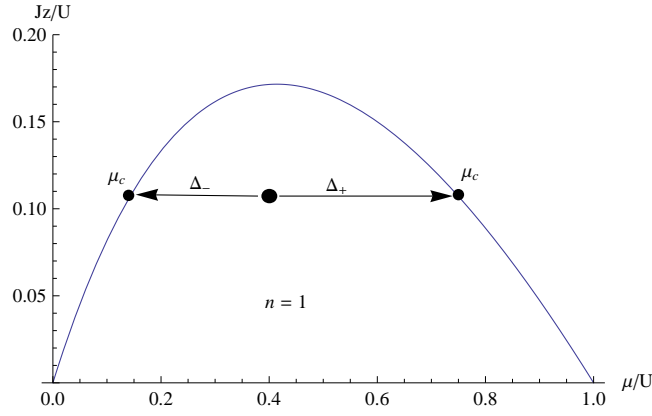


Figure 5.10.: Energy gaps given by the distance, along the  $\mu$  axis, between a point in the phase diagram and the MI-SF phase boundary.

$$\omega \longrightarrow \omega + C, \quad (5.43)$$

$$\mu \longrightarrow \mu - C, \quad (5.44)$$

we see that for a given point of the phase diagram, inside the MI phase, there are two modes whose gaps  $\Delta = \omega(\mathbf{0})$  are related to the two critical chemical potentials  $\mu_c(J)$  by

$$\Delta = \mu_c(J) - \mu. \quad (5.45)$$

This is illustrated in Fig. 5.10 for the first lobe of an optical cubic lattice at zero temperature.

These two modes are also called particle and hole excitations and the gaps associated to each of them are actually the energy necessary to create a particle or a hole with momentum  $\mathbf{k} = \mathbf{0}$ .

From Fig. 5.10, we see that the kind of excitation whose gap vanishes depends on whether the phase boundary is approached at the left or the right side of its lobe tip. If the phase boundary is approached at the left side of the lobe tip, the hole excitation becomes gapless while the particle excitation becomes gapless if the phase boundary is approached at the right side of the lobe tip. If the lobe tip is approached from the Mott phase then the gaps of both particle and hole excitations become simultaneously gapless.

For small values of  $\omega$  and  $|\mathbf{k}|$ , the dispersion relations can be estimated by expanding (5.42) up to second order in both  $\omega$  and  $\mathbf{k}$ , thus giving

$$D_2\omega^2 + D_1\omega + D_0 \approx -Ja^2 |\mathbf{k}|^2. \quad (5.46)$$

By solving this equation for  $\omega$ , we get

$$\omega_{\pm} = -\frac{D_1}{2D_2} \pm \frac{1}{2} \sqrt{\frac{D_1^2}{D_2^2} - 4\frac{D_0 + Ja^2 |\mathbf{k}|^2}{D_2}}. \quad (5.47)$$

## 5. Homogeneous Lattices

The expansion of (5.47) up to second order in  $\mathbf{k}$  gives

$$\omega_{\pm} \approx \Delta_{\pm} \pm \frac{1}{2m'} |\mathbf{k}|^2, \quad (5.48)$$

where the gaps  $\Delta_{\pm}$  associated with each excitation in the system and the effective mass  $m'$  of the excitations are given by

$$\Delta_{\pm} = -\frac{D_1}{2D_2} \pm \frac{1}{2} \sqrt{\frac{D_1^2}{D_2^2} - 4\frac{D_0}{D_2}}, \quad (5.49)$$

$$m' = \frac{\sqrt{D_1^2 - 4D_0D_2}}{2a^2J}. \quad (5.50)$$

For sake of illustration, let us consider the zero-temperature case with  $n = 1$ . In this case, the coefficients are given by

$$D_0 = -Jz - \frac{(\mu - U)\mu}{\mu + U}, \quad (5.51)$$

$$D_1 = -\frac{-U^2 + 2\mu U + \mu^2}{(\mu + U)^2}, \quad (5.52)$$

$$D_2 = -\frac{2U^2}{(U + \mu)^3}. \quad (5.53)$$

By substituting these coefficients into (5.49) and (5.50), we get the gaps  $\Delta_{\pm}$  and the mass  $m'$  in terms of the system parameters. In Fig. 5.11, we present the plots of both the gaps  $\Delta_{\pm}$  and mass  $m'$  for  $\beta \rightarrow \infty$  and  $n = 1$ .

The transformations (5.43) and (5.44) imply that the derivatives of  $\xi_0(\mathbf{k}, \omega)$  with respect to  $\omega$  or  $\mu$  are, actually, identical. Therefore the conditions

$$\xi_0(\mathbf{0}, 0) = 0, \quad (5.54)$$

$$\left. \frac{\partial \xi_0(\mathbf{0}, 0)}{\partial \mu} \right|_{\mu=0} = 0, \quad (5.55)$$

which characterizes the phase boundary and the location of the lobe tip, respectively, are equivalent to

$$D_0 = 0, \quad (5.56)$$

$$D_1 = 0. \quad (5.57)$$

Observe that the expansion (5.48) is not valid if both  $D_0$  and  $D_1$  vanish. In fact, in this case, then Eq. (5.46) can be solved according to

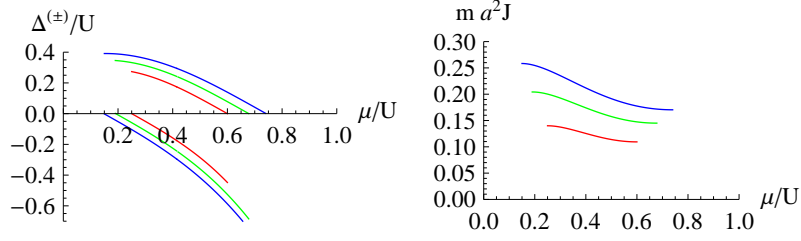


Figure 5.11.: Energy gaps (right) and excitation mass (left) within the MI phase. Left: Excitation mass within the Mott phase for  $\beta \rightarrow \infty$  and  $n = 1$ . The colors red, green, and blue correspond to  $Jz = 0.11U$ ,  $Jz = 0.13U$ , and  $Jz = 0.15U$ , respectively. The vanishing of the gaps and mass of both particle and hole excitations indicates that the spectrum becomes linear at this point.

$$\omega^2 = c_{\text{tip}}^2 |\mathbf{k}|^2, \quad (5.58)$$

where the sound velocity at the tip of the lobe is given by

$$c_{\text{tip}} = \sqrt{-\frac{Ja^2}{D_2}}. \quad (5.59)$$

Another consequence of the conditions (5.54) and (5.55) is that the mass of the excitations must vanish at the Mott lobe according to Eq. (5.50). Fig. 5.11 illustrates the vanishing of the mass and the gaps associated with both particle and hole excitations.

### Spectra in the Superfluid Phase

Let us now consider the perturbations to the order parameter field in the superfluid phase, where we have  $\psi_{\text{eq}} \neq 0$ . To this end, we express the order parameter field as

$$\psi(\mathbf{k}, \omega) = \psi_{\text{eq}}(\mathbf{k}, \omega) + \delta\psi(\mathbf{k}, \omega), \quad (5.60)$$

then substitute (5.60) into (5.9) and expand the effective action up to second order in  $\delta\psi$ , assuming that  $\psi_{\text{eq}}$  is a real number. It leads us to

$$\begin{aligned} -\beta\Gamma[\delta\psi^*, \delta\psi] &\approx \Gamma^{(0)} + \Gamma^{(2)}(\mathbf{0}, 0; \mathbf{0}, 0) + \frac{1}{2!^2}\Gamma^{(4)}(\mathbf{0}, 0, \mathbf{0}, 0; \mathbf{0}, 0, \mathbf{0}, 0)\psi_{\text{eq}}^2 \\ &+ \frac{1}{\beta^2} \left(\frac{a}{2\pi}\right)^{2D} \sum_{\omega, \omega'} \int d^D\mathbf{k} \int d^D\mathbf{k}' \left[ \Gamma^{(2)}(\mathbf{k}, \omega; \mathbf{k}', \omega') + \Gamma^{(4)}(\mathbf{k}, \omega, \mathbf{0}, 0; \mathbf{k}', \omega', \mathbf{0}, 0)\psi_{\text{eq}}^2 \right] \\ &\times \delta\psi^*(\mathbf{k}, \omega) \delta\psi(\mathbf{k}', \omega') \\ &+ \frac{1}{2!^2} \frac{1}{\beta^2} \left(\frac{a}{2\pi}\right)^{2D} \sum_{\omega; \omega'} \int d^D\mathbf{k} \int d^D\mathbf{k}' \Gamma^{(4)}(\mathbf{k}, \omega, \mathbf{k}', \omega'; \mathbf{0}, 0)\psi_{\text{eq}}^2 \\ &\times [\delta\psi(\mathbf{k}, \omega) \delta\psi(\mathbf{k}', \omega') + \delta\psi^*(\mathbf{k}, \omega) \delta\psi^*(\mathbf{k}', \omega')] + \dots \end{aligned} \quad (5.61)$$

However, as we are interested in the real-time dynamics of the system, we must transform our

## 5. Homogeneous Lattices

effective action from imaginary to real time. This is done by performing the transformations (5.37) and (5.38) [52,75,76].

By applying these transformations, the effective action in real-time becomes

$$\begin{aligned} \Gamma_{\text{real}}[\delta\psi^*, \delta\psi] \approx & \Gamma_{\text{pot}} + \frac{1}{2\pi} \left(\frac{a}{2\pi}\right)^{2D} \int d\omega \int d^D \mathbf{k} \xi_1(\mathbf{k}, \omega) |\delta\psi(\mathbf{k}, \omega)|^2 \\ & + \frac{1}{2} \frac{1}{2\pi} \left(\frac{a}{2\pi}\right)^{2D} \int d\omega \int d^D \mathbf{k} \xi_2(\mathbf{k}, \omega) [\delta\psi(\mathbf{k}, \omega) \delta\psi(-\mathbf{k}, -\omega) + \delta\psi^*(\mathbf{k}, \omega) \delta\psi^*(-\mathbf{k}, -\omega)] \end{aligned} \quad (5.62)$$

where, for simplicity, we suppressed the integration limits and made the following identifications

$$\xi_1(\mathbf{k}, \omega) = -\beta^{-1} \Gamma^{(2)}(\mathbf{k}, -i\omega; \mathbf{k}, -i\omega) - \beta^{-1} \Gamma^{(4)}(\mathbf{k}, -i\omega, \mathbf{0}, 0; \mathbf{k}, -i\omega, \mathbf{0}, 0) \psi_{\text{eq}}^2, \quad (5.63)$$

$$\xi_2(\mathbf{k}, \omega) = -\frac{1}{2} \beta^{-1} \Gamma^{(4)}(\mathbf{k}, -i\omega, -\mathbf{k}, i\omega; \mathbf{0}, 0, \mathbf{0}, 0) \psi_{\text{eq}}^2, \quad (5.64)$$

with the equilibrium value of the order-parameter field

$$\psi_{\text{eq}}^2 = -2 \frac{\Gamma^{(2)}(\mathbf{0}, 0; \mathbf{0}, 0)}{\Gamma^{(4)}(\mathbf{0}, 0, \mathbf{0}, 0; \mathbf{0}, 0, \mathbf{0}, 0)}. \quad (5.65)$$

Substituting this expression for  $\psi_{\text{eq}}$  into (5.63) and (5.64), we get the identity

$$\xi_1(\mathbf{0}, 0) = \xi_2(\mathbf{0}, 0). \quad (5.66)$$

In addition, due to the permutation symmetries of  $\Gamma^{(4)}$ , we see that the  $\xi_2(\mathbf{k}, \omega)$  is an even function with respect to both  $\mathbf{k}$  and  $\omega$ . This yields to

$$\left. \frac{\partial \xi_2(\mathbf{k}, \omega)}{\partial k_i} \right|_{k_i=\omega=0} = \left. \frac{\partial \xi_2(\mathbf{k}, \omega)}{\partial \omega} \right|_{k_i=\omega=0} = 0. \quad (5.67)$$

where  $k_i$  stands for the three components of  $\mathbf{k}$ .

By extremalizing (5.62), we finally get the equations of motion for  $\delta\psi$  in frequency-momentum space

$$\xi_1(\mathbf{k}, \omega) \delta\psi(\mathbf{k}, \omega) + \xi_2(\mathbf{k}, \omega) \delta\psi^*(-\mathbf{k}, -\omega) = 0, \quad (5.68)$$

$$\xi_1(\mathbf{k}, \omega) \delta\psi^*(\mathbf{k}, \omega) + \xi_2(\mathbf{k}, \omega) \delta\psi(-\mathbf{k}, -\omega) = 0. \quad (5.69)$$

From these equations, we can immediately observe that any function  $\delta\psi$  which is both stationary and purely imaginary, will automatically solve (5.68) and (5.69). This is a result of the global phase invariance of (5.9) and the non-stationary generalization of these solutions are gapless excitations known as Goldstone modes.

The solution to the equations (5.68) and (5.69) can be obtained by expressing (5.69) as

$$\delta\psi^*(\mathbf{k}, \omega) = -\frac{\xi_2(\mathbf{k}, \omega)}{\xi_1(\mathbf{k}, -\omega)} \delta\psi(\mathbf{k}, \omega) \quad (5.70)$$

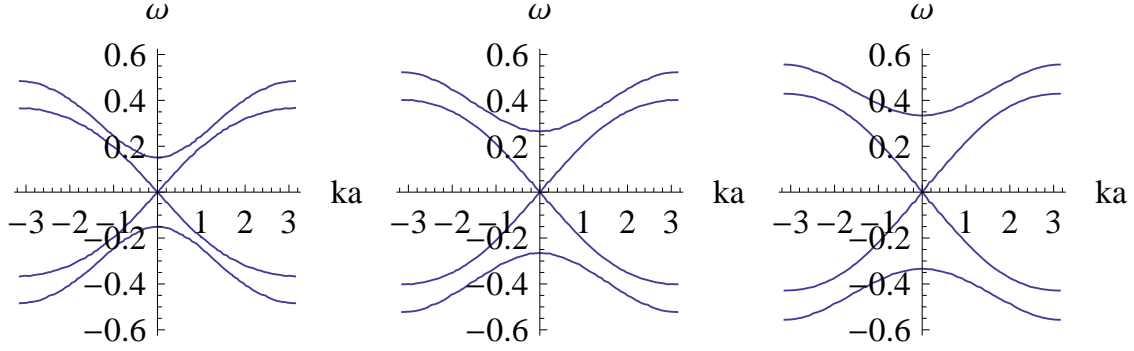


Figure 5.12.: Excitation spectra of a cubic lattice in the superfluid phase with  $\beta = 30/U$ ,  $\mu = 0.4U$  and different values of the hopping parameter. Left:  $Jz = 0.18U$ , middle:  $Jz = 0.20U$ , right:  $Jz = 0.22U$ .

and substituting it back into (5.68), so that we get

$$\left[ \xi_1(\mathbf{k}, \omega) - \frac{\xi_2(\mathbf{k}, \omega)^2}{\xi_1(\mathbf{k}, -\omega)} \right] \delta\psi(\mathbf{k}, \omega) = 0. \quad (5.71)$$

Therefore, the dispersion relations of the excitations in the superfluid phase must obey the equation

$$\xi_1(\mathbf{k}, \omega)\xi_1(\mathbf{k}, -\omega) - \xi_2(\mathbf{k}, \omega)^2 = 0. \quad (5.72)$$

The numerical solution of (5.72) can be seen in Fig. 5.12 for a cubic lattice at finite temperature in the superfluid phase. In this figure, we can observe the gapless mode corresponding to the Goldstone excitation in addition to the gapped mode whose gap becomes smaller as we approach the MI-SF phase boundary. There, we can also see that the Goldstone mode exhibits a linear spectrum for small  $\omega$  and  $\mathbf{k}$ . In fact, such a linear spectrum is a general characteristic of the Goldstone excitations [56].

Observe that over the whole phase boundary, where  $\psi_{\text{eq}} = 0$ , the Eqs. (5.68) and (5.69) are both reduced to (5.41) which describes the particle and hole excitations. This means that, the modes in the SF phase, i.e., both the gapped and the Goldstone excitations are continuously transformed into the particle and hole excitations as the phase boundary is approached from the superfluid side.

In the SF phase, the dispersion relations of the excitations for small  $\omega$  and  $|\mathbf{k}|$  can also be calculated as in the MI phase. To this end, we first expand both  $\xi_1$  and  $\xi_2$  in power series of  $\omega$  and  $\mathbf{k}$ , as follows

$$\xi_1(\mathbf{k}, \omega) \approx A_0 + A_1\omega + A_2\omega^2 + Ja|\mathbf{k}|^2, \quad (5.73)$$

$$\xi_2(\omega) \approx A_0 + B_2\omega^2, \quad (5.74)$$

where the coefficients are given by

$$A_0 = \xi_2(\mathbf{0}, 0) = \xi_1(\mathbf{0}, 0), \quad (5.75)$$

$$A_1 = \left. \frac{\partial \xi_1(\mathbf{0}, \omega)}{\partial \omega} \right|_{\omega=0}, \quad (5.76)$$

$$A_2 = \left. \frac{1}{2} \frac{\partial^2 \xi_1(\mathbf{0}, \omega)}{\partial \omega^2} \right|_{\omega=0}, \quad (5.77)$$

$$B_2 = \left. \frac{1}{2} \frac{\partial^2 \xi_2(\mathbf{0}, \omega)}{\partial \omega^2} \right|_{\omega=0}. \quad (5.78)$$

By substituting the approximations (5.73) and (5.74) into (5.72), we get the equation

$$\left[ 2A_0Ja|\mathbf{k}|^2 + (Ja|\mathbf{k}|^2)^2 \right] + \left[ 2A_0(A_2 - B_2) - A_1^2 + 2A_2Ja|\mathbf{k}|^2 \right] \omega^2 + (A_2^2 - B_2^2)\omega^4 = 0, \quad (5.79)$$

which has the following general solution

$$\begin{aligned} \omega^2 = & -\frac{2A_0(A_2 - B_2) - A_1^2 + 2A_2Ja|\mathbf{k}|^2}{2(A_2^2 - B_2^2)} \\ & \times \left\{ 1 \pm \sqrt{1 - 4 \frac{(A_2^2 - B_2^2) [2A_0Ja|\mathbf{k}|^2 + (Ja|\mathbf{k}|^2)^2]}{[2A_0(A_2 - B_2) - A_1^2 + 2A_2Ja|\mathbf{k}|^2]^2}} \right\}. \end{aligned} \quad (5.80)$$

The dispersion relations for small  $\omega$  and  $|\mathbf{k}|$  can now be obtained by expanding (5.80) up to second order in  $|\mathbf{k}|$ . By considering the plus sign in (5.80), the dispersion relation for the gapped mode is obtained as follows

$$\omega^2 = \frac{A_1^2 - 2A_0(A_2 - B_2)}{A_2^2 - B_2^2} + 2 \frac{A_0(A_2 - B_2)^2 - A_1^2A_2}{(A_2^2 - B_2^2)[A_1 + 2A_0(B_2 - A_2)]} a^2 J |\mathbf{k}|^2. \quad (5.81)$$

This can be further approximated to

$$\omega = \pm \left( \Delta + \frac{1}{2m'} |\mathbf{k}|^2 \right), \quad (5.82)$$

with excitation gap and mass given by

$$\Delta = \sqrt{\frac{A_1^2 - 2A_0(A_2 - B_2)}{A_2^2 - B_2^2}}, \quad (5.83)$$

$$m' = \frac{[A_1^2 - 2A_0(A_2 - B_2)]^2}{2[A_0(A_2 - B_2)^2 - A_1^2A_2]} \sqrt{\frac{A_2^2 - B_2^2}{A_1^2 - 2A_0(A_2 - B_2)}}. \quad (5.84)$$

Now, if we take the minus sign in Eq. (5.80) and expand it up to second order in  $|\mathbf{k}|$ , we get the dispersion relation of the Goldstone mode, as follows

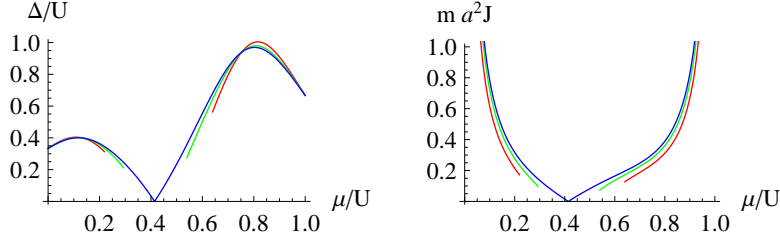


Figure 5.13.: Energy gap (left) and excitation mass (right) within superfluid phase for  $\beta \rightarrow \infty$  and  $n = 1$ . Right: Excitation mass within the superfluid phase. The colors: red, green, and blue correspond to  $Jz = 0.14U$ ,  $Jz = 0.16U$ , and  $Jz = 0.18U$ , respectively.

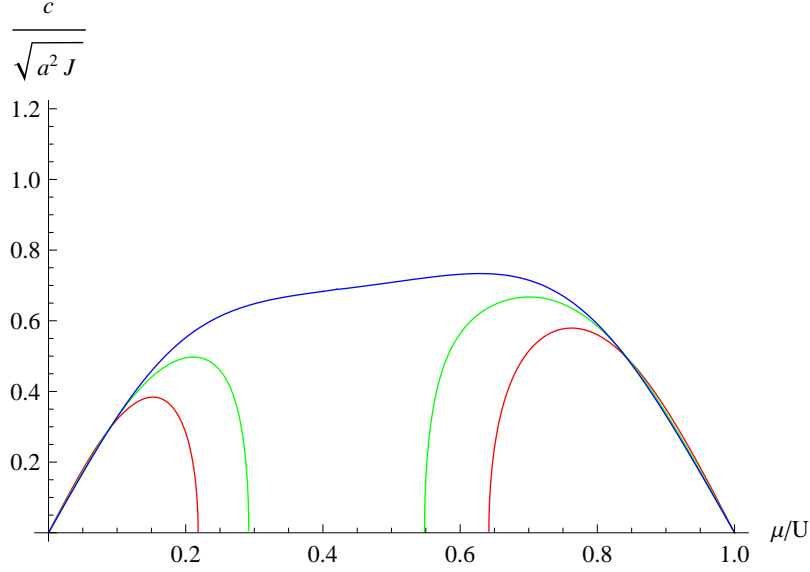


Figure 5.14.: Sound velocity for  $\beta \rightarrow \infty$  and  $n = 1$ . The colors: red, green, and blue correspond to  $Jz = 0.14U$ ,  $Jz = 0.16U$ , and  $Jz = 0.18U$ , respectively.

$$\omega^2 = c^2 |\mathbf{k}|^2, \quad (5.85)$$

where the sound velocity is given by

$$c = \sqrt{\frac{2A_0 J a^2}{A_1^2 - 2A_0(A_2 - B_2)}}. \quad (5.86)$$

At the lobe tip, where the coefficients  $A_0$ ,  $A_1$ , and  $B_2$  vanish, both the gap and the mass of the gapped mode vanish according to Eqs. (5.83) and (5.84). If we look at Eq. (5.81), we see that this comes from the fact that there is no gapped mode at lobe tip. In addition, at the lobe tip,  $A_2$  becomes identical to  $D_2$  which means that Eq. (5.86) becomes equivalent to Eq. (5.59). From this, we conclude that the analysis in both the Mott and the superfluid phase shows that, at the lobe lip, there must exist only one kind of excitation which has a linear spectrum and its sound velocity given by Eq. (5.59).

The analysis in the Mott phase shows that for the points over the phase boundary and out of the lobe tip, there are two excitation modes where both of them are quadratic in  $|\mathbf{k}|$ . This means that

## 5. Homogeneous Lattices

the sound velocity of the Goldstone mode must vanish as these points are approached from the SF phase. This can be checked by considering Eq. (5.86) with  $A_0 = 0$  and  $A_1 \neq 0$ .

For simplicity, let us consider the zero-temperature case with  $n = 1$ . In this case, the coefficients (5.75)–(5.78) can be explicitly calculated, thus yielding

$$A_0 = \frac{(-1 + \mu')\mu' + J'z(1 + \mu')}{1 + \mu'}, \quad (5.87)$$

$$A_1 = \frac{[-2(-1 + \mu')^2\mu'^2(-18 + 42\mu' - 23\mu'^2 + 8\mu'^3 + \mu'^4) + J'z(9 - 66\mu' + 103\mu'^2 + 12\mu'^3 - 117\mu'^4 + 46\mu'^5 - 3\mu'^6)]}{\mu'(1 + \mu')^2(9 - 30\mu' + 46\mu'^2 - 32\mu'^3 + 5\mu'^4 + 2\mu'^5)U}, \quad (5.88)$$

$$A_2 = \frac{[3J'(27 - 135\mu' + 207\mu'^2 - 23\mu'^3 - 185\mu'^4 + 165\mu'^5 - 41\mu'^6 + \mu'^7) + \mu'(-27 + 351\mu' - 1197\mu'^2 + 1907\mu'^3 - 1639\mu'^4 + 739\mu'^5 - 137\mu'^6 + 3\mu'^7)]}{(3 - 2\mu')^2(-1 + \mu')\mu'(1 + \mu')^3(3 - 5\mu' + 5\mu'^2 + \mu'^3)U^2} \quad (5.89)$$

$$B_2 = -\frac{12\mu' [(-1 + \mu')\mu + J'z(1 + \mu')]}{(1 + \mu')^3(3 - 5\mu' + 5\mu'^2 + \mu'^3)U^2}, \quad (5.90)$$

where  $\mu' = \mu/U$  and  $J' = J/U$ .

By substituting these coefficients into (5.83) and (5.84), we obtain the gap and mass of the gapped mode above the first Mott lobe as depicted in Fig. 5.13. The sound velocity above the first Mott lobe is obtained by substituting these coefficients into (5.86) and is shown in Fig. 5.14.

By numerically solving Eqs. (5.42) and (5.72), the properties of the excitation spectra in both the MI and SF phases can be analyzed in an even more precise way. In Fig. 5.15, these properties are exposed in detail according to the various points considered in the phase diagram. In C1 and C3, we see the hole excitations becoming gapless as the phase boundary is approached from the MI phase which indicates that the hole excitation transforms into the Goldstone mode as the phase boundary is crossed. In C2 and C3, the coincidence between both the mass and the gap of the particle excitation and the SF gapped excitation indicates that the particle excitation transforms into the SF gapped mode as the phase boundary is crossed from the MI phase. The roles of particle and hole excitations are exchanged at the other side of the lobe tip, as we can see in A1-A3. In this case, the particle excitation is the one which gives rise to the Goldstone mode while the hole excitation becomes the SF gapped mode, as depicted in A2 and A3. At the Mott lobe, we have a special situation where both particle and hole excitations are merged into single linear excitations as the lobe tip is approached from the MI phase as shown in B1. In addition, the vanishing masses and gaps at the lobe tip in B2 and B3 shows the absence of any gapped or massive mode at the lobe tip. In fact, the only possible mode at this point is the linear mode with finite sound velocity indicated in B3 as opposed to the other points over the boundary, where the vanishing sound velocity in A3 and C3 indicates that only massive modes exist.



### 5.3.3. Critical Exponents

In this chapter, some properties of the excitation spectra such as gaps and masses of the various modes were calculated by means of expansions of the dispersion relations in powers of  $\omega$  and  $|\mathbf{k}|$ , as in Eqs. (5.48) and (5.81). This kind of approximation becomes better and better as the phase boundary is approached, since in the vicinity of the critical points only excitations with low energy and momenta play relevant roles. Therefore, these approximations are enough for the discussion of the critical properties at the MI-SF transition.

At first, it is important to distinguish the transitions at the lobe tip from the ones occurring across the other points of the MI-SF border. At the lobe tip, the relativistic dispersion relations implies that the transitions occurring at this point belong to universality classes which are different from the transitions crossing the other points.

Let us first concentrate on the transitions occurring away from the lobe tip where the phase boundary is crossed vertically with  $\mu$  constant. In the MI phase, the correlation length is related to the coefficient of  $|\psi|^2$  in the effective action according to [56,57,60]

$$\xi^{-2} \sim \Gamma^{(2)}(\mathbf{0}, 0; \mathbf{0}, 0). \quad (5.91)$$

From Eq. (5.40), we have

$$\Gamma^{(2)}(\mathbf{0}, 0; \mathbf{0}, 0) \sim |J - J_c|, \quad (5.92)$$

where  $J_c$  denotes the critical hopping. The critical exponent  $\nu$  is defined according to

$$\xi \sim |J - J_c|^\nu. \quad (5.93)$$

The combination of (5.91)–(5.93) leads to

$$\nu = \frac{1}{2}. \quad (5.94)$$

The definition of the susceptibility [36,56,60] is also related to  $\Gamma^{(2)}(\mathbf{0}, 0; \mathbf{0}, 0)$  according to

$$\chi \sim \Gamma^{(2)}(\mathbf{0}, 0; \mathbf{0}, 0)^{-1}, \quad (5.95)$$

while the critical exponent  $\chi$  is defined by

$$\chi \sim |J - J_c|^{-\gamma}. \quad (5.96)$$

By combining (5.95) and (5.96) with (5.92) we get another coefficient

$$\gamma = 1. \quad (5.97)$$

The critical exponent  $z$  is related to the way in which an excitation vanishes at the critical point [36] according to

$$\Delta \sim |J - J_c|^{\nu z}. \quad (5.98)$$

## 5. Homogeneous Lattices

From (5.49) and (5.83), we see that

$$\Delta \sim |J - J_c|. \quad (5.99)$$

Using the value of  $\nu$  from (5.94) with (5.98) and (5.99), we have

$$z = 2. \quad (5.100)$$

Another possibility is crossing the phase boundary horizontally with  $J$  constant. In this case, all the discussion made above can be repeated by considering  $|\mu - \mu_c|$  instead of  $|J - J_c|$  in such a way that the critical exponents are the same. For both paths, the remaining coefficients can be obtained by using the scaling relations (3.1)–(3.4), thus giving

$$\alpha = -\frac{1}{2}, \quad (5.101)$$

$$\beta = \frac{3}{4}, \quad (5.102)$$

$$\delta = \frac{7}{3}, \quad (5.103)$$

$$\eta = 0. \quad (5.104)$$

Now let us consider the transition where the lobe tip is crossed vertically. Since the equation (5.92) also holds when the lobe tip is approached, the exponents  $\nu$  and  $\gamma$  have the same value. However, in Fig. 5.10, we see that, due to the parabolic shape of the phase boundary near the lobe tip, the gaps of the excitations must vanish according to

$$\Delta \sim |J - J_c|^2. \quad (5.105)$$

From Eq. (5.98), we can then infer for the lobe tip that

$$z = 1. \quad (5.106)$$

By using the scaling relations (3.1)–(3.4), we get the remaining critical exponents at the lobe tip

$$\alpha = 0, \quad (5.107)$$

$$\beta = \frac{1}{2}, \quad (5.108)$$

$$\delta = 3, \quad (5.109)$$

$$\eta = 0. \quad (5.110)$$

Another possible critical behavior can be observed when the lobe tip is approached horizontally from the SF phase without penetrating into the MI phase. To this end, we must use the effective action in the SF phase. In particular, the coefficients  $\nu$  and  $\gamma$  which are related to the correlation length and the susceptibility, respectively, can be obtained from

$$\xi^{-2} \sim \xi_1(\mathbf{0}, 0), \quad (5.111)$$

$$\chi \sim \xi_1(\mathbf{0}, 0)^{-1}, \quad (5.112)$$

where  $\xi_1$  is defined in (5.63). Note that, at the Mott lobe, the derivative of  $\xi_1$  with respect to  $\mu$  vanishes since the derivatives of both  $\Gamma^{(2)}$  and  $\Gamma^{(4)}$  go to zero at this point. Therefore, at the Mott lobe, we must have

$$\xi_1(\mathbf{0}, 0) \sim (\mu - \mu_c)^2. \quad (5.113)$$

This allows us to find the coefficients

$$\nu = 1, \quad (5.114)$$

$$\gamma = 2. \quad (5.115)$$

From (5.83) and Fig. 5.13 we see that the gap of the SF gapped mode behaves according to

$$\Delta \sim |\mu - \mu_c| \quad (5.116)$$

along the horizontal path which touches the Mott lobe. This leads us to our next coefficient

$$z = 1. \quad (5.117)$$

The remaining coefficients can now be calculated using (3.1)–(3.4), thus giving

$$\alpha = -2, \quad (5.118)$$

$$\beta = 1, \quad (5.119)$$

$$\delta = 3, \quad (5.120)$$

$$\eta = 0. \quad (5.121)$$

These results are summarized in Fig. 5.16 with the various transitions corresponding to the different crossings of the MI-SF border discriminated.

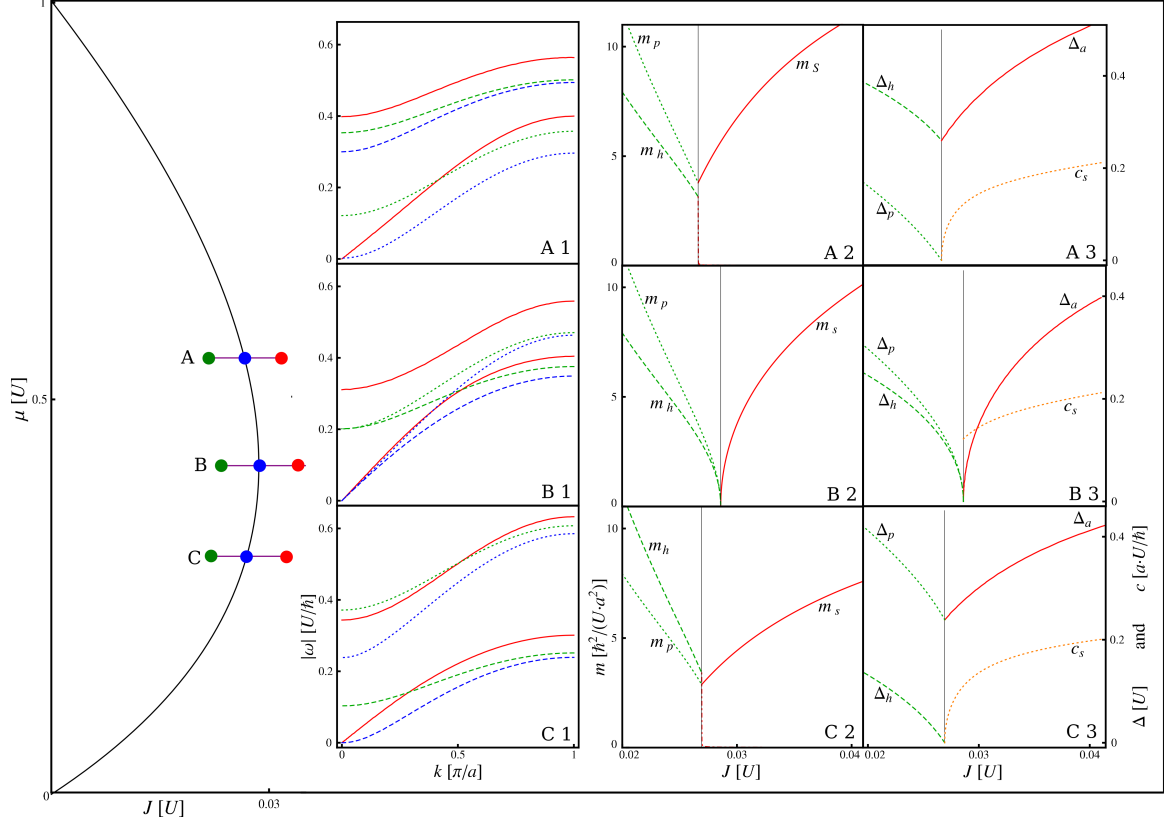


Figure 5.15.: Figure extracted from [45] and [46]. Excitation spectra are plotted in A1–C1 for different values of  $\mu/U$  and  $J/U$ , which are marked in the phase diagram (left). In the MI phase (green lines) and on the phase boundary (blue lines), the two modes can be interpreted as particle (dotted lines) and hole (dashed lines) excitations. At the tip of the Mott lobe (B), both modes become gapless, whereas for larger (smaller) chemical potentials  $\mu$ , only the gap of the particle (hole) mode vanishes. In the SF phase (red), the gapless mode turns into a sound mode, but a gapped mode is also present everywhere in the SF phase. The smooth transition from the MI excitation to the SF excitation is further analyzed in A2–C2 and A3–C3, where the effective mass  $m$  and the gap of each mode are plotted as a function of  $J/U$ . The sound velocity  $c$  of the massless SF excitation, plotted in A3–C3, vanishes at the phase boundary except at the tip, indicating the existence of a different universality class in this configuration.

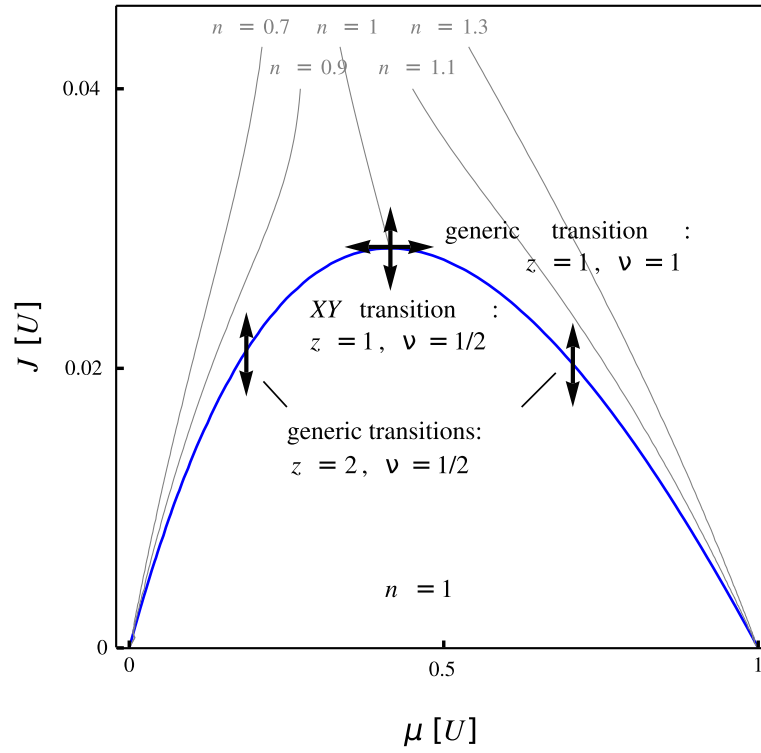


Figure 5.16.: The critical exponents depend on the position and direction of the phase transition. The gray lines of constant densities in the SF phase are obtained via the effective action.



## 6. Collapse and Revival of Matter Waves

This chapter discusses the formation and dynamics of matter waves in an optical lattice loaded with  $2 \times 10^5$   $^{87}\text{Rb}$  atoms which was experimentally observed by Greiner et al. [1]. In particular, we analyse the observed collapse and revival of the condensate field after a sudden change of the potential depth from a small value  $V_A$  to a large value  $V_B$ . Various examples of such effect have been observed not only with the matter waves in a BEC [1,77,78], but also for the coherent light field interacting with a single atom in cavity quantum electrodynamics [79] and for a single ion captured in a trap [80].

Besides the main frequency dependency of the collapse and revival process on the laser potential, the authors in Ref. [1] detected a clear difference between the revival and collapse times which also depend on the external laser potential. Additionally, a damping of those matter waves is perceived which was possibly caused by a loss of coherence due to the harmonic trapping potential. Here we use the results from our effective action theory to reproduce the observed features in Ref. [1] and to test our theory against the experimental results. Therefore, all numeric parameters used here are the same as in Ref. [1].

For sufficiently large values of the laser beam intensity  $V_0$ , the hopping parameter can be neglected, so that our system is described by the Bose-Hubbard Hamiltonian

$$\hat{H}_{\text{BH}} = \frac{U}{2} \hat{n}_i (\hat{n}_i - 1) + V_i \hat{n}_i, \quad (6.1)$$

with  $V_i = (1/2)m\omega^2|\mathbf{r}|_i^2$  and  $\omega^2 = \omega_m^2 + \omega_l^2$ . Here  $\omega_m^2 = 2\pi \times 24$  Hz is the magnetic trap frequency and, due to the Gaussian profile of the laser beams, an additional contribution  $\omega_l^2$  must be taken into account, which reads according to (2.15)

$$\omega_l^2 = \frac{8V_0}{mw_0^2}, \quad (6.2)$$

with  $m$  being the mass of the  $^{87}\text{Rb}$  atoms. Here we consider the values  $V_A = 8 E_R$  and  $V_B = 22 E_R$  as in Ref. [1]. This gives for the laser-generated angular frequencies the values  $\omega_A = 225$  Hz and  $\omega_B = 389$  Hz corresponding to the potentials  $V_A$  and  $V_B$ , respectively, where, we have used the laser beam wavelength  $\lambda = 838$  nm and the beam waists  $w_0 = 125$   $\mu\text{m}$ .

### 6.1. Equations of motion for $J = 0$

The Hamiltonian (6.1) allows us to treat the system as a set of independent lattice points. Therefore, in an analogous way to (5.39), the real-time effective action for a small  $\psi_i$  is given by

$$\Gamma_{\text{real}}[\psi_i^*, \psi_i] = -\beta^{-1}\Gamma^{(0)}/N_S + \frac{1}{2\pi} \int d\omega \xi(\omega) |\psi_i(\omega)|^2, \quad (6.3)$$

## 6. Collapse and Revival of Matter Waves

where, for  $\beta \rightarrow \infty$ , the function  $\xi$  is given by

$$\xi(\omega) = \left[ \frac{n}{\omega + f_i(n-1) - f_i(n)} - \frac{(n+1)}{\omega + f_i(n) - f_i(n+1)} \right]^{-1} \quad (6.4)$$

with the following identification

$$f_i(n) = \frac{U}{2}(n^2 - n) + V_i n. \quad (6.5)$$

By extremalizing (6.3), we obtain the equation of motion

$$\xi(\omega) \psi_i(\omega) = 0. \quad (6.6)$$

Therefore, the order parameter  $\psi_i(\omega)$  is nonzero only for frequencies obeying

$$\xi(\omega) = 0. \quad (6.7)$$

By using (6.6) and (6.5), we conclude that these frequencies are

$$\omega_1 = \frac{U_B n_i}{\hbar} + \frac{m\omega_B^2}{2\hbar} r_i^2, \quad (6.8)$$

$$\omega_2 = \frac{U_B (n_i - 1)}{\hbar} + \frac{m\omega_B^2}{2\hbar} r_i^2, \quad (6.9)$$

where we recovered the explicit dependency on the Planck constant  $\hbar$  by dimensional analysis. This means that the general evolution of  $\psi_i(t)$  is given by

$$\psi_i(t) = \left[ A_i^+ e^{-i \frac{U_B n_i}{\hbar} t} + A_i^- e^{-i \frac{U_B (n_i - 1)}{\hbar} t} \right] e^{-i \frac{m\omega_B^2}{2\hbar} r_i^2 t}, \quad (6.10)$$

where  $A_i^+$  and  $A_i^-$  are constants which are determined by the initial conditions.

### 6.2. Exact solution for $J = 0$

Here we consider that the initial lattice potential is very small so that we can consider our initial state as a direct product of on-site coherent states

$$|\Phi\rangle = \prod_i |\phi_i\rangle, \quad (6.11)$$

with the local states

$$|\phi_i\rangle = e^{-\frac{1}{2}|\psi_i|^2} \sum_{n_i=0}^{\infty} \frac{\psi_i^{n_i}}{\sqrt{n_i!}} |n_i\rangle. \quad (6.12)$$



The time evolution of the order field  $\psi_i$  is then given by

$$\psi_i(t) = \langle \phi_i | e^{\frac{it}{\hbar} \hat{H}_i} a_i e^{-\frac{it}{\hbar} \hat{H}_i} | \phi_i \rangle. \quad (6.13)$$

A direct evaluation of (6.13) with (6.1) finally leads to

$$\psi_i(t) = \psi_i \exp \left\{ |\psi_i|^2 \left[ e^{-\frac{itU_B}{\hbar}} - 1 \right] \right\} e^{-i\frac{m\omega_B^2}{2\hbar} r_i^2 t}. \quad (6.14)$$

### 6.3. Initial conditions

Initial equilibrium situations happening deep in the superfluid phase can be described by the lattice version of the Gross-Pitaevskii equation

$$-J_A \sum_{j \in n.n} \psi_j + U_A |\psi_i|^2 \psi_i + V_i \psi_i = \mu \psi_i. \quad (6.15)$$

Now we use the Thomas-Fermi approximation as solution of (6.15)

$$\psi_i = \sqrt{\frac{zJ_A + \mu - V_i}{U_A}}. \quad (6.16)$$

The constant  $zJ_A + \mu$  is determined from the initial total number of condensed atoms which in our case is  $N_c = 0.6 \times 2 \times 10^5$ . Here the factor 0.6 corresponds to the initial coherent fraction observed in Ref. [1].

Since in Ref. [1], there was around 150,000 populated lattice sites, we can consider the Thomas-Fermi radius as being much larger than the lattice spacing  $a$ , in such a way that  $\mathbf{r}_i$  can be regarded as a continuous variable. The explicit formulas for the constant  $zJ_A + \mu$  and the Thomas-Fermi radius  $R$  are given by

$$zJ_A + \mu = \left( \frac{15U_A a^3 N_c}{8\pi} \right)^{2/5} (m\omega_A^2/2)^{3/5}, \quad (6.17)$$

$$R = \sqrt{\frac{2(zJ_A + \mu)}{m\omega_A^2}}, \quad (6.18)$$

where, in our case, we have  $U_A = 4.84 \times 10^{-31} \text{J}$  which leads to the Thomas-Fermi radius  $R = 32.6a$ .

The solution (6.16) can be directly used as the initial condition of (6.14). However, since Eq. (6.10) determines only the sum  $A_i^+ + A_i^-$ , the difference  $A_i^+ - A_i^-$  between the amplitude modes has to be determined from the minimum of the observed oscillations of  $N_c$ .

### 6.4. Momentum distributions

In the limit of validity of the Bose-Hubbard model the condensate wave function in coordinate space is given by

$$\Psi(\mathbf{r}, t) = \sum_i \mathcal{U}(\mathbf{r} - \mathbf{r}_i) \psi_i(t). \quad (6.19)$$

## 6. Collapse and Revival of Matter Waves

In order to compare our results with the experiments, we must explicitly calculate the momentum distribution of the condensate wave function. Due to the periodicity of the Wannier function  $\mathcal{U}(\mathbf{r})$ , it has the simple form

$$\Psi(\mathbf{k}, t) = \mathcal{U}(\mathbf{k})\psi(\mathbf{k}, t) \quad (6.20)$$

with the quasi-momentum distribution  $\psi(\mathbf{k}, t)$  given by

$$\psi(\mathbf{k}, t) = \sum_l e^{i\mathbf{k}\cdot\mathbf{r}_l} \psi(\mathbf{r}_l, t), \quad (6.21)$$

where the function  $\psi(\mathbf{r}, t)$  is defined in such a way that

$$\psi(\mathbf{r}_i, t) = \psi_i(t). \quad (6.22)$$

In order to compare the results from our equations of motion with the experimental results from Ref. [1], we must take into account that the condensed atoms are observed only in domains  $D_{\mathbf{k}}$  around the interference peaks located at  $\mathbf{k}_n$ . Therefore we must integrate the condensate density distribution only in these domains. As  $\psi(\mathbf{k}, t)$  is a periodic function with period  $\delta k = 2\pi/a$ , the observed number of condensed atoms is given by

$$N_c(t) = \sum_n \int_{D_{\mathbf{k}}} d^3\mathbf{k} |\Psi(\mathbf{k} + \mathbf{k}_n, t)|^2 = \int_{D_{\mathbf{k}}} d^3\mathbf{k} |\psi(\mathbf{k}, t)|^2 \sum_n |\mathcal{U}(\mathbf{k} + \mathbf{k}_n)|^2. \quad (6.23)$$

Here the factor containing the Wannier functions can be further simplified as follows

$$\sum_n |\mathcal{U}(\mathbf{k} + \mathbf{k}_n)|^2 = \frac{1}{(2\pi)^3} \int \int d\mathbf{r} d\mathbf{r}' \mathcal{U}^*(\mathbf{r}') \mathcal{U}(\mathbf{r}) \sum_n e^{i(\mathbf{k} + \mathbf{k}_n) \cdot (\mathbf{r} - \mathbf{r}')}. \quad (6.24)$$

By applying the Poisson's formula

$$\sum_n e^{i\mathbf{k}_n \cdot \mathbf{r}} = a^3 \sum_l \delta(\mathbf{r} - \mathbf{r}_l), \quad (6.25)$$

together with the orthonormality relation

$$\int d\mathbf{r} \mathcal{U}^*(\mathbf{r} + \mathbf{r}_l) \mathcal{U}(\mathbf{r}) = \delta_{0,l}, \quad (6.26)$$

we obtain

$$\sum_n |\mathcal{U}(\mathbf{k} + \mathbf{k}_n)|^2 = \left(\frac{a}{2\pi}\right)^3. \quad (6.27)$$

Substituting this back in (6.23), we finally have

$$N_c(t) = \left(\frac{a}{2\pi}\right)^3 \int_{D_{\mathbf{k}}} d^3\mathbf{k} |\psi(\mathbf{k}, t)|^2. \quad (6.28)$$

Additionally, the quasi-momentum distribution can be written in terms of the continuous Fourier

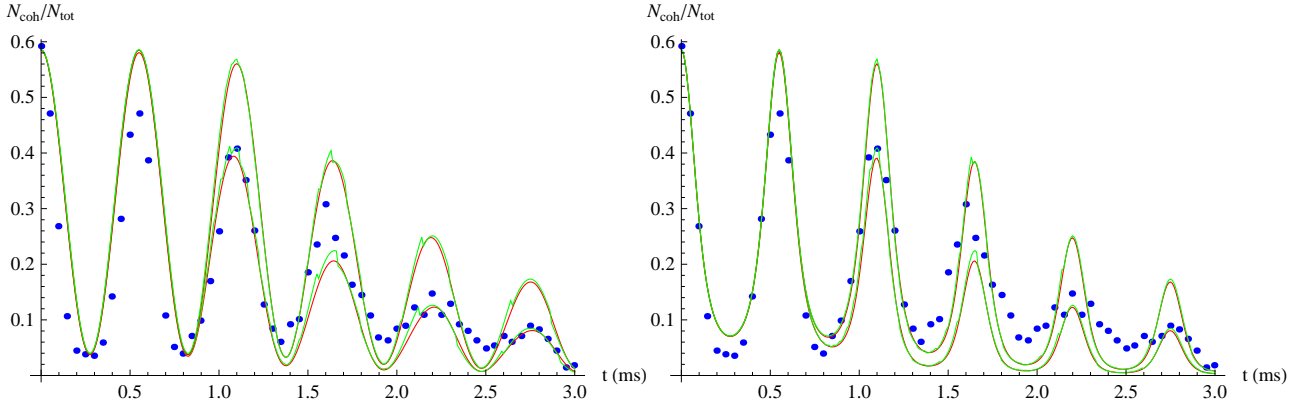


Figure 6.1.: Observed coherent fraction. Left: calculated from formula (6.10). Right: calculated from formula (6.14). The green lines are obtained using approximation (6.36). The red lines stem from a numerical calculation of Eq. (6.21). The blue dots are experimental points from [1]. The lower lines correspond to the momentum-space window  $\delta k = 2.0 \times 10^6 \text{m}^{-1}$  whereas the upper lines correspond to  $\delta k = 3.0 \times 10^6 \text{m}^{-1}$ .

transform. In order to see this, we rewrite Eq. (6.21) in the following form

$$\psi(\mathbf{k}, t) = \sum_l \int d^3\mathbf{r} \delta(\mathbf{r} - \mathbf{r}_l) e^{i\mathbf{k} \cdot \mathbf{r}} \psi(\mathbf{r}, t). \quad (6.29)$$

Using the Poisson formula (6.25) once more, we have

$$\psi(\mathbf{k}, t) = \frac{(2\pi)^{3/2}}{a^3} \sum_n \psi_c(\mathbf{k} + \mathbf{k}_n, t), \quad (6.30)$$

where  $\psi_c(\mathbf{k}, t)$  is the usual continuous Fourier transform of the order parameter field

$$\psi_c(\mathbf{k}, t) = \frac{1}{(2\pi)^{3/2}} \int d\mathbf{r} e^{i\mathbf{k} \cdot \mathbf{r}} \psi(\mathbf{r}, t). \quad (6.31)$$

Now observe that Eqs. (6.10) and (6.14) can both be written in the form

$$\psi(\mathbf{r}_l, t) = p(\mathbf{r}_l, t) e^{-i \frac{m\omega_B^2}{2\hbar} r_l^2 t}, \quad (6.32)$$

where  $p(\mathbf{r}, t)$  is a periodic function in  $t$  with period  $U/\hbar$ . Substitution of (6.32) into (6.21), reveals an additional frequency mode with period  $T = 4\pi/m\omega_B^2 a^2$ . Eq. (6.32) also enables us to evaluate the integral (6.31) for large times by using a saddle-point approximation which gives

$$\psi_c(\mathbf{k}, t) \approx \frac{1}{(im\omega_B^2 t)^{3/2}} \exp\left(i \frac{\mathbf{k}^2}{2m\omega_B^2 t}\right) p\left(\frac{\mathbf{k}}{m\omega_B^2 t}, t\right). \quad (6.33)$$

Additionally, if the function  $\psi_c(\mathbf{k}, t)$  is localized in a region with side smaller than  $\delta k$ , we can ignore

## 6. Collapse and Revival of Matter Waves

all terms with  $n \neq 0$  in Eq. (6.30), which leads to

$$\psi(\mathbf{k}, t) \approx \frac{(2\pi)^{3/2}}{a^3} \psi_c(\mathbf{k}, t). \quad (6.34)$$

Now we can substitute (6.33) into (6.28) and obtain

$$N_c(t) \approx \frac{1}{a^3} \int_{D_{\mathbf{r}}} d^3\mathbf{r} |p(\mathbf{r}, t)|^2, \quad (6.35)$$

where  $D_{\mathbf{r}}$  is the domain  $D_{\mathbf{k}}$  contracted by a factor  $m\omega_B^2 t$ . As the width of the function  $p(\mathbf{r}, t)$ , which is given by the Thomas-Fermi radius in Eq. (6.18), can be considered as much larger than the lattice spacing  $a$ , we can approximate the above integral as a sum over the lattice points

$$N_c(t) \approx \sum_{i \in D_{\mathbf{r}}} |p(\mathbf{r}_i, t)|^2. \quad (6.36)$$

In order to be consistent with the results obtained from the time-of-flight pictures in Ref. [1], the region  $D_{\mathbf{k}}$  must be taken as a rectangular parallelepiped with dimensions  $\delta k \times \delta k \times 2\pi/a$ . This leads to a loss of the observed condensed fraction to the region outside of  $D_{\mathbf{k}}$  as the momentum distribution  $|\psi(\mathbf{k}, t)|^2$  becomes less localized. From Eqs. (6.35) and (6.36) we see that the loss process starts exactly at the moment when the function  $|p(\mathbf{r}, t)|^2$  stops fitting into the domain  $D_{\mathbf{r}}$  due to its contraction. This allows us to calculate the critical time when the loss process starts

$$t_c = \frac{\delta k}{2m\omega_B^2 R}. \quad (6.37)$$

## 6.5. Comparison with Experiments

Now we compare the results obtained in Ref. [1] for  $N_c(t)$  with the exact numerical evaluation of (6.28) using Fast-Fourier transform algorithms as well as with the analytical approximation of (6.28) given by (6.36). In Fig. 6.1, we present the results for  $N_c$  calculated both numerically, using Fast-Fourier transform algorithms, and using formula (6.36).

In Eq. (6.37), we see that the critical time, after which the loss in the observed coherent density begins, depends linearly on the side  $\delta k$  of the observed momentum domain  $D_{\mathbf{k}}$ . In the experiments of Ref. [1], the observations are restricted to a squares with width  $\delta x = 130\mu\text{m}$ , around the interference peaks in the pictures obtained after the time-of-flight  $t_{\text{flight}} = 16\text{ms}$ . The corresponding  $\delta k$  is related to the width  $\delta x = 130\mu\text{m}$  according to

$$\delta x = \frac{\hbar \delta k}{m} t_{\text{flight}}. \quad (6.38)$$

This leads us to a momentum domain with width  $\delta k = 1.11 \times 10^7 \text{m}^{-1}$ . According to our theory, such a big momentum domain should give no observable loss of the condensate during the time interval between 0 and  $t_c = 2.4\text{ms}$ . In fact, our theoretical results become comparable with the the experimental data only if we consider  $\delta k$  to be one order of magnitude smaller, as we can see in Fig. 6.1. A possible explanation for such a disagreement may come from the fact that, in Ref. [1], part of the atoms

inside the domain  $D_{\mathbf{k}}$  are considered as belonging to the thermal cloud. This may lead to systematic underestimations of the coherent fraction and, therefore, to a condensate loss much higher than the theoretically expected.



## 7. Summary and Conclusion

Since 1989, despite many experimental and theoretical advancements, the most accurate analytical calculation of the MI-SF quantum phase diagram was based on the mean-field theory in Ref. [28]. In comparison with the high-precision Quantum Monte Carlo data [34], it underestimates by 16% the location of the first lobe tip for three-dimensional cubic lattices. An alternative way to obtain the MI-SF phase boundary at zero temperature is based on a strong-coupling expansion as is worked out in detail in Ref. [37]. However, the position of the first MI-SF lobe tip in the third-order hopping expansion is overestimated by 24% in three-dimensional lattices. For the two-dimensional case, the situation is in favor of the third-order hopping expansion which overestimate the position of the first lobe tip by 13% while the mean-field theory underestimates it by 28% [35]. The strong-coupling expansion has a clear advantage when one-dimensional systems are considered as it is even capable of reproducing the correct Kosterlitz-Thouless behavior in these systems.

This constituted the state-of-the-art treatment of bosons in a optical lattice at the time this thesis work was started. Precise results could be extracted from numerical simulations while physical understanding of the system was limited by inadequate analytical theories. Moreover, since numerical simulations are necessarily restricted to finite regions of the phase diagram, all published numerical studies concerning the MI-SF phase transition were concentrated in the region around the first Mott lobe. This means that there was a total lack of precise results for the regions with densities larger than one particle per lattice site. In view of a better quantitative comparison with experimental results, where the harmonic confinement is dealt within the local density approximation and, thus, usually involves more than one Mott lobe, it was indispensable to further develop analytical approximation methods.

Driven by this necessity of new precise analytical methods to deal with bosons in optical lattices, this thesis was dedicated to elaborate a set of tools which culminated in the development of an elegant and powerful Ginzburg-Landau theory [39,40]. This method turned out to provide not only a better qualitative understanding of the lattice system, but also to improve the former analytical methods. Actually, the first-order hopping expansion reproduces the above mentioned mean-field results and our second-order hopping expansion already exhibits a relative error of less than 3% for the phase boundary in the three-dimensional case which can be considered as exact for most practical purposes. In this way, our accurate analytical results for the phase boundary at arbitrary dimensions, chemical potentials, and temperatures, yields new insights beyond the purely numerical data provided by Quantum Monte Carlo simulations.

After the initial application of our new Ginzburg-Landau theory to cubic lattices in two and three dimensions [39,40], a stream of papers were published both using the quantum phase diagram obtained from our method as reference data [81–83] and applying our Ginzburg-Landau theory in various situations involving bosons in optical lattices [41–46,84–86].

## 7. Summary and Conclusion

In our first two papers, where the general techniques were introduced [39,40], the actual computations were performed only at first and second hopping order. A systematic study of our theory for higher orders of the hopping parameter was performed by the group of Martin Holthaus in Oldenburg [41–44] and demonstrated an impressive convergence for the hopping expansion. In fact, their extrapolation of the 10th hopping order results are indistinguishable from the Quantum Monte Carlo data [34]. After that, our theory was applied by the authors of Ref. [84] to obtain the phase boundary separating the Mott insulator phase from the so called pair superfluid phase (PSF) which is induced by excited molecules loaded into the optical lattice. In Ref. [85], the authors used our theory to study the phase diagram of attractive atoms with three-body constraint in optical lattices. In particular, they calculated the MI-SF phase boundary as well as the phase boundary separating the MI phase and a dimer superfluid phase (DSF). The application for triangular and hexagonal optical lattices was made in Ref. [86] where the authors generated the first reference data for optical lattices with these geometries. In Refs. [45,46], our effective action approach was combined with the Keldysh formalism in order to describe cubic optical lattices in out-of-equilibrium conditions.

The first three chapters of this thesis introduce the physics of optical lattices and serve as an overview over some subjects which are relevant for a better understanding of the methods developed here. The last three chapters contain the original contributions of my PhD work.

In Chapter 2, the general theory of optical lattices was discussed. It was described how laser generated standing waves are used to produce periodic potentials as in Eq. (2.21). These potentials are capable of reproducing many features of solid-state systems with the advantage of a defect-free lattice whose tunnel coupling can be tuned by both the intensity and the frequency of the lasers. Due to the ac-Stark effect, the atoms are trapped in the maxima or minima of the laser field depending on whether the lasers are red or blue detuned, respectively. The Bloch theorem states that the spectrum of free particles moving through the lattice has a band structure as depicted in Fig. 2.1. Since the separation between Bloch bands increases with the lattice depth, the assumption of deep enough lattices at temperatures close to zero allows to describe these systems in terms of the so called Bose-Hubbard Hamiltonian (2.52). By an explicit calculation of the Wannier function (2.25), it was possible to obtain the Bose-Hubbard parameters defined in Eqs. (2.53)–(2.55). Approximate expressions for the hopping parameter and the on-site energy are shown in (2.61) and (2.65), which are compared with the numerically calculated parameters in Figs. 2.4 and 2.6. The effects due to the inhomogeneities of the generating laser beams are considered in the inhomogeneous Bose-Hubbard Hamiltonian (2.73) and the corresponding expressions for system parameters are provided in Eqs. (2.74), (2.79)–(2.81), and (2.85).

In Chapter 3, a general introduction to second-order phase transitions was provided according to the modern classification of critical phenomena. In particular, the symmetry breaking mechanism was addressed, which applies when the system passes from one more ordered to a less ordered phase. A discussion was also made on the role of the order parameter and the concept of *universality* as well as its relation to the different critical exponents characterizing the immediate vicinity of a phase transition. Special attention was given to quantum phase transitions which are transitions that can happen even at zero temperature. Most of these discussions are made in the context of bosons in optical lattices so that the theory of second-order phase transitions was specifically applied to the



MI-SF transition. It was also described how to apply quantum statistical mechanics to systems with spontaneous symmetry breaking. This method consists in minimizing the Von Neumann entropy (3.13) subjected to constraints in the order parameter in addition to the constraints of the considered ensemble. In the grand-canonical ensemble, this generates the effective potential (3.14) which depends on the order parameter. The first step for the actual calculation of the effective potential is to obtain the free energy according to Eq. (3.15). This free energy depends on the symmetry-breaking sources which are also the Lagrange multipliers used to enforce the constraints in the order parameter. The effective potential itself must be obtained from the Legendre transformation of (3.15). By analyzing the expansion of the effective potential in a power series of the order parameter (3.23), it is possible to determine the phase of the system depending on the values of its control parameters. The effective potential was also generalized to the so called effective action by allowing the order parameter to vary both in space and imaginary time. This generalization was essential for the diagrammatic approach developed in Chapter 4 and for the calculation of dynamical properties like the excitation spectra in Chapter 5. The explicit expression for the MI-SF phase boundary calculated using mean-field theory is given by Eq. (3.46) and the corresponding phase diagram is displayed in Fig. 3.2. The unphysical decreasing of the total particle density with the chemical potential shown in Fig. 3.3 and the consequent negative compressibility in Fig. 3.4 are pointed out as weaknesses of the mean-field theory.

In Chapter 4, a perturbation theory was developed by taking advantage of a diagrammatic notation which has been specially developed to deal with bosons in optical lattices. Such a notation follows the ideas introduced in Ref. [63], where a diagrammatic expansion for the fermionic Hubbard model is considered. In the bosonic case, the calculation of the effective action, which is defined through a Legendre transformation of the free energy, leads to an automatic resummation of the hopping expansion. This allows the description of the system properties in both the Mott insulator and superfluid phase. By defining a set of diagrammatic rules, the effective action was calculated up to second hopping order. At first, by analyzing the expansion of the partition function (4.7) in a power series of both the order parameter and the hopping parameter, it was possible to find the general formula (4.29). This formula not only simplifies the computation of the terms in the partition function but also allows us to construct the set of diagrammatic rules for our calculations. Further simplification of our calculations was possible by defining the generating functional of connected diagrams (4.32) and the generating functional of the 1PI diagrams (4.47) which represent the diagrammatic content of the free energy and the effective action, respectively. The Matsubara representation was introduced and it was shown that, in this representation, the same rules used for imaginary time can also be applied if we take into account the transformations (4.58) and (4.59). The most relevant terms in the effective action are then systematically calculated up to second hopping order and are given by (4.71), (4.88), (4.92), and (4.101). In order to facilitate the comprehension of calculations in Matsubara space, some computational details are relegated to the appendices A and B.

In Chapter 5, the effective action was used to calculate various static and dynamical properties of cubic bosonic lattices at both zero and finite temperature. In Fig. 5.4, the comparison of the total particle density and the compressibility in the superfluid phase with the mean-field results shows that the unphysical features of the mean-field results are not present in our theory. Eq. (5.30) gives the critical hopping based on our second-order hopping expansion. This result shows an impressive

accordance with the numerically calculated phase diagrams for two and three dimensions, as depicted in Fig. 5.6. This indicates that already at second-hopping order our theory has enough precision for most practical applications. In addition, the equivalence between condensed density and superfluid density was demonstrated at first hopping order by using the definition of superfluid density (5.33). Here it should be noted, however, that this property does not necessarily hold for higher orders of the hopping expansion [87]. By considering the fluctuations of the order parameter around its equilibrium value in (5.9) and using (5.37) and (5.38) to Wick rotate from imaginary time to real time, it was possible to find the equations defining the dispersion relations for collective excitations in the MI phase (5.42) and SF phase (5.68), (5.69). In the MI phase, the solution of Eq. (5.42) shown in Fig. 5.9 indicates the existence of two excitations which are known as particle and hole excitations with positive and negative gaps, respectively. In order to evaluate the gaps and masses associated with these excitations in (5.49) and (5.50), the Eq. (5.42) was solved in the limit of large wavelengths and small frequencies. In the SF phase, the solution of (5.68) and (5.69) in Fig. 5.12 exhibits a gapless excitation known as Goldstone mode in addition to the gapped mode. By solving Eqs. (5.68) and (5.69) in the limit of large wavelengths and small frequencies, the gap and mass of the gapped mode in Eqs. (5.83) and (5.84) as well as sound velocity in Eq. (5.86) associated with the Goldstone mode are calculated. The mass and gap of the gapped mode are shown in Fig. 5.13, while the sound velocity was depicted in Fig. 5.14.

Chapter 6 discusses the formation and dynamics of matter waves in an optical lattice loaded with  $^{87}\text{Rb}$  atoms which was experimentally observed by Greiner et al. [1]. The results from our theory are used to reproduce the features observed in Ref. [1] and to test our theory against the respective experimental results. The real-time effective action for small oscillations of the order parameter was considered in Eq. (6.3) which makes it possible to construct the general solution (6.10). The exact solution for the order parameter time evolution was also considered in (6.14). The initial conditions are taken from the Thomas-Fermi approximation (6.16). In order to reproduce the experimentally observed decay of the coherent fraction, it was necessary to consider the fact that the experiment is restricted to a finite region of momentum space according to Eq. (6.28). This allows us to compare the time evolution of the coherent fraction obtained from the solutions (6.10) and (6.14) with the experimental results as shown in Fig. 6.1. In addition, the critical time after which the coherent fraction starts to decay was calculated in Eq. (6.37).

In this thesis, a new effective action approach combined with diagrammatic techniques was developed and applied to analyze static and dynamic properties of spinless bosons in optical lattices. These new tools can also be applied to a wide range of atomic systems in optical lattices by adapting the diagrammatic rules to the Hamiltonian of interest where the Legendre transformation leading to the effective action must be made according to the order parameters of the considered system. More precisely, a new source term must be added to the Hamiltonian for each order parameter considered. By making such modifications, our formalism was already applied, for example, in Refs. [84,85]. Among other possible systems, where this formalism can be applied, we have Bose-Bose [88,89] and Bose-Fermi mixtures, optical lattices with non-trivial geometries such as triangular [86,90] and Kagomé [22], and even other realizations of lattice systems as QED lattices [91].

Bose-Bose mixtures can be obtained, for instance, by using heteronuclear mixtures as in Ref. [89],

where the authors trapped  $^{87}\text{Rb}$  and  $^{41}\text{K}$  atoms in a 3D optical lattice, or by confining a mixture of atoms of the same species but in different hyperfine states as in Ref. [88], where the hyperfine states  $|F = 2, m_F = -2\rangle$  and  $|F = 1, m_F = -1\rangle$  of  $^{87}\text{Rb}$  were used. In these cases a two-species Bose-Hubbard Hamiltonian has to be considered [92–95]. A natural generalization for such systems consists in considering two order parameter fields corresponding to the macroscopic wave function of each species.

Bose-Fermi mixtures can be realized for example by using  $^{40}\text{K}$ - $^{87}\text{Rb}$  or  $^{40}\text{K}$ - $^{23}\text{Na}$  mixtures as in Ref. [96]. There, in addition to the usual superfluid order parameter, extra order parameters must be included in order to distinguish between different non-superfluid phases as the charge density and spin density waves [96].

Different geometries can also be treated with our approach, as was shown in Ref. [86] for triangular and hexagonal lattices. Another geometry, which could be considered, is the Kagomé geometry [22].

A straightforward application of the methods developed here is in the field of optical QED lattices where the so called Jaynes-Cummings-Hubbard model can be used to describe the Bose-Einstein condensation of polaritons in a way analogous to the condensation of bosonic atoms in optical lattices. This problem was treated in the diploma thesis in Ref. [91], where further references to this interesting topic can be found.

We conclude that our Ginzburg-Landau theory for bosons in optical lattices has successfully passed various tests against numerical simulations and experimental results. Therefore, we expect it to be useful for planning and analyzing future lattice experiments.



## A. Appendix 1

This appendix contain the derivation of the general formula used in Chapter 4 to simplify the calculation of Matsubara transformed Green functions.

The objective is to calculate the general multiple integral

$$C(\omega_n, \dots, \omega_1) = \int_0^\beta d\tau_n \cdots \int_0^\beta d\tau_1 e^{i(\omega_1\tau_1 + \dots + \omega_n\tau_n)} \text{Tr} \left\{ e^{-\beta\hat{H}} \hat{T} \left[ \hat{O}_n(\tau_n) \cdots \hat{O}_1(\tau_1) \right] \right\}, \quad (\text{A.1})$$

here Matsubara frequencies are  $\omega_n = (2\pi/\beta)n$ , where  $n$  are integer numbers.  $\hat{H}$  is an arbitrary time-independent Hamiltonian and  $\hat{O}_i(\tau_i)$  are arbitrary operators in Heisenberg representation, i.e.,  $\hat{O}_i(\tau_i) = e^{\tau\hat{H}} \hat{O}_i(0) e^{-\tau\hat{H}}$ .

The first observation that we have to make is that, due to invariance of the trace under cyclic permutations, we have

$$\text{Tr} \left\{ e^{-\beta\hat{H}} \hat{T} \left[ \hat{O}_n(\tau_n) \cdots \hat{O}_1(\tau_1) \right] \right\} = \text{Tr} \left\{ e^{-\beta\hat{H}} \hat{T} \left[ \hat{O}_n(\tau_n - \tau_1) \cdots \hat{O}_2(\tau_2 - \tau_1) \hat{O}_1(0) \right] \right\}. \quad (\text{A.2})$$

By making the transformation  $\tau_i \rightarrow \tau_i + \tau_1$  in the variables  $\{\tau_n, \dots, \tau_2\}$ , we can rewrite (A.1) as

$$C(\omega_n, \dots, \omega_1) = \int_0^\beta d\tau_1 e^{i(\omega_1 + \dots + \omega_n)\tau_1} \int_{-\tau_1}^{\beta-\tau_1} d\tau_n \cdots \int_{-\tau_1}^{\beta-\tau_1} d\tau_2 e^{i(\omega_2\tau_2 + \dots + \omega_n\tau_n)} \text{Tr} \left\{ e^{-\beta\hat{H}} \hat{T} \left[ \hat{O}_n(\tau_n) \cdots \hat{O}_2(\tau_2) \hat{O}_1(0) \right] \right\}. \quad (\text{A.3})$$

The integration interval  $(-\tau_1, \beta - \tau_1)$  of the variables  $\{\tau_n, \dots, \tau_2\}$  can be spited into the two sub-intervals  $(-\tau_1, 0)$  and  $(0, \beta - \tau_1)$ , i.e.,

$$\begin{aligned} & \int_{-\tau_1}^{\beta-\tau_1} d\tau_n \cdots \int_{-\tau_1}^{\beta-\tau_1} d\tau_2 e^{i(\omega_2\tau_2 + \dots + \omega_n\tau_n)} \text{Tr} \left\{ e^{-\beta\hat{H}} \hat{T} \left[ \hat{O}_n(\tau_n) \cdots \hat{O}_2(\tau_2) \hat{O}_1(0) \right] \right\} \\ &= \left( \int_0^{\beta-\tau_1} d\tau_n + \int_{-\tau_1}^0 d\tau_n \right) \cdots \left( \int_0^{\beta-\tau_1} d\tau_2 + \int_{-\tau_1}^0 d\tau_2 \right) e^{i(\omega_2\tau_2 + \dots + \omega_n\tau_n)} \text{Tr} \left\{ e^{-\beta\hat{H}} \hat{T} \left[ \hat{O}_n(\tau_n) \cdots \hat{O}_2(\tau_2) \hat{O}_1(0) \right] \right\} \end{aligned} \quad (\text{A.4})$$

It means that Eq. (A.4) is composed by a sum of multiple integrals where, in each of these terms, a given variable  $\tau_i$  is integrated in either the interval  $(-\tau_1, 0)$  or  $(0, \beta - \tau_1)$ . Let us consider an arbitrary

## A. Appendix 1

term which has  $l - 1$  variables  $\{\tau_{i_l}, \dots, \tau_{i_2}\}$  integrated in the interval  $(0, \beta - \tau_1)$  and  $n - l$  variables  $\{\tau_{i_n}, \dots, \tau_{i_{l+1}}\}$  integrated in the interval  $(\tau_1, 0)$ . Such a term can be expressed as

$$\begin{aligned} & \int_{-\tau_1}^0 d\tau_{i_n} \cdots \int_{-\tau_1}^0 d\tau_{i_{l+1}} \int_0^{\beta-\tau_1} d\tau_{i_l} \cdots \int_0^{\beta-\tau_1} d\tau_{i_2} e^{i(\omega_{i_2}\tau_{i_2} + \cdots + \omega_{i_n}\tau_{i_n})} \text{Tr} \left\{ e^{-\beta\hat{H}} \hat{T} \left[ \hat{O}_{i_n}(\tau_{i_n}) \cdots \hat{O}_{i_2}(\tau_{i_2}) \hat{O}_1(0) \right] \right\} \\ &= \int_{-\tau_1}^0 d\tau_{i_n} \cdots \int_{-\tau_1}^0 d\tau_{i_{l+1}} \int_0^{\beta-\tau_1} d\tau_{i_l} \cdots \int_0^{\beta-\tau_1} d\tau_{i_2} e^{i(\omega_{i_2}\tau_{i_2} + \cdots + \omega_{i_n}\tau_{i_n})} \\ & \quad \times \text{Tr} \left\{ e^{-\beta\hat{H}} \hat{T} \left[ \hat{O}_{i_l}(\tau_{i_l}) \cdots \hat{O}_{i_2}(\tau_{i_2}) \right] \hat{O}_1(0) \hat{T} \left[ \hat{O}_{i_n}(\tau_{i_n}) \cdots \hat{O}_{i_{l+1}}(\tau_{i_{l+1}}) \right] \right\}, \end{aligned} \quad (\text{A.5})$$

where the right-hand side of this equation is obtained by observing that  $\tau < 0$  if  $\tau \in \{\tau_{i_n}, \dots, \tau_{i_{l+1}}\}$  and  $\tau > 0$  if  $\tau \in \{\tau_{i_l}, \dots, \tau_{i_2}\}$ .

Now, by making the transformation  $\tau \rightarrow \tau - \beta$  in the variables  $\{\tau_{i_n}, \dots, \tau_{i_{l+1}}\}$  we have

$$\begin{aligned} & \int_{-\tau_1}^0 d\tau_{i_n} \cdots \int_{-\tau_1}^0 d\tau_{i_{l+1}} \int_0^{\beta-\tau_1} d\tau_{i_l} \cdots \int_0^{\beta-\tau_1} d\tau_{i_2} e^{i(\omega_{i_2}\tau_{i_2} + \cdots + \omega_{i_n}\tau_{i_n})} \text{Tr} \left\{ e^{-\beta\hat{H}} \hat{T} \left[ \hat{O}_{i_n}(\tau_{i_n}) \cdots \hat{O}_{i_2}(\tau_{i_2}) \hat{O}_1(0) \right] \right\} \\ &= \int_{\beta-\tau_1}^{\beta} d\tau_{i_n} \cdots \int_{\beta-\tau_1}^{\beta} d\tau_{i_{l+1}} \int_0^{\beta-\tau_1} d\tau_{i_l} \cdots \int_0^{\beta-\tau_1} d\tau_{i_2} e^{i(\omega_{i_2}\tau_{i_2} + \cdots + \omega_{i_n}\tau_{i_n})} \\ & \quad \times \text{Tr} \left\{ e^{-\beta\hat{H}} \hat{T} \left[ \hat{O}_{i_l}(\tau_{i_l}) \cdots \hat{O}_{i_2}(\tau_{i_2}) \right] \hat{O}_1(0) e^{-\beta\hat{H}} \hat{T} \left[ \hat{O}_{i_n}(\tau_{i_n}) \cdots \hat{O}_{i_{l+1}}(\tau_{i_{l+1}}) \right] e^{\beta\hat{H}} \right\} \\ &= \int_{\beta-\tau_1}^{\beta} d\tau_{i_n} \cdots \int_{\beta-\tau_1}^{\beta} d\tau_{i_{l+1}} \int_0^{\beta-\tau_1} d\tau_{i_l} \cdots \int_0^{\beta-\tau_1} d\tau_{i_2} e^{i(\omega_{i_2}\tau_{i_2} + \cdots + \omega_{i_n}\tau_{i_n})} \\ & \quad \times \text{Tr} \left\{ e^{-\beta\hat{H}} \hat{T} \left[ \hat{O}_{i_n}(\tau_{i_n}) \cdots \hat{O}_{i_{l+1}}(\tau_{i_{l+1}}) \right] \hat{T} \left[ \hat{O}_{i_l}(\tau_{i_l}) \cdots \hat{O}_{i_2}(\tau_{i_2}) \right] \hat{O}_1(0) \right\} \\ &= \int_{\beta-\tau_1}^{\beta} d\tau_{i_n} \cdots \int_{\beta-\tau_1}^{\beta} d\tau_{i_{l+1}} \int_0^{\beta-\tau_1} d\tau_{i_l} \cdots \int_0^{\beta-\tau_1} d\tau_{i_2} e^{i(\omega_{i_2}\tau_{i_2} + \cdots + \omega_{i_n}\tau_{i_n})} \\ & \quad \times \text{Tr} \left\{ e^{-\beta\hat{H}} \hat{T} \left[ \hat{O}_{i_n}(\tau_{i_n}) \cdots \hat{O}_{i_2}(\tau_{i_2}) \hat{O}_1(0) \right] \right\}, \end{aligned} \quad (\text{A.6})$$

This means that the integration limits  $(0, -\tau_1)$  in Eq. (A.4) can actually be substituted by the new limits  $(\beta, \beta - \tau_1)$ , i.e.,

$$\begin{aligned} & \left( \int_0^{\beta-\tau_1} d\tau_n + \int_{-\tau_1}^0 d\tau_n \right) \cdots \left( \int_0^{\beta-\tau_1} d\tau_2 + \int_{-\tau_1}^0 d\tau_2 \right) e^{i(\omega_2\tau_2 + \cdots + \omega_n\tau_n)} \text{Tr} \left\{ e^{-\beta\hat{H}} \hat{T} \left[ \hat{O}_n(\tau_n) \cdots \hat{O}_2(\tau_2) \hat{O}_1(0) \right] \right\} \\ &= \left( \int_0^{\beta-\tau_1} d\tau_n + \int_{\beta-\tau_1}^{\beta} d\tau_n \right) \cdots \left( \int_0^{\beta-\tau_1} d\tau_2 + \int_{\beta-\tau_1}^{\beta} d\tau_2 \right) e^{i(\omega_2\tau_2 + \cdots + \omega_n\tau_n)} \\ & \quad \times \text{Tr} \left\{ e^{-\beta\hat{H}} \hat{T} \left[ \hat{O}_n(\tau_n) \cdots \hat{O}_2(\tau_2) \hat{O}_1(0) \right] \right\}, \end{aligned} \quad (\text{A.7})$$

which is equivalent to

$$\begin{aligned}
& \int_{-\tau_1}^{\beta-\tau_1} d\tau_n \cdots \int_{-\tau_1}^{\beta-\tau_1} d\tau_2 e^{i(\omega_2\tau_2+\cdots+\omega_n\tau_n)} \text{Tr} \left\{ e^{-\beta\hat{H}} \hat{T} \left[ \hat{O}_n(\tau_n) \cdots \hat{O}_2(\tau_2) \hat{O}_1(0) \right] \right\} \\
& = \int_0^\beta d\tau_n \cdots \int_0^\beta d\tau_2 e^{i(\omega_2\tau_2+\cdots+\omega_n\tau_n)} \text{Tr} \left\{ e^{-\beta\hat{H}} \hat{T} \left[ \hat{O}_n(\tau_n) \cdots \hat{O}_2(\tau_2) \hat{O}_1(0) \right] \right\}
\end{aligned}$$

Substituting this result back into (A.3), we finally obtain our final result

$$C(\omega_n, \cdots, \omega_1) = \beta \delta_{0, \omega_n + \cdots + \omega_1} \int_0^\beta d\tau_n \cdots \int_0^\beta d\tau_2 e^{i(\omega_2\tau_2+\cdots+\omega_n\tau_n)} \text{Tr} \left\{ e^{-\beta\hat{H}} \hat{T} \left[ \hat{O}_n(\tau_n) \cdots \hat{O}_2(\tau_2) \hat{O}_1(0) \right] \right\} \quad (\text{A.8})$$





## B. Appendix 2

Consider a function  $f(x)$  which decays faster than  $|x|^{-1}$  as  $|x| \rightarrow \infty$  and whose only divergences are simple poles located at  $\omega_i^\pm = ia_i^\pm$  with  $a_i^+ > 0$  and  $a_i^- < 0$ . Then

$$\begin{aligned} \sum_{n=-\infty}^{\infty} f\left(\frac{2\pi}{\beta}n\right) &= \int_{-\infty}^{\infty} d\omega \sum_{n=-\infty}^{\infty} \delta\left(\omega - \frac{2\pi}{\beta}n\right) f(\omega) = \frac{\beta}{2\pi} \sum_{n=-\infty}^{\infty} \int_{-\infty}^{\infty} d\omega e^{i\beta\omega n} f(\omega) \\ &= \frac{\beta}{2\pi} \left( 2\pi i \sum_{i^+} \sum_{n=0}^{\infty} e^{-\beta a_i^+ n} c_i^+ - 2\pi i \sum_{i^-} \sum_{n=-\infty}^{-1} e^{-\beta a_i^- n} c_i^- \right), \end{aligned} \quad (\text{B.1})$$

where we used the Poisson formula. The coefficients  $c_i^\pm$  are the residues associated with the poles  $\omega_i^\pm$ . The sum over  $n$  gives

$$\sum_{n=-\infty}^{\infty} f\left(\frac{2\pi}{\beta}n\right) = i\beta \left( \sum_{i^+} \frac{c_i^+}{1 - e^{-\beta a_i^+}} - \sum_{i^-} \frac{e^{\beta a_i^-} c_i^-}{1 - e^{\beta a_i^-}} \right) \quad (\text{B.2})$$

$$= i\beta \sum_i \frac{c_i}{1 - e^{-\beta a_i}}. \quad (\text{B.3})$$

Here the index  $i$  labels all poles above and below the real line of the complex plane.

Below we show some very useful application of this formula

$$\sum_{n=-\infty}^{\infty} \frac{1}{\omega_n - i\mu} = i\beta \frac{1}{1 - e^{-\beta\mu}} \quad (\text{B.4})$$

$$\sum_{n=-\infty}^{\infty} \frac{1}{(\omega_n - i\mu)(\omega_n - i\nu)} = i\beta \left( \frac{1}{1 - e^{-\beta\mu}} \frac{1}{i\mu - i\nu} + \frac{1}{1 - e^{-\beta\nu}} \frac{1}{i\nu - i\mu} \right) = \beta \frac{e^{-\beta\mu} - e^{-\beta\nu}}{(1 - e^{-\beta\mu})(1 - e^{-\beta\nu})(\mu - \nu)} \quad (\text{B.5})$$

$$\begin{aligned}
\sum_{n=-\infty}^{\infty} \frac{1}{(\omega_n - i\mu)(\omega_n - i\nu)(\omega_n - i\eta)} &= i\beta \left( \frac{1}{1 - e^{-\beta\mu}} \frac{1}{(i\mu - i\nu)(i\mu - i\eta)} \right. \\
&\quad \left. + \frac{1}{1 - e^{-\beta\nu}} \frac{1}{(i\nu - i\mu)(i\nu - i\eta)} + \frac{1}{1 - e^{-\beta\eta}} \frac{1}{(i\eta - i\mu)(i\eta - i\nu)} \right) \\
&= i\beta \left[ \frac{1}{(\nu - \mu)(\nu - \eta)} \left( \frac{1}{1 - e^{-\beta\mu}} - \frac{1}{1 - e^{-\beta\nu}} \right) \right. \\
&\quad \left. + \frac{1}{(\eta - \nu)(\eta - \mu)} \left( \frac{1}{1 - e^{-\beta\mu}} - \frac{1}{1 - e^{-\beta\eta}} \right) \right] \quad (\text{B.6})
\end{aligned}$$

In the cases where we have higher-order divergences, we can calculate the sums by taking derivatives of functions with only single poles. Here are some examples

$$\sum_{n=-\infty}^{\infty} \frac{1}{(\omega_n - i\mu)^2} = -i\partial_\mu \sum_{n=-\infty}^{\infty} \frac{1}{\omega_n - i\mu} = -\beta^2 \frac{e^{-\beta\mu}}{(1 - e^{-\beta\mu})^2} = \beta^2 \left[ \frac{1}{1 - e^{-\beta\mu}} - \frac{1}{(1 - e^{-\beta\mu})^2} \right] \quad (\text{B.7})$$

$$\begin{aligned}
\sum_{n=-\infty}^{\infty} \frac{1}{(\omega_n - i\mu)^2 (\omega_n - i\nu)} &= -i\partial_\mu \sum_{n=-\infty}^{\infty} \frac{1}{(\omega_n - i\mu)(\omega_n - i\nu)} \\
&= i\beta \left[ \frac{e^{-\beta\mu} - e^{-\beta\nu}}{(\mu - \nu)^2 (1 - e^{-\beta\mu})(1 - e^{-\beta\nu})} + \frac{\beta e^{-\beta\mu}}{(\mu - \nu)(1 - e^{-\beta\mu})^2} \right]
\end{aligned}$$

$$\sum_{n=-\infty}^{\infty} \frac{1}{(\omega_n - i\mu)^3} = \frac{-i}{2} \partial_\mu \sum_{n=-\infty}^{\infty} \frac{1}{(\omega_n - i\mu)^2} = -i\beta^3 \left[ \frac{e^{-2\beta\mu}}{(1 - e^{-\beta\mu})^3} + \frac{e^{-\beta\mu}}{2(1 - e^{-\beta\mu})^2} \right] \quad (\text{B.8})$$

# Bibliography

- [1] M. Greiner, O. Mandel, T. W. Hänsch, and I. Bloch. Collapse and revival of the matter wave field of a Bose-Einstein condensate. *Nature*, 419:51, 2002.
- [2] S. N. Bose. Plancks Gesetz und Lichtquantenhypothese. *Z. Phys.*, 26:178, 1924.
- [3] A. Einstein. *Siz. Kgl. Preuss. Akad. Wiss.*, page 261, 1924.
- [4] A. Einstein. *Siz. Kgl. Preuss. Akad. Wiss.*, page 3, 1925.
- [5] F. London. The  $\lambda$  -Phenomenon of Liquid Helium and the Bose-Einstein Degeneracy. *Nature*, 141:643, 1938.
- [6] E. C. Svensson and V. F. Sears. Neutron Scattering by  $^4\text{He}$  and  $^3\text{He}$ . *Prog. Low Temp. Phys.*, 11:189, 1987.
- [7] W. Ketterle and N. V. Druten. Evaporative cooling of trapped atoms. *Adv. Atom. Mol. Opt. Phys.*, 37:181, 1996.
- [8] M. H. Anderson, J. R. Ensher, M. R. Matthews, C. E. Wieman, and E. A. Cornell. Observation of Bose-Einstein condensation in a dilute atomic vapor. *Science*, 269:198, 1995.
- [9] K. B. Davis, M. Mewes, M. R. Andrews, N. J. van Druten, D. S. Durfee, D. M. Kurn, and W. Ketterle. Bose-Einstein condensation in a gas of sodium atoms. *Phys. Rev. Lett.*, 75:3969, 1995.
- [10] E. P. Gross. Structure of a quantized vortex in boson systems. *Nuovo Ciminto*, 20:454, 1961.
- [11] L. P. Pitaevskii. Vortex Lines in an Imperfect Bose Gas. *JETP*, 13:451, 1961.
- [12] N. N. Bogoliubov. On the theory of superfluidity. *J. Phys. (USSR)*, 11:23, 1947.
- [13] H. Moritz, T. Stöferle, M. Köhl, and T. Esslinger. Exciting Collective Oscillations in a Trapped 1D Gas. *Phys. Rev. Lett.*, 91:1, 2003.
- [14] B. Paredes, A. Widera, V. Murg, O. Mandel, S. Fölling, I. Cirac, G.V. Shlyapnikov, T.W. Hänsch, and I. Bloch. Tonks-Girardeau gas of ultracold atoms in an optical lattice. *Nature*, 429:277, 2004.
- [15] T. Kinoshita, T. Wenger, and D. S. Weiss. Observation of a one-dimensional Tonks-Girardeau gas. *Science (New York, N.Y.)*, 305:1125, 2004.
- [16] T. Stöferle, H. Moritz, C. Schori, M. Köhl, and T. Esslinger. Transition from a Strongly Interacting 1D Superfluid to a Mott Insulator. *Phys. Rev. Lett.*, 92:1, 2004.

- [17] G. Grynberg, B. Lounis, P. Verkerk, J. Courtois, and C. Salomon. Quantized motion of cold cesium atoms in two- and three-dimensional optical potentials. *Phys. Rev. Lett.*, 70:2249, 1993.
- [18] A. Hemmerich and T. Hänsch. Two-dimensional atomic crystal bound by light. *Phys. Rev. Lett.*, 70:410, 1993.
- [19] Z. Hadzibabic, P. Krüger, M. Cheneau, B. Battelier, and J. Dalibard. Berezinskii-Kosterlitz-Thouless crossover in a trapped atomic gas. *Nature*, 441:1118, 2006.
- [20] M. Weidemüller, A. Hemmerich, A. Görlitz, T. Esslinger, and T. W. Hänsch. Bragg diffraction in an atomic lattice bound by light. *Phys. Rev. Lett.*, 75:4583, 1995.
- [21] D. Jaksch and P. Zoller. The cold atom Hubbard toolbox. *Ann. of Phys.*, 315:52, 2005.
- [22] L. Santos, M. Baranov, J. Cirac, H.-U. Everts, H. Fehrmann, and M. Lewenstein. Atomic Quantum Gases in Kagomé Lattices. *Phys. Rev. Lett.*, 93:4, 2004.
- [23] Q. Niu, X. G. Zhao, G. A. Georgakis, and M. G. Raizen. Atomic Landau-Zener tunneling and Wannier-Stark ladders in optical potentials. *Phys. Rev. Lett.*, 76:4504, 1996.
- [24] B. M. Dahan, E. Peik, J. Reichel, Y. Castin, and C. Salomon. Bloch oscillations of atoms in an optical potential. *Phys. Rev. Lett.*, 76:4508, 1996.
- [25] B. P. Anderson and M. A. Kasevich. Macroscopic Quantum Interference from Atomic Tunnel Arrays. *Science*, 282:1686, 1998.
- [26] O. Morsch and M. Oberthaler. Dynamics of Bose-Einstein condensates in optical lattices. *Rev. Mod. Phys.*, 78:179, 2006.
- [27] D. Jaksch, C. Bruder, J. Cirac, C. Gardiner, and P. Zoller. Cold Bosonic Atoms in Optical Lattices. *Phys. Rev. Lett.*, 81:3108, 1998.
- [28] M. P. A. Fisher, P. B. Weichman, G. Grinstein, and D. S. Fischer. Boson localization and the superfluid-insulator transition. *Phys. Rev. B*, 40:546, 1989.
- [29] M. Greiner, O. Mandel, T. Esslinger, T. W. Hänsch, and I. Bloch. Quantum phase transition from a superfluid to a Mott insulator in a gas of ultracold atoms. *Nature*, 415:39, 2002.
- [30] F. Gerbier, A. Widera, S. Fölling, O. Mandel, T. Gericke, and I. Bloch. Interference pattern and visibility of a Mott insulator. *Phys. Rev. A*, 72:053606, 2005.
- [31] F. Gerbier, A. Widera, S. Fölling, O. Mandel, T. Gericke, and I. Bloch. Phase Coherence of an Atomic Mott Insulator. *Phys. Rev. Lett.*, 95:050404, 2005.
- [32] T. D. Kühner and H. Monien. Phases of the one-dimensional Bose-Hubbard model. *Phys. Rev. B*, 58:R14741, 1998.
- [33] G. G. Batrouni, R. T. Scalettar, and G. T. Zimanyi. Quantum critical phenomena in one-dimensional Bose systems. *Phys. Rev. Lett.*, 65:1765, 1990.

- [34] B. Capogrosso-Sansone, N. Prokof'ev, and B. Svistunov. Phase diagram and thermodynamics of the three-dimensional Bose-Hubbard model. *Phys. Rev. B*, 75:134302, 2007.
- [35] B. Capogrosso-Sansone, S. Söyler, N. Prokof'ev, and B. Svistunov. Monte Carlo study of the two-dimensional Bose-Hubbard model. *Phys. Rev. A*, 77:015602, 2008.
- [36] S. Sachdev. *Quantum Phase Transitions*. Cambridge University Press, Cambridge, 1999.
- [37] J. K. Freericks and H. Monien. Strong-Coupling expansions for the pure and disordered Bose-Hubbard model. *Phys. Rev. B*, 53:2691, 1996.
- [38] N. Elstner and H. Monien. Dynamics and thermodynamics of the Bose-Hubbard model. *Phys. Rev. B*, 59:12184, 1999.
- [39] F. E. A. dos Santos and A. Pelster. Quantum phase diagram of bosons in optical lattices. *Phys. Rev. A*, 79:013614, 2009.
- [40] B. Bradlyn, F. E. A. dos Santos, and A. Pelster. Effective action approach for quantum phase transitions in bosonic lattices. *Phys. Rev. A*, 79:013615, 2009.
- [41] A. Eckardt. Process-chain approach to high-order perturbation calculus for quantum lattice models. *Phys. Rev. B*, 79:195131, 2009.
- [42] N. Teichmann, D. Hinrichs, M. Holthaus, and A. Eckardt. Bose-Hubbard phase diagram with arbitrary integer filling. *Phys. Rev. B*, 79:100503, 2009.
- [43] N. Teichmann, D. Hinrichs, M. Holthaus, and A. Eckardt. Process-chain approach to the Bose-Hubbard model: Ground-state properties and phase diagram. *Phys. Rev. B*, 79:224515, 2009.
- [44] N. Teichmann and D. Hinrichs. Scaling property of the critical hopping parameters for the Bose-Hubbard model. *Eur. Phys. J. B*, 71:219, 2009.
- [45] T. D. Grass, F. E. A. dos Santos, and A. Pelster. Real-Time Ginzburg-Landau Theory for Bosons in Optical Lattices. *Laser Physics*, 21:1459, 2011.
- [46] T. D. Grass, F. E. A. dos Santos, and A. Pelster. Excitation Spectra of Bosons in Optical Lattices from Schwinger-Keldysh Calculation. *Phys. Rev. A*, 84:013613, 2011.
- [47] C. J. Pethick and H. Smith. *Bose-Einstein Condensates in Dilute Gases*. Cambridge University Press, Cambridge, 2nd edition, 2008.
- [48] L. Pitaevskii and S. Stringari. *Bose-Einstein Condensation*. Oxford University Press, Oxford, 2003.
- [49] L. Mandel and E. Wolf. *Optical Coherence and Quantum Optics*. Cambridge University Press, Cambridge, 1995.
- [50] N. W. Ashcroft and N. D. Mermin. *Solid State Physics*. Saunders College Publishing, 1976.

- [51] M. Greiner, I. Bloch, O. Mandel, T. Hänsch, and T. Esslinger. Exploring Phase Coherence in a 2D Lattice of Bose-Einstein Condensates. *Phys. Rev. Lett.*, 87:2, 2001.
- [52] A. L. Fetter and J. D. Walecka. *Quantum theory of many-particle systems*. Dover Publications, New York, 2003.
- [53] W. Zwerger. Mott Hubbard transition of cold atoms in optical lattices. *J. of Opt. B: Quantum and Semiclass. Opt.*, 5:S9, 2003.
- [54] A. Albus, F. Illuminati, and J. Eisert. Mixtures of bosonic and fermionic atoms in optical lattices. *Phys. Rev. A*, 68:1, 2003.
- [55] K. Huang. *Statistical Mechanics*. John Wiley & Sons, Singapore, 1987.
- [56] H. Kleinert and V. Schulte-Frohlinde. *Critical Properties of  $\phi^4$ -Theories*. World Scientific, Singapore, 2001.
- [57] J. Zinn-Justin. *Quantum Field Theory and Critical Phenomena*. Claredon Press, Oxford, 2002.
- [58] P. Hohenberg and B. Halperin. Theory of dynamic critical phenomena. *Rev. Mod. Phys.*, 49:435, 1977.
- [59] H. E. Stanley. *Introduction to Phase Transitions and Critical Phenomena*. Oxford University Press, London, 1971.
- [60] M. A. Continentino. *Quantum Scaling in Many-Body Systems*. World Scientific, Singapore, 2001.
- [61] J. von Neumann. *Mathematische Grundlagen der Quantenmechanik*. Springer, Berlin, 1995.
- [62] A. Eckardt, P. Hauke, P. Soltan-Panahi, C. Becker, K. Sengstock, and M. Lewenstein. Frustrated quantum antiferromagnetism with ultracold bosons in a triangular lattice. *EPL*, 89:10010, 2010.
- [63] W. Metzner. Linked-cluster atomic Hubbard. *Phys. Rev. B*, 43:8549, 1991.
- [64] M. P. Gelfand, R. R. P. Singh, and D. A. Huse. Perturbation expansions for quantum many-body systems. *J. Stat. Phys.*, 59:1093, 1990.
- [65] J. M. Kosterlitz and D. J. Thouless. Ordering, metastability and phase transitions in two-dimensional systems. *J. Phys. C*, 6:1181, 1973.
- [66] M.E. Fisher, M.N. Barber, and D. Jasnow. Helicity modulus, superfluidity, and scaling in isotropic systems. *Phys. Rev. A*, 8:1111, 1973.
- [67] R. Roth and K. Burnett. Superfluidity and interference pattern of ultracold bosons in optical lattices. *Phys. Rev. A*, 67:1, 2003.
- [68] J. Stenger, S. Inouye, A. P. Chikkatur, D. M. Stamper-Kurn, D. E. Pritchard, and W. Ketterle. Bragg spectroscopy of a Bose-Einstein condensate. *Phys. Rev. Lett.*, 82:4569, 1999.

- [69] M. Kozuma, L. Deng, E. W. Hagley, J. Wen, R. Lutwak, K. Helmerson, S. L. Rolston, and W. D. Phillips. Coherent splitting of Bose-Einstein condensed atoms with optically induced Bragg diffraction. *Phys. Rev. Lett.*, 82:871, 1999.
- [70] P. T. Ernst, S. Götze, J. S. Krauser, K. Pyka, D.-S. Lühmann, D. Pfannkuche, and K. Sengstock. Probing superfluids in optical lattices by momentum-resolved Bragg spectroscopy. *Nature Physics*, 6:56, 2009.
- [71] D. Clément, N. Fabbri, L. Fallani, C. Fort, and M. Inguscio. Exploring Correlated 1D Bose Gases from the Superfluid to the Mott-Insulator State by Inelastic Light Scattering. *Phys. Rev. Lett.*, 102:1, 2009.
- [72] A. Polkovnikov, S. Sachdev, and S. Girvin. Nonequilibrium Gross-Pitaevskii dynamics of boson lattice models. *Phys. Rev. A*, 66:1, 2002.
- [73] S. Huber, E. Altman, H. Büchler, and G. Blatter. Dynamical properties of ultracold bosons in an optical lattice. *Phys. Rev. B*, 75:085106, 2007.
- [74] C. Menotti and N. Trivedi. Spectral weight redistribution in strongly correlated bosons in optical lattices. *Phys. Rev. B*, 77:1, 2008.
- [75] A. A. Abrikosov, L. P. Gorkov, and I. E. Dzyaloshinski. *Quantum field theoretical methods in statistical physics*. Dover Publications, New York, 1975.
- [76] A. J. Leggett. Bose-Einstein condensation in the alkali gases: Some fundamental concepts. *Rev. Mod. Phys.*, 73:307, 2001.
- [77] J. Sebby-Strabley, B. Brown, M. Anderlini, P. Lee, W. Phillips, J. Porto, and P. Johnson. Preparing and Probing Atomic Number States with an Atom Interferometer. *Phys. Rev. Lett.*, 98:1, 2007.
- [78] S. Will, T. Best, U. Schneider, L. Hackermüller, D.-S. Lühmann, and I. Bloch. Time-resolved observation of coherent multi-body interactions in quantum phase revivals. *Nature*, 465:197, 2010.
- [79] M. Brune, F. Schmidt-Kaler, A. Maali, J. Dreyer, E. Hagley, J. M. Raimond, and S. Haroche. Quantum Rabi oscillation: A direct test of field quantization in a cavity. *Phys. Rev. Lett.*, 76:1800, 1996.
- [80] D. M. Meekhof, C. Monroe, B. E. King, W. M. Itano, and D. J. Wineland. Generation of nonclassical motional states of a trapped atom. *Phys. Rev. Lett.*, 76:1796, 1996.
- [81] A. Hubener, M. Snoek, and W. Hofstetter. Magnetic phases of two-component ultracold bosons in an optical lattice. *Phys. Rev. B*, 80:1, 2009.
- [82] M. Snoek, J. L. Song, and F. Zhou. Hyperfine spin-two ( $F=2$ ) atoms in three-dimensional optical lattices: Phase diagrams and phase transitions. *Phys. Rev. A*, 80:1, 2009.
- [83] A. Mering and M. Fleischhauer. Multiband and nonlinear hopping corrections to the three-dimensional Bose-Fermi-Hubbard model. *Phys. Rev. A*, 83:1, 2011.

- [84] X.-F. Zhou, Y.-S. Zhang, and G.-C. Guo. Pair tunneling of bosonic atoms in an optical lattice. *Phys. Rev. A*, 80:1, 2009.
- [85] Y.-W. Lee and M.-F. Yang. Superfluid-insulator transitions in attractive Bose-Hubbard model with three-body constraint. *Phys. Rev. A*, 81, 2010.
- [86] N. Teichmann, D. Hinrichs, and M. Holthaus. Reference data for phase diagrams of triangular and hexagonal bosonic lattices. *Europhys. Lett.*, 91:10004, 2010.
- [87] I. Hen and M. Rigol. Analytical and numerical study of trapped strongly correlated bosons in two- and three-dimensional lattices. *Phys. Rev. A*, 82:1, 2010.
- [88] O. Mandel, M. Greiner, A. Widera, T. Rom, T. W. Hänsch, and I. Bloch. Controlled collisions for multiparticle entanglement of optically trapped atoms. *Nature*, 425:937, 2003.
- [89] S. Söyler, B. Capogrosso-Sansone, N. Prokof'ev, and B. V. Svistunov. Sign-alternating interaction mediated by strongly correlated lattice bosons. *New J. Phys.*, 11:073036, 2009.
- [90] C. Becker, P. Soltan-Panahi, J. Kronjäger, S. Dörscher, K. Bongs, and K. Sengstock. Ultracold quantum gases in triangular optical lattices. *New J. Phys.*, 12:065025, 2010.
- [91] C. Nietner. Diploma Thesis. Quantum Phase Transition of Light in the Jaynes-Cummings Lattice, 2010.
- [92] E. Altman, W. Hofstetter, E. Demler, and M. D. Lukin. Phase diagram of two-component bosons on an optical lattice. *New J. Phys.*, 5:113, 2003.
- [93] L.-M. Duan, E. Demler, and M. Lukin. Controlling Spin Exchange Interactions of Ultracold Atoms in Optical Lattices. *Phys. Rev. Lett.*, 91:1, 2003.
- [94] A. B. Kuklov and B. V. Svistunov. Counterflow Superfluidity of Two-Species Ultracold Atoms in a Commensurate Optical Lattice. *Phys. Rev. Lett.*, 90:12, 2003.
- [95] A. Kuklov, N. Prokof'ev, and B. Svistunov. Commensurate Two-Component Bosons in an Optical Lattice: Ground State Phase Diagram. *Phys. Rev. Lett.*, 92:3, 2004.
- [96] D.-W. Wang, M. Lukin, and E. Demler. Engineering superfluidity in Bose-Fermi mixtures of ultracold atoms. *Phys. Rev. A*, 72:051604(R), 2005.



# List of Publications

1. F. E. A. dos Santos and A. Pelster. Quantum phase diagram of bosons in optical lattices. Phys. Rev. A, 79:013614, 2009.
2. B. Bradlyn, F. E. A. dos Santos, and A. Pelster. Effective action approach for quantum phase transitions in bosonic lattices. Phys. Rev. A, 79:013615, 2009.
3. T. D. Grass, F. E. A. dos Santos, and A. Pelster. Real-Time Ginzburg-Landau Theory for Bosons in Optical Lattices. Laser Physics, 21:1459, 2011.
4. T. D. Grass, F. E. A. dos Santos, and A. Pelster. Excitation Spectra of Bosons in Optical Lattices from Schwinger-Keldysh Calculation. Phys. Rev. A , 84: 013613, (2011).
5. F. E. A. dos Santos and A. Pelster. Collapse and revival of matter waves in bosonic lattices, (*in preparation*).



# Acknowledgements

This thesis is the result of four stimulating years of work at the Physics Department of the Free University of Berlin. It could not be accomplished without the valuable support of my advisor Priv.-Doz. Dr. Axel Pelster, to whom I am very grateful for his guidance in the art of scientific research. His deep mathematical understanding and commitment to his students provided me with exceptional lessons not only in Physics but also in life, which I will keep as a treasure.

I also want to express my gratitude to Prof. Dr. Dr. h.c. mult. Hagen Kleinert for accepting me in his group. It was inspiring to observe his urge to transmit knowledge which is so great that his lessons during the lunch time became known as “The universe in a piece of napkin”.

It gives me great pleasure in acknowledging my co-advisor Prof. Dr. Jürgen Bosse for his wise words when I had many doubts about my career as a physicist. I also would like to thank him for all the support letters for extensions of my DAAD scholarship as well as for his critical suggestions to this manuscript.

Special thanks goes to the Brazilian guys also known as “The Brazilian Mafia” for their friendship: Aristeu Lima, Victor Bezerra, Flavio Nogueira and the honorary member Tobias Graß. I specially thank Flavio Nogueira and my another office colleague Jürgen Dietel for being always available to discuss various topics in physics.

I am indebted to my many colleagues with whom I had the privilege to work at the Free University of Berlin: Konstantin Glaum, Walja Korolewski, Christian Nietner, Alexander Hoffmann, Matthias Ohliger, Mahmoud Ghabour, Hamid Al-Jibbouri, and Mohammad Mobarak.

I cannot find words to express my gratitude to Prof. Vanderlei Bagnato for his support at the later stages of this work. Without his help, the accomplishment of this thesis would be seriously compromised.

Very special thanks go to my wife Lorena for being by my side during these years even with the personal sacrifices that this implied.

I acknowledge the financial support from the German Academic Exchange Service (DAAD). I am particularly indebted to Mrs. Maria Salgado for her kind support during all the period of my DAAD-scholarship.